AD-A091 012 OKLAHOMA UNIV NORMAN DEPT OF PHYSICS AND ASTRONOMY F/G 20/5
ELECTRON IMPACT OF LASER MEDIA.(U)
AUG 80 D E GOLDEN AFOSR-75-2866
UNCLASSIFIED AFOSR-TR-80-1000 NL

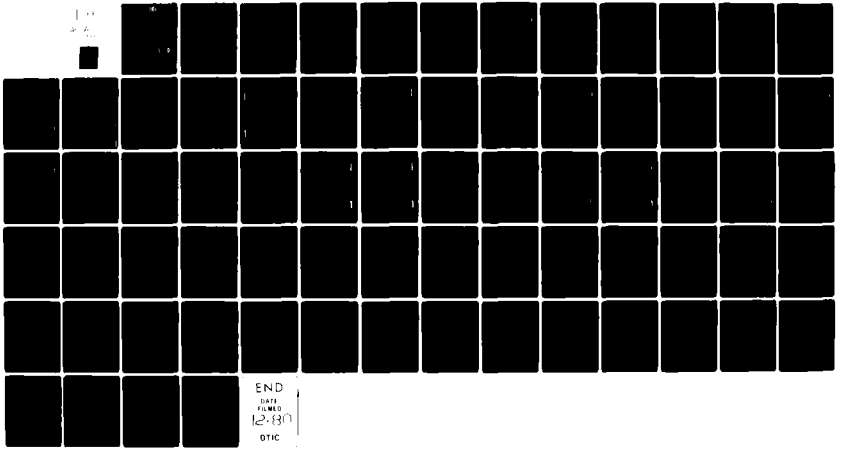

END
DATE FILMED
12-80
DTIC

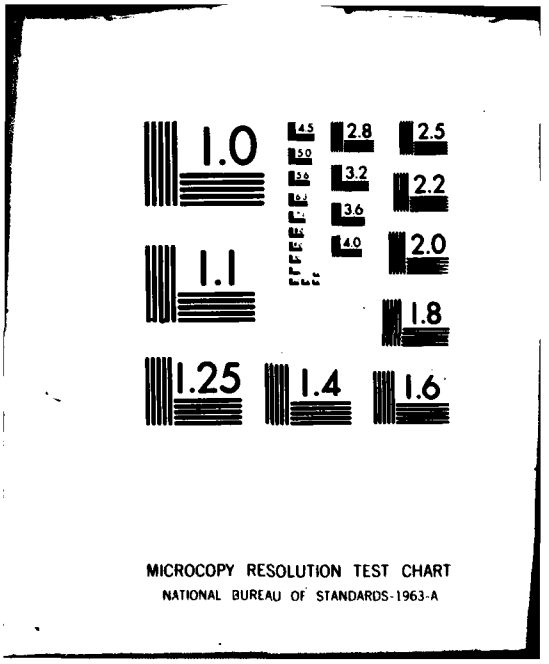
1.0
1.1
1.25
1.4
1.6
1.8
2.0
2.2
2.5
2.8
3.2
3.6
4.0
4.5
5.0
5.6
MICROCOPY RESOLUTION TEST CHART
NATIONAL BUREAU OF STANDARDS-1963-A

UNCLASSIFIED

SECURITY CLASSIFICATION OF THIS PAGE (When Data Entered)

LEVEL III

REPORT DOCUMENTATION PAGE

READ INSTRUCTIONS BEFORE COMPLETING FORM

1. REPORT NUMBER	2. GOVT ACCESSION NO.	3. RECIPIENT'S CATALOG NUMBER
AFOSR-TR-80-1000	AD-A091012	

4. TITLE (and Subtitle)

Electron Impact of Laser Media

5. TYPE OF REPORT & PERIOD COVERED

Final Scientific Report.
6-15-79 — 6-14-80

6. PERFORMING ORG. REPORT NUMBER

15 Jun 79-14 Jun 80

7. AUTHOR(s)

David E. Golden

8. CONTRACT OR GRANT NUMBER(s)

AFOSR-75-2866

9. PERFORMING ORGANIZATION NAME AND ADDRESS

Office of Research Administration
University of Oklahoma
1000 Asp, Avenue Room 314
Norman, Oklahoma 73019

10. PROGRAM ELEMENT, PROJECT, TASK AREA & WORK UNIT NUMBERS

61102F 2301/A4

11. CONTROLLING OFFICE NAME AND ADDRESS

AFOSR/NP
Bolling AFB, Bldg. #410
Wash DC 20332

12. REPORT DATE

14 August 1980

13. NUMBER OF PAGES

70

14. MONITORING AGENCY NAME & ADDRESS (if different from Controlling Office)

A4

15. SECURITY CLASS. (of this report)

unclassified

15a. DECLASSIFICATION/DOWNGRADING SCHEDULE

16. DISTRIBUTION STATEMENT (of this Report)

Approved for public release; distribution unlimited.

17. DISTRIBUTION STATEMENT (of the abstract entered in Block 20, if different from Report)

DTIC ELECTE OCT 28 1980 S D

18. SUPPLEMENTARY NOTES

19. KEY WORDS (Continue on reverse side if necessary and identify by block number)

Lasers, electron impact excitation cross sections, optical branching of decays, excited state lifetimes, polarization of radiation, collisional deactivation, energy transfer rates

20. ABSTRACT (Continue on reverse side if necessary and identify by block number)

The experimental program is aimed at an understanding of the physics necessary for the design of lasers which are excited by electron impact. Electron impact excitation cross sections, optical branching ratios of the subsequent decays, excited state lifetimes, polarization of radiation, collisional deactivation, and energy transfer rates are measured. Cross sections for the excitation of fine structure levels and alignment and orientation parameters are also measured.

407645 DM UNCLASSIFIED

AD A091012

DDC FILE COPY

A phase shift analysis of relative differential cross section measurements was developed to very accurately place such measurements on an absolute scale. This method was used to analyze all previous differential elastic cross section measurements for e-He scattering.

We have measured the prompt and delayed excitation functions of the $b^3\Sigma^+$ and $d^3\Delta$ states of CO as well as the optical decay of these states in delayed coincidence to make definite measurements of the lifetimes and quenching cross sections for these states. In addition we have extracted the $(d \rightarrow x)/(d \rightarrow a)$ branching ratios for the $v' = 4, 5$ levels from this data. Briefly, measured lifetimes take account of the presence of cascades which has not been accounted for in the analysis of previous measurements.

The electron photon angular correlation function in the scattering plane for excitation of the 2^1P state of He for electron energies from 80 to 500 eV and for a range of electron scattering angles from 5° to 100° were measured. These measurements, together with other measurements, are used to examine the behavior of the Fano-Macek alignment and orientation parameters for electron energies from 40 to 500 eV.

The angular correlation measurements are only in agreement with one calculation (the distorted wave calculation of Madison) over the entire energy and angular range. The study of the alignment and orientation has permitted explanation of this scattering process in terms of the small angle scattering being due to the attractive atomic polarizibility and the large angle scattering as being due to repulsive scattering from the bound electrons over the entire energy range.

Electron Impact of Laser Media . . .

TECHNICAL REPORT

FINAL

AFOSR 75-2866
period ending 14 June 1980

AFOSR-TR- 80 - 1000

The experimental program is aimed at an understanding of the physics necessary for the design of lasers which are excited by electron impact. We measure electron impact excitation cross sections, optical branching ratios of the subsequent decays, excited state lifetimes, polarization of radiation, collisional deactivation and energy transfer rates. We also measure cross sections for the excitation of fine structure levels and alignment and orientation parameters. The measurements are performed with sufficient electron energy resolution so that the role of resonances in the excitation process may be studied.

The experiments thus far have been carried out in two apparatuses. In one apparatus a pulsed electron gun with less than 500 p sec cut off is used to excite atoms or molecules contained in a gas cell. Time resolved spectroscopy is used to study prompt and delayed excitation functions, lifetimes, quenching cross sections, collisional energy transfer rates and branching ratios. In a second apparatus an electron beam is cross fired with an atomic or molecular beam target. Electrons which have excited a particular state of the target are detected in delayed coincidence with photons emitted in the decay of that target state in the scattering plane. For a particular electron impact energy the angular correlation function for a particular excitation is studied. From this information, cross sections for exciting fine structure levels, alignment and orientation parameters, target multipole moments, and even excited state wave functions within an arbitrary phase factor are extracted. A third apparatus has been recently constructed. In this apparatus an electron beam will be cross fired with a very well collimated neutral beam source. A tunable dye laser will be interacted

with a target neutral beam to select a particular target state. Following the electron impact a second tunable dye laser will be used to interrogate the scattered neutrals as to their final states. This laser spectroscopy technique will allow an energy resolution of about 5×10^{-8} eV which represents an improvement of about 5 1/2 orders of magnitude in every resolution over the standard technology used in this type of experiment.

Present Results

We have developed a phase shift analysis of relative differential cross section measurements to very accurately place such measurements on an absolute scale. We have used this method to analyze all previous differential elastic cross section measurements for e-He scattering. This is discussed in detail in Publication (1).

We have used apparatus I to measure the prompt and delayed excitation functions of the $b^3\Sigma^+$ and $d^3\Delta$ states of CO. We have also used this apparatus to study the optical decay of these states in delayed coincidence to make definite measurements of the lifetimes and quenching cross sections for these states. In addition we have extracted the $(d \rightarrow x)/(d \rightarrow a)$ branching ratios for the $v' = 4, 5$ levels from our data. The apparatus, technique used and results obtained are described in Publications (2) and (6). Briefly, our measured lifetimes take account of the presence of cascades. This fact has not been accounted for in the analysis of previous measurements.

The second apparatus was to measure the electron photon angular correlation function in the scattering plane for excitation of the 2^1P state of He for electron energies from 80 to 500 eV and for a range of electron scattering angles from 5° to 100°. This work is described in Publications (3), (4), and (5). We have used the measurements together with other measurements to examine the behavior of the Fano-Macek alignment and orientation parameters for electron energies from 40 to 500 eV.

The angular correlation measurements are only in agreement with one calculation (the distorted wave calculation of Madison) over the entire energy and angular range. The study of the alignment and orientation has allowed us to explain this scattering process in terms of the small angle scattering being due to the attractive atomic polarizibility and the large angle scattering as being due to repulsive scattering from the bound electrons over the entire energy range.

Professor Golden has been asked to give an invited talk on Electron-Photon Correlation in Electron Impact Excitation at the next annual DEAP Meeting in Los Angeles.

AFOSR 75-2866
Period June 15, 1979 to
June 14, 1980

Publications

1) N.C. Steph, L. McDonald and D.E. Golden, Analysis of Low Energy Scattering Cross Sections, I - Electron-Helium Elastic Scattering, J. Phys. B. 12, 1507 (1979)

2) J.R. Twist, W. Paske, T.O. Rhymes, G.N. Haddad, and D.E. Golden, Low Energy Electron Impact Excitation of the $b^3\Sigma^+$ State of CO, J. Chem. Phys. 71, 2345 (1979)

3) D.E. Golden and N.C. Steph, Correlation Effects in Electron-Atom Scattering, in Coherence and Correlation Effects in Atomic Physics, Plenum Press (1979)

4) N.C. Steph and D.E. Golden, Electron-Photon Angular Correlation Measurements of He 1^1S-2^1P Excitation at 80 eV, Phys. Rev. A (March 1980)

5) N.C. Steph and D.E. Golden, Alignment and Orientation in the Electron Impact Excitation of the 2^1P State of He from 40-500 eV, Phys. Rev. A (accepted for publication January 1980)

6) W.C. Paske, J.R. Twist, A.W. Garrett and D.E. Golden, Low Energy Electron Impact Excitation and Radiative Decay of the $d^3\Delta$ State of CO, J. Chem. Phys. (accepted for publication February 1980)

Abstracts and Proceeding's

W. C. Paske, J. R. Twist and D. E. Golden, Low Energy Electron Impact Excitation of the d and e States of CO, Bull. Am. Phys. Soc. 24, 1170 (1979)

N. C. Steph and D. E. Golden, Alignment and Orientation Parameters for He 1^1S-2^1S Excitation, Bull. Am. Phys. Soc. 24, 1189 (1979)

D. E. Golden, Orientation in Electron Impact Excitation, Invited Paper, Second George Schulz Memorial Symposium, Yale University (1979)

From: COHERENCE AND CORRELATION IN ATOMIC COLLISIONS
Edited by H. Kleinpoppen and J.F. Williams
(Plenum Publishing Corporation, 1980)

7

Correlation in Electron–Atom Excitation

D. E. GOLDEN AND N. C. STEPH

The use of delayed coincidences and photon polarization measurements to study correlation effects in electron–atom inelastic scattering is detailed. Sources of systematic error in experimental results with respect to determination of the correlation parameters λ and χ for helium are discussed. The results of several calculations are compared to the experimental data for the 2^1P_1 state of helium.

Correlation, which indicates a lack of internal independence, has not been discussed as such in the atomic physics literature until relatively recently. However, correlation has been discussed extensively in high-energy, nuclear, and solid-state physics. The underlying idea is that internal symmetries may be uncovered by fixing the external symmetries in the preparation of an experiment or calculation. This certainly must be true in any case where structure is attributed to an object. The trick is to figure out how to probe the structure. For example, by proper experimental design, one might be able to probe the excitation of fine and even hyperfine levels.

The subject of coherent excitation of different fine and hyperfine levels begins with the beam–foil measurements in the mid-1960's.[†] These experiments were aimed at the measurement of atomic lifetimes by looking at radiation from foils excited by ion impact. While the measurements were made under supposed zero external field conditions, oscillations in the light intensity were observed. These oscillations were attributed to Stark mixing due to a small electric field in the ion beam itself.[‡]

[†] See, for example, Reference 1.

D. E. GOLDEN AND N. C. STEPH • Department of Physics and Astronomy, University of Oklahoma, Norman, Oklahoma 73019.

However, the correct explanation, given by Macek,[2] is that the oscillations were beats due to interferences between the various hyperfine levels. Thus Macek postulated the coherent excitation of fine and hyperfine levels.

Correlation effects in electron–atom excitation were first studied in a scattering experiment using the technique of delayed coincidence.[3] While this measurement technique has been used extensively in nuclear physics,[4] it is only relatively recently that it has become widely used in atomic physics. It was first used to study atomic lifetimes in 1955.[5] Since that time it has been used to study ionization,[6] excitation of metastables,[7] energy transfer from a metastable to radiating state,[8] and to separate excitation cross sections for levels that could not be separated in a scattered electron detector.[9] This last application has most recently been used to separate the 3^3D and 3^1D excitation cross sections in Kr by McGregor and Kleinpoppen at the University of Stirling. These levels are separated by only 0.0004 eV and so this experiment would not be possible within present electron energy analyzer technology without the use of the delayed coincidence technique.

The work of Macek[2] was extended by Macek and Jaecks[10] to point out that more insight regarding inelastic scattering could be obtained by studying angular correlations between inelastically scattered electrons and photons from the decay of an excited state than from the measurement of an inelastic cross section. The basis of the work of Macek and Jaecks[10] is the first consistent theoretical treatment of electron impact excitation due to Percival and Seaton[11] and the notion of Macek[2] that radiation from different fine and hyperfine levels introduces oscillatory terms into the radiative decay of atoms. Macek and Jaecks[10] took the magnetic substates to be excited coherently and developed a time-dependent theory. This theory has been reformulated by many others. Most recently the subject of electron–photon angular correlations in atomic physics has been reviewed by Blum and Kleinpoppen.[12] In this work the e –H correlation parameters are also developed for the first time.

The first electron–photon angular correlation measurements were reported by Eminyan *et al.*[3] for excitation of the 2^1P state of helium. We should point out that the kind of information to be obtained can also be obtained from experiments with laser-excited atoms such as have been performed at Kaiserslautern and New York University. However, the interpretation of the data is less clear-cut because the laser excites some distribution of excited states. Electron–photon angular correlations have since been studied in Ne and Ar by the Flinders group, in Kr and Hg by the Stirling group, in H_2 by the Kaiserlautern group, and in Ar and H by the Windsor group. However, the interpretation of the results of scattering from targets other than helium is incomplete, as was pointed by Slevin and Farago[13] for argon.

The standard way to treat the 2^1P state of helium is to describe it by a coherent superposition of the degenerate sublevels and neglect spin–orbit and spin–spin interactions in the collision. In addition, the 2^1P state will be excited from the 1^1S state in a field free region. With reference to Figure 1, the electrons are incident along the Z direction and both the scattered electron detector and the photon detector are free

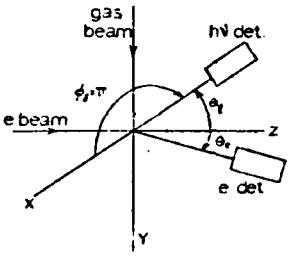

Figure 1. Schematic diagram of the electron–photon coincidence experiment in the scattering plane.

to move in the X–Z plane, which is the scattering plane. In this case the excitation amplitudes, a_m with $m = 0 \pm 1$, are only functions of the electron energy E and the electron scattering angle θ_e. In addition, since there is a mirror symmetry through the scattering plane, $a_{-1} = -a_1$ and the wave function can be normalized such that the scattering amplitudes a_m are very simply related to the scattering cross sections for excitation of the sublevels σ_m,

$$\begin{aligned} |a_0|^2 &= \sigma_0 \\ |a_1|^2 &= \sigma_1 \\ |a_0|^2 + 2|a_1|^2 &= \sigma \end{aligned} \tag{1}$$

where σ is the differential cross section for exciting the 2^1P level. The relative phase χ between a_0 and a_1 is simply given by $a_1 = |a_1| e^{i\chi}$ and $a_0 = |a_0|$. The wave function at a given E and θ_e is completely described within an arbitrary phase factor by σ_0, σ_1, and χ, and the scattering completely determined by a measurement of these parameters. The parameters are determined with the exception of the sign of χ by a measurement of the electron–photon coincidence rate $\dot{N}_c$, which was given by Macek and Jaecks,[10]

$$\frac{d\dot{N}_c}{d\Omega_e\, d\Omega_\gamma\, dz} = A\{\lambda \sin^2\theta_\gamma + (1-\lambda)\cos^2\theta_\gamma - 2[\lambda(1-\lambda)]^{1/2}\cos\chi \sin\theta_\gamma \cos\theta_\gamma\} \tag{2}$$

Here $\lambda = \sigma_0/\sigma$ and

$$A = \frac{3}{8\pi}\,\frac{I_e}{e}\,\varrho(z)\,\frac{\gamma'}{\gamma}\,\varepsilon_e\varepsilon_\gamma\sigma$$

where I_e is the incident electron beam current, $\varrho(z)$ is the density of the target atoms in the interaction volume, γ'/γ is the branching ratio for the decay of the 2^1P state, ε_e and ε_γ are the detector efficiencies, and e is the electron charge. Since the sign of χ is not given by equation (2) this must be determined by a separate measurement such as the polarization of the radiation. We can rewrite equation (2) as the sum of two cosine functions as follows:

$$\begin{aligned} \frac{d\dot{N}_c}{d\Omega_e\, d\Omega_\alpha\, dz} &= \frac{A}{2}\,[(1-\cos\chi)\cos^2(\theta_\gamma - \beta) + (1+\cos\chi)\cos^2(\theta_\gamma + \beta)] \\ &= Af(\lambda, \chi, \theta_\gamma) \end{aligned} \tag{3}$$

where $\sin\beta = \lambda$. When $\cos\chi \simeq 1$, the first term in equation (3) may be neglected so that

$$\frac{d\dot{N}_c}{d\Omega_e\, d\Omega_\gamma\, dz} \simeq \frac{A}{2}(1 + \cos\chi)\cos^2(\theta_\gamma + \beta) \tag{4}$$

Thus, for small χ we have a simple periodic function whose amplitude depends only on χ and whose phase depends only on λ. This is instructive from the point of view of unfolding values of λ and χ from measurements of $\dot{N}_c$. In Figure 2, $f(\lambda, \chi, \theta_\gamma)$ is plotted as a function of θ_γ for $\lambda = 0.48$, $\chi = 0.20$ (solid line, 1); $\lambda = 0.48$, $\chi = 0.30$ (dotted line, 2); and for $\lambda = 0.58$, $\chi = 0.20$ (dash-dotted line, 3). The difference between curves 1 and 2 is due to about a 2% change in amplitude, which is caused by a 50% change in $|\chi|$ so that small errors in amplitude give very large errors in $|\chi|$. The situation in regard to λ is not quite so bad. The difference between curves 1 and 3 is about a 5.5° change in phase, which is due to a 20% change in λ.

When we perform an experiment, we will study coincidences with detectors that view finite solid angles for some time T so that equation (3) must be integrated over the solid angles of the detectors and the time. We perform the integration over the two solid angles and write

$$\frac{\dot{N}_c}{\dot{N}_e} = \frac{3}{8\pi}\varepsilon_\gamma \frac{J_c}{J_e} f(\lambda, \chi, \theta_\gamma) \tag{5}$$

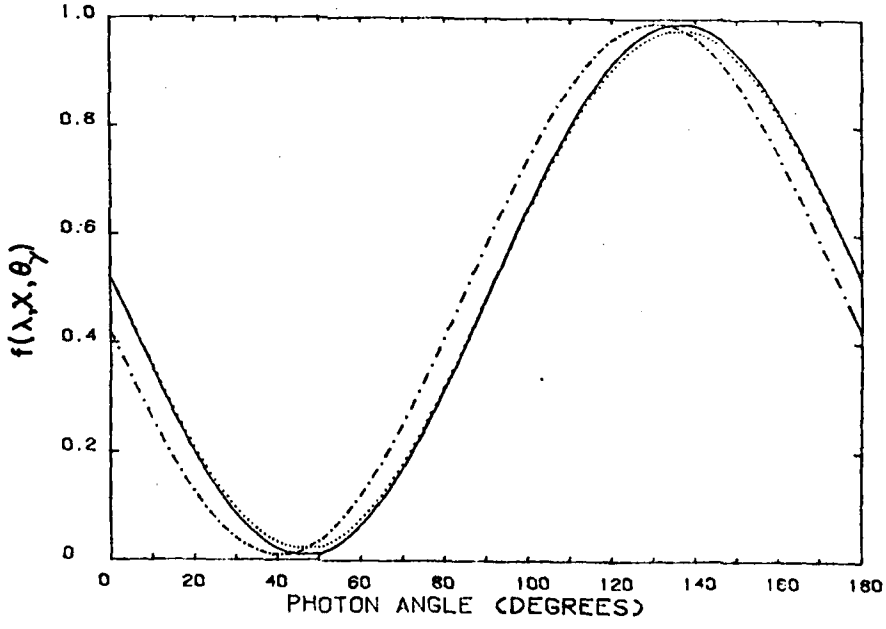

Figure 2. $f(\lambda, \chi, \theta_\gamma)$ vs. photon angle (θ_γ). (1) ——, $\lambda = 0.48$, $\chi = 0.20$; (2) · · ·, $\lambda = 0.48$, $\chi = 0.30$; (3) —·—, $\lambda = 0.58$, $\chi = 0.20$.

where

$$\frac{J_c}{J_e} = \frac{\int [\varrho(z)/\varrho_0]\, d\Omega_e\, d\Omega_\gamma\, dz}{\int [\varrho(z)/\varrho_0]\, d\Omega_e\, dz}$$

and $\dot{N}_e$ is the scattered electron rate. For the case where the atomic beam density is very large compared to the background gas density and uniform over the extent of the beam and for infinite angular resolution, equation (5) reduces to

$$\frac{\dot{N}_c}{\dot{N}_e} = \frac{3}{8\pi}\, \varepsilon_\gamma\, \Delta\Omega_\gamma f(\lambda, \chi, \theta_\gamma) \tag{6}$$

Then one counts for a time T at fixed θ_e for various values of θ_γ and fits to the equation

$$\frac{N_c}{N_e} = Bf(\lambda, \chi, \theta_\gamma) \tag{7}$$

One can then determine the parameters B, λ, and $\cos\chi$ as was done by Eminyan *et al.*[14] Alternatively, for $\theta_\gamma = \pi/2$, one may write

$$\frac{N_c}{N_e} = \frac{3}{8\pi}\, \varepsilon_\gamma \frac{J_c}{J_e}\left(\theta_e, \frac{\pi}{2}\right)\lambda \tag{8}$$

and coincidence measurements at this angle can be used to obtain λ as a function of E and θ_e, as was done by Sutcliffe *et al.*[15] In addition, the coincidence rate for photons observed perpendicular to the scattering plane is given by

$$\dot{N}_c = K\sigma[(1 - \lambda)\sin^2\phi_\gamma + \lambda] \tag{9}$$

Equation (9) was used by Tan *et al.*,[16] together with measurements of $\dot{N}_c$ at $\phi_\gamma = 0$ and $\pi/2$ to obtain values of λ. Also they used a linear polarization filter to obtain values of λ and $|\chi|$. In this later experiment they studied coincidences between electrons which had excited the 2^1P state of helium and photons perpendicular to the scattering plane whose linear polarization made an angle β with the incident electron beam. Then

$$\lambda = \frac{N_c(\beta{=}0)}{N_c(\beta{=}\pi/4) + N_c(\beta{=}3\pi/4)} \tag{10}$$

$$2\left(\frac{1-\lambda}{\lambda}\right)^{1/2}\cos\chi = \frac{N_c(\beta{=}\pi/4) - N_c(\beta{=}3\pi/4)}{N_c(\beta{=}0)}. \tag{11}$$

Now let us consider the experimental questions: (1) What it the effect of the finite angular resolution of the detectors? (2) What is the effect of a nonnegligible background gas density? The effect of the finite resolution of the photon detector can be seen with the aid of Figure 3, where $f(\lambda, \chi, \theta_\gamma)$ is plotted for $\lambda = 0.48$ and $\chi = 0.20$ (solid curve). Suppose we assume that this is the "true" function and

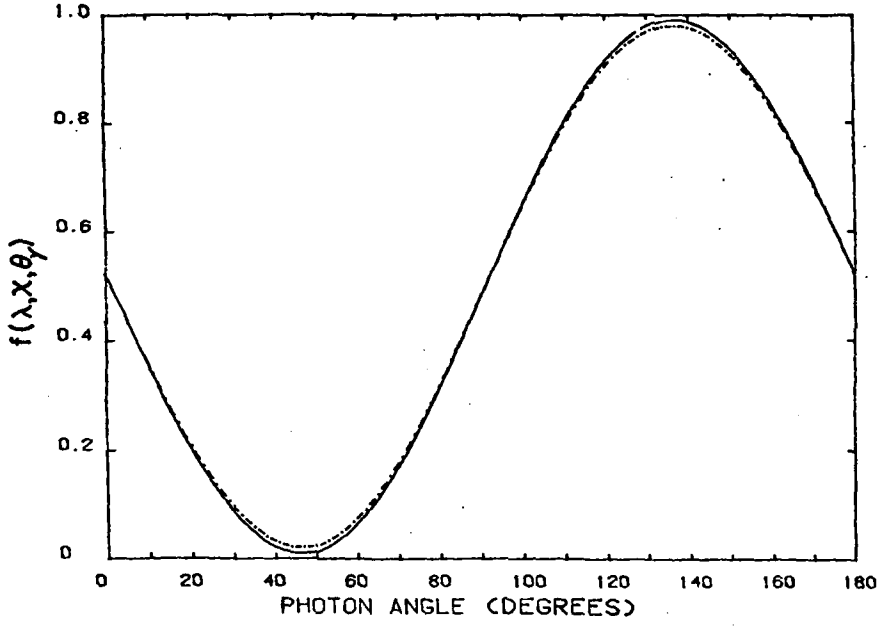

Figure 3. $f(\lambda, \chi, \theta_\gamma)$ vs. photon angle (θ_γ). ——, $\lambda = 0.48$, $\chi = 0.20$; —·—, obtained by averaging solid line over 20° intervals to simulate a flat detector response over 20°.

ask what is the effect of a flat detector response over, say, 20°. The effect would be to draw a new curve that is constructed from points obtained by averaging over 20° intervals from the solid curve of Figure 3. This curve is drawn as a dash-dotted line in Figure 3. The period of the curve remains the same, but the amplitude is decreased. As has been discussed above, for small χ the effect of decreasing the amplitude is to increase the value of χ. This change of about 2% in the amplitude looks like a 50% change in $|\chi|$. This effect, as well as a similar effect due to the detection of photons out of the scattering plane, was corrected for by Eminyan *et al.*[14] by using the following equation:

$$\frac{N_c}{N_e} = \frac{3}{8\pi}\,\varepsilon_\gamma\,\Delta\Omega_\gamma\left[\varkappa f(\lambda, \chi, \theta_\gamma) + \frac{2}{3}(1 - \varkappa)\right] \tag{12}$$

where $\varkappa$ is given by† $(1 - \Delta\Omega_\gamma/4\pi)(1 - \Delta\Omega_\gamma/2\pi)$. Of course it is possible to make $\Delta\Omega_\gamma$ sufficiently small so that the correction represented by equation (12) is unnecessary. The effect of a finite background gas density is to give too large a measured value of N_c/N_e at both small and large values of either θ_e or θ_γ. This is a

† *Note added in proof.* It should be noted that this definition of $\varkappa$ is slightly different than that given in Reference 14. This typographical error was pointed out to us by Professor K. B. MacAdam.

correction that is symmetric about 90° and affects both λ and χ. This correction requires knowledge of the solid angles of the detectors, the variation of these solid angles with path length, and the atomic beam profile, and can be written as $(J_c/J_e)(\theta_e, \theta_\gamma)$. This expression has been evaluated by Sutcliffe *et al.*[15] for $\theta_\gamma = \pi/2$ from auxiliary measurements of elastic angular distributions with the atomic beam on and with the atomic beam off and the chamber flooded to the same background gas density as with the beam on. The correction to the data of Sutcliffe *et al.*[15] is plotted as $(J_c/J_c)(\theta_e, \pi/2)$ in Figure 4. One would expect a similar correction to be obtained if θ_e is kept fixed and θ_γ varied. It should be noted that in the range $40° < \theta_e < 140°$ the graph is relatively flat. Therefore, provided one makes the solid angle of the detector sufficiently small and avoids both small and large angles, this correction is unnecessary.

The problem of measuring the number of coincidences at a given θ_e, θ_γ, and E can be further complicated by accidental coincidences. These occur when the clock is started and stopped by electrons and photons from different scattering events and is given by the product of the two rates and the time window of the coincidence detector

$$\dot{N}_A = \dot{N}_e \dot{N}_\gamma \, \Delta t \tag{13}$$

An example from the work of Sutcliffe *et al.*[15] is shown in Figure 5. The background is due to the accidental coincidences spread out in time (channel number). Once a start pulse is obtained the *a priori* probability of a stop pulse is p. Then the probability of obtaining a stop in the ith channel is given by $P_i = (1 - p)^i p$. Then the background distribution due to accidental coincidences is given by

$$\dot{N}_{A_i} = \dot{N}_e \dot{N}_\gamma \, \Delta t p (1 - p)^i T \tag{14}$$

The number of true coincidences is obtained by fitting the background and sub-

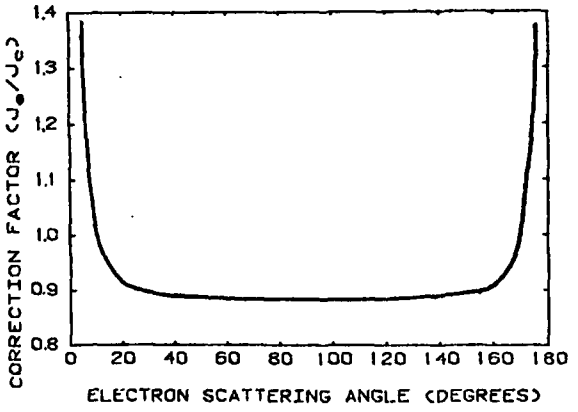

Figure 4. $(J_e/J_c)(\theta_e, \pi/2)$ vs. electron scattering angle (θ_e) from Reference 15.

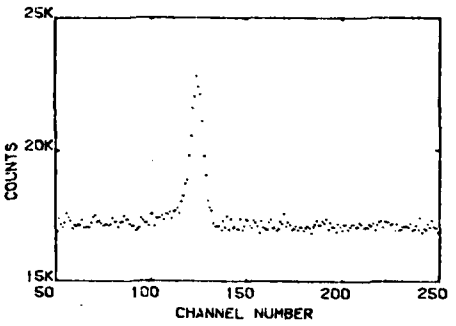

Figure 5. Coincidence peak for $\theta_y = \pi/2$, $\phi_y = \pi$, $\theta_e = 10°$, $\phi_e = 0$ from Reference 15.

tracting it from the signal. Since the coincidence rate divided by the accidental rate is inversely proportional to the gas beam density and the electron current, the background can be suppressed by lowering these quantities. However, the signal-to-noise ratio is increased as these quantities are increased, up to the point where resonance trapping takes place. Then, bearing in mind that not a great deal of attention has been paid as yet to some of these considerations, the data in helium for λ at 80 eV are presented in Figure 6. The data, for the most part, are in reasonably good agreement below 70°. That includes data from Oklahoma, Sutcliffe *et al.*,[15] Belfast,

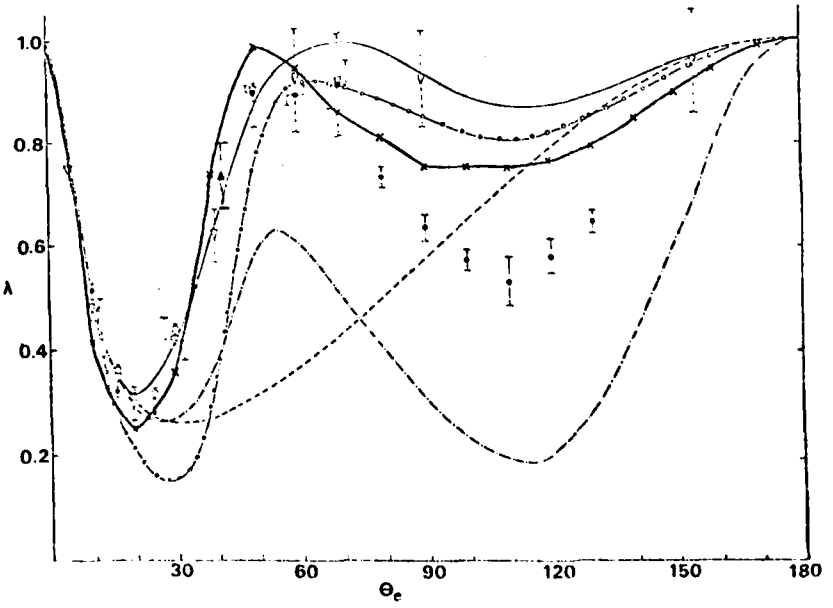

Figure 6. λ vs. θ_e for He($2^1P \rightarrow 1^1S$) at 80 eV. ▽, Sutcliffe *et al.*;[15] ●, Hollywood *et al.*;[17] ○, Eminyan *et al.*;[14] [ ], Ugbabe *et al.*;[18] ▲, Tan *et al.*;[16] ——, Madison and Calhoun;[19] —○—, Thomas *et al.*;[27] – – –, Born calculation; —·—, Baluja and McDowell;[20] —×—, Fon *et al.*[29]

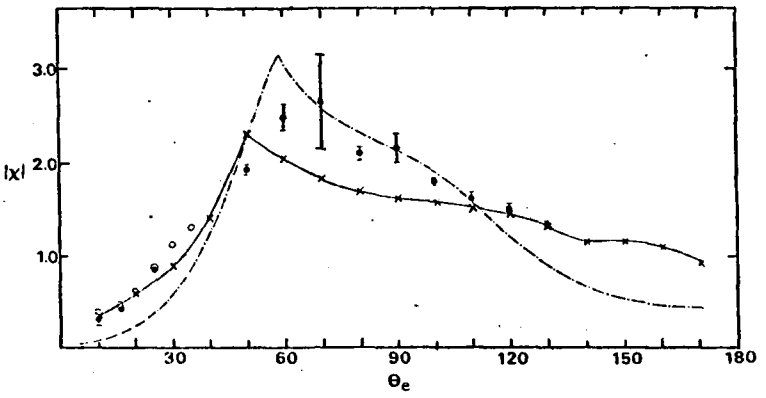

Figure 7. $|\chi|$ vs. θ_e for He($2^1P \rightarrow 1^1S$) at 80 eV. ●, Hollywood *et al.*;[17] ○, Eminyan *et al.*;[14] □, Ugbabe *et al.*;[18] ---·---, Baluja and McDowell;[20] —×—, Fon *et al.*[22]

Hollywood and Williams,[17] Stirling, Eminyan *et al.*,[14] Flinders, Ugbade *et al.*,[18] and Windsor, Tan *et al.*[16] The large-angle data are another story, where on the face of it a considerable difference exists between the Belfast and Oklahoma data. However, the difference only involves the points at 80° and 90° thus far. (Both groups are repeating the measurements.) The distorted-wave calculations of Madison and Calhoun[19] agree with all of the small-angle data and the large-angle data of Sutcliffe *et al.*[15] The other calculations included on the plot are the distorted-wave calculation of Baluja and McDowell,[20] the many-body calculation of Thomas *et al.*,[21] a first Born approximation calculation, and the most recent *R*-matrix calculation of Fon *et al.*[22] The measurements of $|\chi|$ vs. θ_e at 80 eV in He are presented in Figure 7,

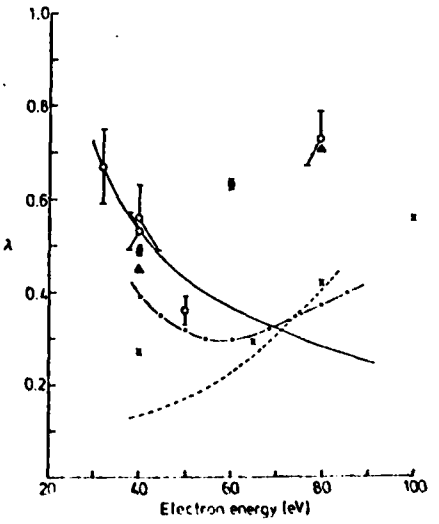

Figure 8. λ vs. electron energy (E) for He($2^1P \rightarrow 1^1S$) for $\theta_e = 42°$. ○, Tan *et al.*;[16] ■, Eminyan *et al.* (40°);[14] ▲, Madison and Shelton;[19] ×, Scott and McDowell;[23] – – –, Thomas *et al.*;[21] ---·---, Flannery and McCann;[24] ——, first Born approximation.

together with the calculations of Baluja and McDowell,[20] and Fon *et al.*[22] Here the agreement is fair between the measurements and both of the calculations.

The variation of λ with electron energy for a fixed electron scattering angle of 42° is presented in Figure 8. As before, the picture is not completely clear as yet. Below 40 or 50 eV, the first Born approximation agrees with the data quite well, while at 80 eV the distorted-wave calculations of Madison and Calhoun[19] agree with the data. In between there is a minimum which is not very well predicted by the remaining calculations of Scott and McDowell,[23] Thomas *et al.*,[21] or Flannery and McCann.[24]

Linear and circular polarization measurements of the $3^1P \rightarrow 2^1S$ photons detected in delayed coincidence with electrons that have excited the 3^1P state of helium have been made by Standage and Kleinpoppen.[25] A schematic diagram of their apparatus is shown in Figure 9. The photons are detected perpendicular to the scattering place. The polarization vector is defined in terms of the intensity component at an angle β with respect to the electron direction

$$\begin{aligned} P_1 &= N_e(\beta=0) - N_e(\beta=\pi/2) \\ P_2 &= N_e(\beta=\pi/4) - N_e(\beta=3\pi/4) \\ P_3 &= N_e(\mathrm{RHC}) - N_e(\mathrm{LHC}) \end{aligned} \tag{15}$$

where RHC and LHC denote left- and right-hand circular polarization. The measurements of the components of the polarization vector, the degree of polarization, and

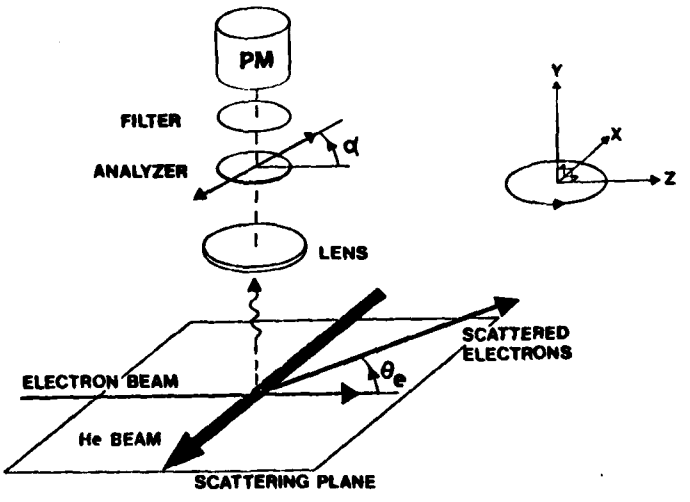

Figure 9. Schematic diagram of the polarization measurement of Reference 25. The X–Z plane is the scattering plane; the photons are detected by the photomultiplier (PM) along the Y axis. Scattering angle θ_e and linear polarizer angle α are measured in the X–Z plane. Positive scattering angle is shown.

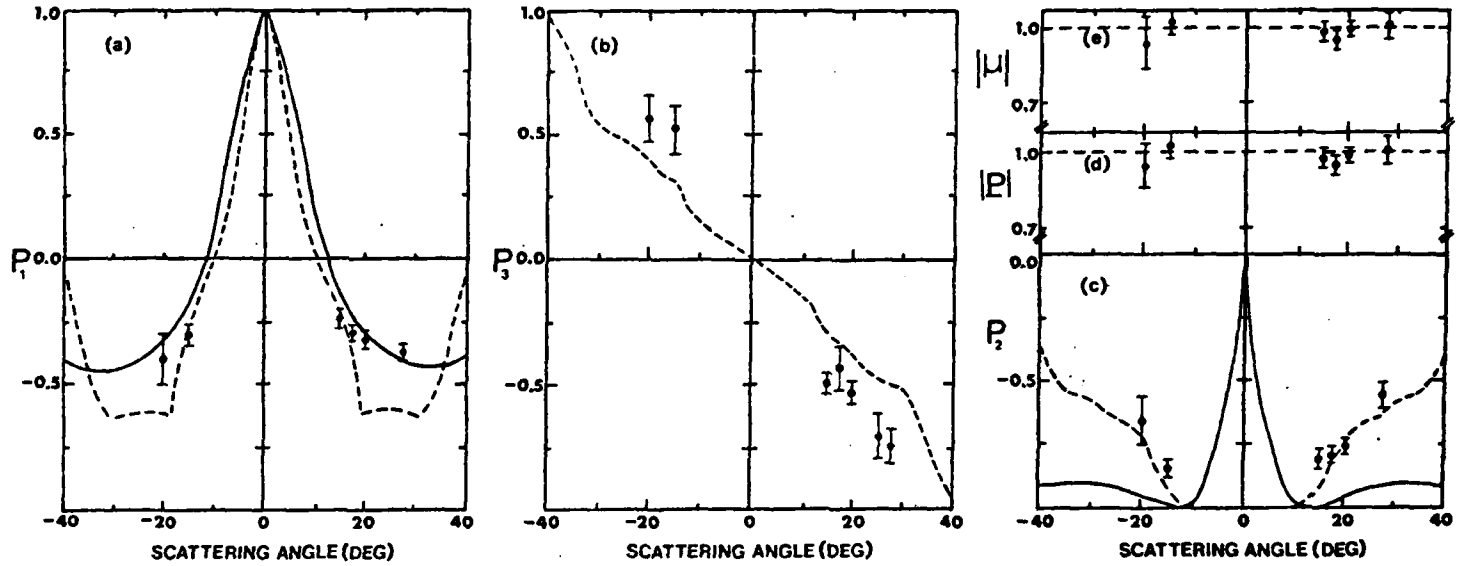

Figure 10. Experimental results of Reference 25. (a)–(c) Experimental data for the vector polarization components P_1, P_3, and P_2 respectively, of He ($3^1P \rightarrow 2^1S$) coincident photons at 80 eV incident electron energy vs. electron scattering angle. ——, first Born approximation; – – –, multichannel eikonal approximation. (d) Degree of polarization. (e) Degree of coherence.

the degree of coherence from the measurements of Standage and Kleinpoppen[25] are shown in Figure 10. These measurements show that the excitation is completely polarized and completely coherent.

ACKNOWLEDGMENT

This work was supported in part by the NSF and the AFOSR.

References

1. S. Bashkin and G. Beauchemin, *Can. J. Phys.* **44**, 1603 (1966).
2. J. Macek, *Phys. Rev. Lett.* **23**, 1 (1969); *Phys. Rev. A* **1**, 618 (1970).
3. M. Eminyan, K. B. MacAdam, J. Slevin, and H. Kleinpoppen, *Phys. Rev. Lett.* **31**, 576 (1973).
4. R. E. Bell, in *Alpha, Beta, and Gamma Ray Spectroscopy*, K. Siegbahn, ed., p. 905, North-Holland, Amsterdam (1966).
5. E. Brannen, F. R. Hunt, R. H. Adlington, and R. W. Nichols, *Nature (London)* **175**, 810 (1955).
6. H. Ehrhardt, M. Schulyz, T. Tekaat, and K. Willmann, *Phys. Rev. Lett.* **2**, 89 (1969).
7. D. E. Golden, D. J. Burns, and V. C. Sutcliffe, *Phys. Rev. A* **10**, 212 (1974).
8. D. J. Burns, D. E. Golden, and D. Galliard, *J. Chem. Phys.* **65**, 266 (1976).
9. A. Pochat, D. Rozuel, and J. Perrose, *J. Phys. (Paris)* **34**, 701 (1973).
10. J. Macek and D. H. Jaecks, *Phys. Rev. A* **4**, 2288 (1971).
11. I. Percival and M. Seaton, *Phil. Trans. R. Soc. London A* **251**, 113 (1958).
12. K. Blum and H. Kleinpoppen, *Phys. Rep.* **52**, 203 (1979).
13. J. Slevin and P. S. Farago, *J. Phys. B* **8**, 1407 (1975).
14. M. Eminyan, K. B. MacAdam, J. Slevin, and H. Kleinpoppen, *J. Phys. B* **7**, 1519 (1974).
15. V. C. Sutcliffe, G. N. Haddad, N. C. Steph, and D. E. Golden, *Phys. Rev. A* **17**, 100 (1978).
16. K. H. Tan, J. Fryar, P. S. Farago, and J. W. McConkey, *J. Phys. B* **10**, 1073 (1977).
17. M. T. Hollywood, A. Crowe, and J. F. Williams, *J. Phys. B* **12**, 819 (1979).
18. A. Ugbabe, P. J. O. Teubner, E. Weingold, and H. Arriola, *J. Phys. B* **10**, 71 (1977).
19. D. H. Madison and R. V. Calhoun (unpublished).
20. K. L. Baluja and M. R. C. McDowell, *J. Phys. B* **12**, 835 (1979).
21. L. D. Thomas, G. Csanak, H. S. Taylor, and G. S. Yarlagadda, *J. Phys. B* **10**, 1073 (1977).
22. W. C. Fon, K. A. Berrington, and A. Kingston *J. Phys. B* **12**, L171 (1979).
23. T. Scott and M. R. C. McDowell, *J. Phys. B* **8**, 1851 (1975).
24. M. R. Flannery and K. J. McCann, *Phys. Rev. A* **12**, 846 (1975).
25. M. C. Standage and H. Kleinpoppen, *Phys. Rev. Lett.* **36**, 577 (1976).

J. Phys. B: Atom. Molec. Phys., Vol. 12, No. 9, 1979. Printed in Great Britain

Analysis of low-energy scattering cross sections I. Electron–helium elastic scattering†

N C Steph, L McDonald and D E Golden

Department of Physics and Astronomy, University of Oklahoma, Norman, Oklahoma 73019, USA

Received 25 April 1978, in final form 20 November 1978

Abstract. The e^-–He differential scattering cross section measurements for selected energies between 2 and 19 eV have been re-analysed to obtain phaseshifts and associated errors which are consistent with the measurements. The phaseshifts obtained from different angular distribution measurements are shown to be consistent with each other within their associated errors and are also consistent with the best available phaseshifts determined by theory. These phaseshifts have also been used to determine total and momentum transfer cross sections which are compared with direct determinations of these quantities. The re-analysis of the differential cross section measurements does not reduce the uncertainty which presently exists in the total cross section at lower energies. It is suggested that the uncertainty, which is as large as 20% at the lower energies, can be reduced by more precise measurements and analysis of the ^2S resonance profile at 19·35 eV coupled with precise relative measurements and analysis at other energies and/or accurate cross section calculations which include an *ab initio* error determination.

1. Introduction

It would be very useful if some easily measurable electron scattering cross section were accurately known so that it could be used as a standard against which all other cross section measurements could be calibrated. The elastic e^-–He scattering cross section should, in principle, provide such a case. Helium is a gas at room temperature possessing no low-lying levels and thus low-energy ($\lesssim$19 eV) elastic cross sections are, in principle, easily measurable. It is also the simplest two-electron target and so elastic e^-–He cross sections are, in principle, also easily calculable. The experimental and theoretical results prior to 1969 have been discussed in detail by Massey and Burhop (1969) and thus are only briefly summarised here.

The problem of e^-–H scattering is the simplest case to treat theoretically. In this case the wavefunctions of the target states are completely known, so that one may find the phaseshifts for the scattering problem theoretically to any degree of accuracy required (see Schwartz 1961). In the case of more complicated targets, the degree of accuracy to which the phaseshifts may be calculated has not yet been established. In general, if one has the exact target ground-state wavefunction, one can obtain a lower bound on the phaseshifts in the case of elastic scattering (see Burke and Robb 1975).

† Partially supported by grants from NSF and AFOSR.

0022-3700/79/091507+21$01.00

However in the case of e^-–He elastic scattering we are dealing with a three-electron problem which precludes the use of exact atomic wavefunctions in the calculations. Thus, one is left with the question of how close to a lower bound are the phaseshifts obtained using non-exact target wavefunctions.

The best calculations available for elastic e^-–He scattering at the present time appear to be the polarised-orbital calculations of Duxler *et al* (1971), the variational calculations of Sinfailam and Nesbet (1972) and Wichmann and Heiss (1974), the many-body calculations of Yarlagadda *et al* (1973) (at the higher energies), and the recent *R*-matrix calculation of Berrington *et al* (1978). The S-wave phaseshifts from all of these calculations agree to within about 2 or 3% while the P-wave phaseshifts generally agree to within 10 to 15% (within their range of validity). The higher order phaseshifts may be approximated with sufficient accuracy by the Born approximation. However, even if we take the differences in the theoretically obtained S- and P-wave phaseshifts as their range of reliability, it is insufficient to be able to predict elastic scattering cross sections to within a few per cent. The variational calculations can probably be used to do a meaningful error analysis. However, until an *ab initio* error analysis is performed, the value of further e^-–He scattering calculations is uncertain. We therefore turn our attention to the reliability of e^-–He cross section measurements.

Absolute total e^-–He scattering cross section measurements were first obtained by Ramsauer (1921). Additional absolute total cross section measurements were obtained by Normand (1930) and Ramsauer and Kollath (1929, 1931, 1932). The measurements of Ramsauer and Kollath (1932) are of the order of 20% larger than the measurements of Normand (1930). Furthermore no error bars were given in these or other early measurements. The first absolute total cross section measurements which included an error analysis were made by Golden and Bandel (1965) for energies from 0·3 to 28 eV. The principal limitation of these measurements was the absolute measurement of pressure, and the measurements were stated to have a probable error of ±3% with a maximum error of ±7%. The results of Golden and Bandel (1965) are about 20% lower than the results of Ramsauer (1921) and 8–10% lower than the results of Ramsauer and Kollath (1932). Momentum transfer cross section determinations were put on an absolute basis by Frost and Phelps (1964) and Crompton *et al* (1967, 1970). These latter measurements were extended to higher energies by Milloy and Crompton (1977). The determinations of Crompton *et al* (1967, 1970) and Milloy and Crompton (1977) which have maximum error bars of ±2% from 0·008 to 3·0 eV, ±3% from 3·0 to 7·0 eV and ±5% from 7·0 to 12 eV are the most precise.

Effective-range theory as given by O'Malley *et al* (1962) and O'Malley (1963) was used by Golden (1966) to fit the data of Golden and Bandel (1965) from 0·3 to 2 eV. This fitting procedure allowed comparison with the momentum transfer cross section determinations of Crompton and Jory (1965) and showed that agreement could only be established to about 10% between the two different kinds of measurement. More recently the same conclusion was reached by Bederson and Kieffer (1971) and Milloy and Crompton (1977). These latter authors used the momentum transfer cross section measurements of Crompton *et al* (1967, 1970) and the form of the differential cross section calculations of Sinfailam and Nesbet (1972) to determine total cross sections. In this latter case, the maximum error bars of the two kinds of experiment were estimated to overlap in the range of 4 to 12 eV.

Differential scattering cross section measurements were made early on by Bullard and Massey (1931) and Ramsauer and Kollath (1932), although no error analysis was included in either measurement. More recently, absolute differential cross section

measurements were obtained by Gibson and Dolder (1969b), McConkey and Preston (1975), Andrick and Bitsch (1975) and Williams (1978).

A phaseshift analysis of the experimental data in He consistent with the forward dispersion relation has been performed and discussed by a number of authors including Gerjuoy and Krall (1960, 1962), Bransden and McDowell (1969), Naccache and McDowell (1974) and Bransden and Hutt (1975). While it is well known that the forward dispersion relation holds for a variety of potential scattering problems, it has not been proved in general. It had generally been assumed (see Gerjuoy 1958) that if the many-body Green's function has reasonable analytic properties, the forward dispersion relation would hold for electron–atom scattering. More recently it has become clear (Byron *et al* 1975, Blum and Burke 1976, Hutt *et al* 1976) that the forward dispersion relation does not hold, in general, for electron–atom scattering. Specifically, it does not hold in the e^-–He case.

Because of this development, greater emphasis must be placed on an accurate experimental determination of the first several phaseshifts. This can be done by making absolute differential cross section measurements and then performing a phaseshift analysis of the measurements. In this case, the absolute measurement of a number of quantities such as target density, overlap integrals, etc is required. Alternatively, in the proper energy domain, the structure of the angular distribution can be sufficiently well defined so that relative differential cross section measurements may be placed on an absolute scale solely by a phaseshift analysis. Finally, the fitting of a resonance in a particular partial wave of a particular reaction channel to a Breit–Wigner analytic form leads to a determination of the non-resonant part of the phaseshift of that particular partial wave in that particular reaction channel at the resonance energy. Since the structure of a resonance is, in general, better defined than the structure of the differential cross section, one might reasonably expect this latter method to produce a more accurate determination of the first several phaseshifts than a partial-wave analysis where there are no resonances.

The first analysis of the angular distribution at a resonance in elastic scattering is due to Andrick and Ehrhardt (1966) who showed that the resonance in e^-–He scattering at about 19·35 eV is an S-wave resonance. Later, an angular distribution measurement and phaseshift analysis of this resonance profile, using three partial waves, was performed by Gibson and Dolder (1969a). This analysis produced a derived total cross section in very good agreement with the direct measurement of Golden and Bandel (1965). A similar procedure was used by McConkey and Preston (1975). In this latter case, the phaseshifts for $l > 2$ obtained from the calculations of LaBahn and Callaway (1970) were included. The total cross section derived from this analysis is also in good agreement with the direct result of Golden and Bandel (1965). A third measurement and phaseshift analysis of this resonance by Williams and Willis (1975) was obtained using the Born approximation for the $3 \leq l \leq 10$ phaseshifts. Their result gives a total cross section which is approximately midway between the total cross section given by Golden and Bandel and that given by Ramsauer and Kollath (1932).

Angular distribution measurements and a phaseshift analysis using the sum of all the Born scattering amplitudes for $l > 2$ were performed by Andrick and Bitsch (1975) for energies below the 19·35 eV resonance. This procedure resulted in a total elastic scattering cross section at 19 eV in agreement with the direct measurement of Ramsauer (1921). The non-resonant angular distribution measurements of Gibson and Dolder (1969b) and McConkey and Preston (1975) are substantially lower than those of Andrick and Bitsch (1975) in the forward direction and therefore yield smaller

derived total cross sections. The recent angular distribution measurements of Williams (1978) are in agreement with the measurements of Andrick and Bitsch (1975) and McConkey and Preston (1975) within their combined error limits.

Recently, three additional low-energy absolute total e^-–He scattering cross section measurements have become available. An axial magnetic field transmission technique has been used by Stein *et al* (1978), a modified Ramsauer technique has been used by Bullis (1977), and a time-of-flight technique has been used by Kennerly and Bonham (1977). The measurements of Stein *et al* (1978) cover the range of 1·5 to 30 eV and are about 12% higher than Golden and Bandel (1965) although no error analysis of these results has been given. The measurements of Bullis cover the range of 0·05 to 3·0 eV and are a maximum of about 5% lower than the measurements of Golden and Bandel (1965). Within the stated errors, these two results are in very good agreement with each other. However the measurements of Kennerly and Bonham (1977), which have a stated maximum error of ±3% from 1 to 50 eV, are in general about 10 to 15% higher than those of Golden and Bandel (1965) and consequently 15 to 20% higher than those of Bullis (1977). Thus, it is fair to say that while more experimental measurements are now available, the situation is slightly worse than that in 1971 which led Bederson and Kieffer (1971) to conclude in their review that the total elastic cross section for e^-–He was known to about ±10%.

A comparison between total and momentum transfer cross sections requires a precise knowledge of relative differential cross sections. However, absolute differential cross section measurements provide an independent determination of both the total and momentum transfer cross sections to compare with direct measurements. In light of the present situation it is therefore important to investigate in more detail the measurements and analysis of differential elastic scattering cross sections. The questions to be addressed are: what is the present state of the art and how well can one hope to measure the elastic differential scattering cross section?

2. Experimental considerations in angular distribution measurements

In this section we will discuss two techniques which have been used to make elastic differential scattering cross section measurements. Both of the techniques have been used to study the angular distribution of scattered electrons and will be referred to as electron-beam–gas-cell and crossed electron-beam–gas-beam experiments. A third technique is the atomic-beam recoil technique which has been used to study the scattered atoms (see Collins *et al* 1971). This technique has not been used as yet to obtain accurate angular distributions and will not be discussed here. For a previous discussion of some of the points of this section, the reader is referred to the review articles of Andrick (1973) and Golden (1978) and the work of Williams and Willis (1975).

If the incident electron beam can be considered narrow then the scattered-electron count rate, $\dot{N}_e$, in both the electron-beam–gas-cell and crossed electron-beam–gas-beam experiments can be represented by (see Sutcliffe *et al* 1978),

$$\dot{N}_e = \frac{I_e}{e}\rho_0 \epsilon_e \sigma(E, \theta) J_e(\theta) + \dot{n}_e \tag{1}$$

where I_e/e is the number of incident electrons per second in the electron beam, ρ_0 is the

background gas density which is assumed to be composed of the same species as the target gas, ϵ_e is the efficiency of the electron detector, $\sigma(E, \theta)$ is the differential elastic scattering cross section at energy E and electron scattering angle θ, $\dot{n}_e$ is the count rate due to electronic noise, and

$$J_e(\theta) = \int_{\Delta\Omega} \int_{l_e} \frac{\rho(z)}{\rho_0} \, d\Omega \, dz \tag{2}$$

where $\rho(z)$ is the density of target particles which may be spatially dependent, $d\Omega$ is the solid angle viewed by the electron detector, dz is the element of path length of the electron beam through the interaction region viewed by the electron detector, and l_e is the length over which dz is integrated. In the usual case $\dot{n}_e$ can be made sufficiently small so that it can be neglected. It has been assumed in equation (1) that the variation of $\sigma(E, \theta)$ with E over the energy distribution in the incident electron beam is sufficiently small that averaging over the energy distribution is unnecessary. This is the usual case. It has also been assumed that the half-angle viewed by the electron detector, α, is small compared to the electron scattering angle. This is not necessarily the case, and if this condition is not satisfied, $\sigma(E, \theta)$ needs to be averaged over the angular detection function of the scattered-electron detector. In addition if the angular divergence of the incident electron beam is not small, $\sigma(E, \theta)$ must be averaged over the angular distribution of the incident electron beam. If these averages are not performed one may introduce systematic errors into the measured angular distribution. In order to determine the extent of both of these sources of systematic error it is necessary to measure the angular divergence of the incident electron beam and the acceptance profile of the scattered-electron detector. If one studies the angular divergence of the incident electron beam with the scattered-electron detector, in general, one measures the folding together of the two desired angular functions. However, these two functions may be unfolded, as was described by Hertel and Ross (1969) or Sutcliffe *et al* (1978). This involves moving the scattered-electron detector through the unscattered electron beam, when it has a geometrically defined acceptance profile, to define the electron beam profile. Once the electron beam profile has been determined, the measurements may be repeated with the proper voltages on the lens elements of the scattered-electron detector to determine the acceptance profile of the scattered-electron detector. It was found in the work of Sutcliffe *et al* (1978) that the electron beam angular profile was sometimes subject to instabilities so that the measurement of this profile was a necessary consistency check before and after every scattering measurement. These authors also found that tuning the electron gun for maximum electron beam current to the Faraday cup did not insure that the electron beam profile had a narrow angular divergence. In fact, it resulted in an angular profile which had a half-width of 15°. It was therefore necessary to set the voltages of the output lenses of the electron gun to insure that the electron beam profile was of acceptable divergence. Furthermore, it is also important to collect the scattered incident electron beam. That is, a Faraday cup must be included which has a sufficiently large acceptance angle and an efficient means of collecting the incident electron beam. Since low-energy electrons are not collected efficiently on metal surfaces, this condition is not always easy to satisfy. If the incident beam is not collected efficiently, the electron flux in the interaction region may be higher than has been accounted for by the beam current leaving the electron gun. This can lead to significant errors in the measurement of angular distributions. In fact this may introduce a systematic error which has an angular dependence.

Absolute differential cross sections may be obtained from angular distribution measurements by using equations (1) and (2). This requires measurement of the ratio $\dot{N}_e/(I_e/e)$ and absolute measurement of ρ_0, ϵ_e and J_e.

In the case of electron-beam–gas-cell experiments, the gas density in the interaction region has no spatial dependence and the integral J_e given by equation (2) becomes

$$L_e = \int_{\Delta\Omega_e} \int_{l_e} d\Omega \, dz. \tag{3}$$

For $\alpha \ll \theta$, and a very narrow stable electron beam

$$L_e(\theta) = \frac{L_e(90°)}{\sin\theta}. \tag{4}$$

In order to apply equations (1), (3) and (4) to the data one has to take care to insure that the electrons in the interaction region do not undergo multiple collisions. This is simply done by showing that the scattered intensity is proportional to the interaction region density. If the target gas is contained in the interaction region and the scattered electrons leave the interaction region through a hole, one has to take great care to insure that scattered electrons from angles other than that being studied cannot bounce off the interaction region walls and into the scattered-electron detector. In fact, this kind of effect can also introduce a systematic error which has an angular dependence.

In the case of crossed electron-beam–gas-beam experiments, equations (1) and (2) are used. The correction for the variation in path length through the background gas may be made by using a subtraction technique (see Andrick and Bitsch 1975). The procedure used is to turn the target gas beam off and flood the chamber to the same background pressure with the gas beam off as existed with the gas beam on. When the target gas beam is off, we call the electron count rate $\dot{N}'_e$. Then

$$\dot{N}'_e = \frac{I_e}{e} \rho_0 \epsilon_e \sigma(E, \theta) L_e. \tag{5}$$

If the target beam is sharply defined, we may write

$$\frac{\rho(z)}{\rho_0} = \frac{\rho_J(z)}{\rho_0} + 1 \tag{6}$$

where $\rho_J(z)$ is the target density in the target gas beam. Then,

$$\dot{N}_e - \dot{N}'_e = \frac{I_e}{e} \rho_0 \epsilon_e \frac{d\sigma}{d\Omega} \Delta\Omega \int_{l_J} \frac{\rho_J(z)}{\rho_0} dz \tag{7}$$

where it has been assumed that the spatial extent of the gas beam l_J is sufficiently small that the integration over $d\Omega$ just yields the solid angle of the scattered electron detector, $\Delta\Omega$. If $\rho_J(z)/\rho_0$ or

$$\int_{l_J} \frac{\rho_J(z)}{\rho_0} dz$$

is measured, then equation (7) can be used to measure $\sigma(E, \theta)$. In fact since

$$\int_{l_J} \frac{\rho_J(z)}{\rho_0} dz$$

is independent of θ, the measurement of relative values of $\dot{N}_e - \dot{N}'_e$ as a function of θ at

constant E yields relative values of $\sigma(E, \theta)$. This is the procedure used by Andrick and Bitsch (1975) to measure $\sigma(E, \theta)$ at each energy studied. It should be noted that corrections for double scattering events in which the first scattering takes place in the interaction region and the second takes place in the background gas, or vice versa are not accounted for by the subtraction technique. Furthermore, as the signal $\dot{N}_e'(\theta)$ becomes comparable to $\dot{N}_e(\theta)$ the time required to achieve a good signal-to-noise ratio becomes increasingly long. Therefore attention should be given to the problem of making the ratio of gas density in the beam large compared to the background gas density. This is especially important if one is going to study scattering angles close to either 0° or 180°.

An assumption inherent in equation (7) is that the electron beam is of uniform density and of the same spatial extent as the gas beam. Equation (7) may still be usable for relative measurements if this is not true. For example, if the electron beam is larger in spatial extent than the gas beam and uniform over the spatial extent of the gas beam which is itself not uniform, this type of equation is still valid. In fact, in this case, spatial fluctuations of the electron beam which are small compared to the spatial extent of the gas beam do not contribute a significant error to the measurement. Suppose, however, that the electron beam is smaller in spatial extent than the gas beam. If the electron beam is uniform in spatial extent, while the gas beam is not, equation (7) will be valid if the electron beam is stable. However if $\rho_J(z)$ is a rapidly varying function of z, small fluctuations in the position of the electron beam can lead to large fluctuations in the measured angular distributions. Such fluctuations can be caused by small instabilities in the electron gun, or by small stable residual magnetic fields in the interaction region which cause the relative position of the electron beam in the gas beam to change as a function of time or electron scattering angle. This may be the case if the electron scattering angle is varied by rotating the electron gun relative to the scattered-electron detector. The latter effect gives a systematic error which has an angular dependence.

3. Phaseshift analysis of angular distribution measurements

Differential cross sections for elastic e⁻–He scattering may be analysed by the method of partial waves. In this procedure, the scattering amplitude $f(\theta, k)$ is represented by the sum

$$f(\theta, k) = \frac{1}{2ik} \sum_{l=0}^{\infty} (2l+1)[\exp(2i\eta_l(k)) - 1]P_l(\cos\theta) \tag{8}$$

where θ is the electron scattering angle, k is the wavenumber of the incident electron, $P_l(\cos\theta)$ is the lth Legendre polynomial, and $\eta_l(k)$, the phaseshift for elastic scattering of the lth partial wave at energy $E = k^2$, is real. If the $\eta_l(k)$ are known, the differential cross section $\sigma(\theta, k)$, the total cross section $\sigma_T(k)$ and the momentum transfer cross section $\sigma_{MT}(k)$ are all determined from $|f(\theta, k)|^2$

$$\sigma(\theta, k) = |f(\theta, k)|^2 \tag{9}$$

$$\sigma_T(k) = 2\pi \int_0^{\pi} \sigma(\theta, k) \sin\theta \, d\theta \tag{10a}$$

$$= \frac{4\pi}{k^2} \sum_{l=0}^{\infty} (2l+1) \sin^2 \eta_l \tag{10b}$$

$$\sigma_{MT}(k) = 2\pi \int_0^{\pi} \sigma(\theta, k)(1-\cos\theta)\sin\theta \, d\theta \tag{11a}$$

$$= \frac{4\pi}{k^2} \sum_{l=0}^{\infty} (l+1)\sin^2(\eta_l - \eta_{l+1}). \tag{11b}$$

If absolute measurements of $\sigma(\theta, k)$ at fixed E could be made for the full angular range from 0 to π at sufficiently small angular intervals, equations (10*a*) and (11*a*) could be integrated numerically to obtain σ_T and σ_{MT}. In such a case a phaseshift analysis of the data using equations (10*b*) and (11*b*) would serve as a validity check and the set of phaseshifts which reproduce the helium data should have the following properties. The S-wave phaseshift should be π at $E = 0$ and should decrease smoothiy as E increases. All other phaseshifts should be 0 for $E = 0$ and should increase smoothly as E increases (see Massey and Burhop 1969). If the data are not measured over the complete angular range, a phaseshift analysis eliminates the errors associated with extrapolating the data to 0 and π.

For low-energy electron–atom scattering, the first few partial waves dominate. However, the higher order waves cannot be neglected because they also can affect the shape of the calculated differential cross section.

The phaseshifts for $l \geq 1$ may be obtained from the Born approximation for electron scattering from a polarisable system of polarisibility α,

$$\eta_l(l \geq 1) = \frac{\pi\alpha k^2}{(2l-1)(2l+1)(2l+3)}. \tag{12}$$

The values of η_l calculated from equation (12) may be inaccurate for small values of l, but the accuracy improves as l increases. Moreover, the contribution to the scattering amplitude decreases as l increases. Thus one may treat the first several values of $\eta_l(l \leq L)$ as variable parameters in a fitting procedure, and derive the higher order values of $\eta_l(L < l < L')$ from equation (12) to fit equation (8) to the data. However, as many as 50 terms may be necessary to describe the scattering at small angles and the value of L' necessary is energy dependent. A more satisfactory method is to sum all of the Born scattering amplitudes for $l > L$ analytically. It has been shown by Thompson (1966) that this can be done provided the $l = 0$ term is excluded. Then the difference between the Born sum f_B and the contribution from the $l = 0$ term f_B^0 is given by

$$f_B - f_B^0 = \pi\alpha k(\tfrac{1}{3} - \tfrac{1}{2}\sin\tfrac{1}{2}\theta). \tag{13}$$

The procedure used by Andrick and Bitsch (1975) was to subtract all terms for $l \leq L$ from equation (13). Then the scattering amplitude for $L < l < \infty$, f_B^l is given by

$$f_B^l = \pi\alpha k\left(\tfrac{1}{3} - \tfrac{1}{2}\sin\tfrac{1}{2}\theta - \sum_{l=1}^{L} \frac{P_l(\cos\theta)}{(2l+3)(2l-1)}\right). \tag{14}$$

This result may be used to rewrite equations (8) and (9) as

$$f(\theta, k) = \frac{1}{2ik}\left(\sum_{l=0}^{L} (2l+1)[\exp(2i\eta_l) - 1]P_l + 2ikf_B^L\right) \tag{15}$$

$$\sigma(\theta, k) = \frac{1}{4k^2}\left[\left(\sum_{l=0}^{L} (2l+1)\sin 2\eta_l P_l + 2kf_B^L\right)^2 + \left(\sum_{l=0}^{L} (2l+1)(\cos 2\eta_l - 1)P_l\right)^2\right]. \tag{16}$$

It is desirable to make L as small as possible so that the time necessary to perform the

fitting may be kept to a minimum. To find a reasonable value for L, let us consider the centrifugal barrier term for the lth partial wave, $l(l+1)/r^2$. The distance of closest approach of the lth partial wave of an incident electron of energy k^2 in the absence of a scattering potential should be r_l, where $r_l = [l(l+1)]^{1/2}/k$ is the point where the kinetic energy is equal to the centrifugal barrier potential. If the point r_l is 'outside' the atom, then the lth partial wave does not penetrate the atom. That is, it is unaffected by the nuclear potential and 'sees' only the long-range dipole potential due to the polarisation of the target. Since r_l varies inversely with k, it is sufficient to consider 19·6 eV electrons as we will treat no higher energies. A 19·6 eV electron has $k = 1{\cdot}2$ Bohr^{-1}, so that $r_1 = 1{\cdot}18$, $r_2 = 2{\cdot}04$, and $r_3 = 2{\cdot}89$. These numbers are approximate in that they were obtained by setting the potential equal to zero. The presence of the potential will decrease them. Calculations by Boyd (1977) give the size of a helium atom as 1·8 Bohr. Therefore, the $l = 3$ partial wave does not penetrate the atom at all and may be handled by the Born approximation. The $l = 2$ partial wave is a borderline case and should be retained as a variable parameter. It should be noted that changing the $l = 3$ or 4 phaseshifts by 20–30% would not significantly affect the results.

Setting $L = 2$, equation (16) may be fitted to the data by starting with a trial set of η_0, η_1 and η_2 and subsequently varying these phaseshifts to determine the combination leading to the best fit. The best fit is defined as the fit which gives a minimum reduced chi square, χ^2, which is defined

$$\chi^2 = \frac{1}{N-P}\sum_{\theta_i}\left(\frac{\sigma_c(\theta_i)-\sigma_m(\theta_i)}{\Delta\sigma_m(\theta_i)}\right)^2 \tag{17}$$

where N is the number of angles measured, σ_c is the calculated cross section, σ_m is the measured cross section, $\Delta\sigma_m$ is the error in measured cross section, P is the number of variable parameters, $P = 3$ in this case, and θ_i is the angle of ith measurement. If the measurements have not already been brought to an absolute scale by some independent procedure, then the phaseshift analysis itself enables relative measurements to be brought to an absolute scale provided certain conditions are satisfied. It can be seen that equation (16) yields a curve which is an interference pattern of Legendre polynomials weighted by the terms containing the variable parameters. At energies above about 5 eV this interference produces a curve of pronounced structure. Provided the errors are small enough so that the structure is clearly defined, the measurements may be brought to an absolute scale by introducing an additional parameter κ which multiplies the angular distribution measurements. This is done to insure that there is not only agreement between the measured and calculated angular distributions but also between their absolute magnitudes. This may be done by altering equation (17) to

$$\chi^2 = \frac{1}{N-P}\sum_{\theta_i}\left(\frac{\kappa^{-1}\sigma_c(\theta_i)-\sigma_m(\theta_i)}{\Delta\sigma_m(\theta_i)}\right)^2 \tag{18}$$

where the parameter κ is used to bring the relative measurements to an absolute scale, and now $P = 4$. As the energy is decreased, for energies below 5 eV, the η_0 term begins to dominate and the cross section becomes nearly linear with angle and finally uniform. Thus, as the energy decreases, the structure in the curve is insufficient to uniquely determine the phaseshifts or the value of κ. The procedure therefore breaks down since the curve is equally well represented by a wide range of the parameters. In particular the parameter κ is subject to an uncertainty which must be included in the error

analysis. This type of analysis was introduced by Andrick and Bitsch (1975) but they did not explicitly include an uncertainty in κ. This point is discussed further in § 5.

An alternative method of analysis is based on measurement of the cross section at fixed angles as a function of energy over a resonance. Such a resonance exists in e^-–He scattering at 19·35 eV. One can analyse this S-wave resonance structure using a Breit–Wigner formula for the resonant part of the S-wave phaseshift without introducing the parameter κ. We write the S-wave phaseshift as

$$\eta_0 = \eta_0^0 + \eta_0^r \tag{19}$$

$$\eta_0^r = -\tan^{-1}\left(\frac{\frac{1}{2}\Gamma}{E - E_r}\right) \tag{20}$$

where η_0^0 is the background S-wave phaseshift, E_r is the resonance energy, and Γ the natural width of the resonance. The expression for η_0 given by equation (19) may be substituted into equation (16) and values of the cross section calculated as a function of energy for fixed angle. Since the value of Γ is not precisely known it may be used as a parameter to be optimised in the fitting procedure. Before these calculated values may be compared to a measurement, it is necessary to account for the broadening of the measured width by instrumental effects (see Gibson and Dolder 1969a or Andrick 1973). If the variations of the phaseshifts η_0^0, η_1 and η_2 over the energy range of the resonance are negligible, equation (16) may be fitted to the data as a function of energy to find the best values for η_0^0, η_1 and η_2 in the region of the resonance. Such a determination may then be compared to values obtained by fitting to angular distribution measurements at energies below but near the resonance energy. Also, such resonance measurements may form the basis for the normalisation of raw data which has not been corrected for variations in scattered intensity due to variations in scattering volume or any other energy and time independent variations (see discussion of the results of Gibson and Dolder 1969a in § 5).

4. Error analysis

In order to make a meaningful comparison between the best values of η_0, η_1 and η_2 obtained from analyses of relative differential cross section measurements with the values obtained by other methods, it is necessary to determine the errors in the phaseshifts that arise from the uncertainties in the experimental data. The equation to be used in the present case (equation (16)) is not linear in η_0, η_1 and η_2, and therefore one cannot give an analytic form for the errors in the best values of the fitting parameters (see Bevington 1969). Furthermore, the problem of finding errors for total and momentum transfer cross sections determined from the best values of the phaseshifts is even more complicated, since the errors in the phaseshifts are correlated. It is clear from equations (10*b*) and (11*b*) that changes in η_0 can be offset by changes in η_1 so that σ_T or σ_{MT} remain unchanged. Therefore, the best one can do is choose some well defined justifiable criterion for an acceptable fit to an experimental differential cross section data set which thus defines the errors in η_0, η_1, η_2, κ, σ_T and σ_{MT}.

When the errors are purely statistical, the χ^2 of the best fit, χ^2_{min} should be about 1. Such a χ^2_{min} indicates that the measured and calculated values deviate from each other by one standard deviation, on the average. The probability that a measured point differs from the average of many measurements by less than one standard deviation is

0·68. Since a measured point can be any place in the distribution of points which would be obtained by making many measurements, a common criterion is to accept any fit with $\chi^2 \leq 2\chi^2_{\min}$ (see Bevington 1969). This criterion is roughly equivalent to saying that all of the allowed calculated curves fall within about two standard deviations of the measured points and the errors thus obtained represent a 95% confidence level.

An additional question to be resolved is how to deal with systematic errors. Corrections can be made to the data to compensate for systematic errors where the type and extent of the error is known. If this is not the case, it still may be possible to determine the maximum uncertainty introduced into the measurement by the systematic error. However, in most cases, the uncertainties resulting from systematic errors must be estimated, considered as probable errors, combined with uncertainties from statistical error and treated in the same way as statistical errors. However, it should be noted that unlike statistical errors, systematic errors are not random. In fact, systematic errors affect the measured points in some definite but unknown way as a function of energy and/or angle.

If the shape of the non-resonant angular distribution is being used to normalise the data, this problem is particularly serious. It has been found in this work that a small change in the shape of the angular distribution measurement can result in a very different best value of κ. So a given systematic error may result in an even larger error in the normalisation. If the errors are absolute, all calculated fits which fall within the errors of the points must be accepted equally, but the best fit is undefined. When, as is the usual case, systematic and statistical errors are both present, any criterion is somewhat arbitrary. Andrick and Bitsch (1975) were aware of this problem and chose to find the best fit to their data using statistical errors only. They then added their systematic error, which they considered absolute, to the statistical error and accepted any fit with no more than three points falling outside the combined error bars. However, when large systematic errors are present, finding the best fit using statistical error only may lead one to attach undue importance to the best fit and also to underestimate the errors in the phaseshifts. Furthermore, there is no *a priori* way to determine the correlations between the errors in the phaseshifts and this is necessary in order to calculate the errors in σ_T and σ_{MT}.

After consideration of all the problems associated with choosing a criterion for error determination, the following procedure was chosen. Statistical and systematic errors were treated equally and therefore all fits to a given data set for which $\chi^2 \leq 2$ were accepted. The accepted fits were generated by varying all phaseshifts for $l \leq L$ and κ and using a grid search technique to determine the set of acceptable curves. The range in each phaseshift contained in the set of accepted fits was taken as the error in that phaseshift and the range in κ contained in the set of accepted fits was taken as the error in κ. It is important to note that if the range of κ is restricted, the errors in the derived phaseshifts may be seriously underestimated. In addition, values of σ_T and σ_{MT} were generated for each accepted fit and the range in σ_T and σ_{MT} contained in the set of accepted fits was taken as the error in these quantities.

5. Results of phaseshift analysis

In this section we review the most recent measurements of the elastic differential cross section and the S-wave resonance at 19·35 eV in helium. The earlier measurements of Bullard and Massey (1931) and Ramsauer and Kollath (1932) are not considered

because of the extreme enhancement of the small-angle scattering data at all energies and because they are given without estimates of the error. The results of Stein *et al* (1978) are not discussed because they were given without error bars.

An electron-beam–gas-cell experiment was performed by Gibson and Dolder (1969b) but a phaseshift analysis of their results is complicated by their normalisation procedure. Their raw data were in the form of ratios of scattered to primary beam currents. In order to relate these raw data to relative differential cross sections experimentally, accurate knowledge of the variations of scattering volume with scattering angle and the electron current within this volume is needed. In addition, to bring the relative measurements to an absolute scale experimentally, the absolute pressure is needed. These authors decided that it would be too difficult to make the necessary measurements with sufficient precision and devised the following alternative method to make their results absolute.

In an earlier paper (Gibson and Dolder 1969a) these authors deduced the first three phaseshifts for scattering at 19·35 eV from measurements of the S-wave resonance profiles. The phaseshifts were obtained from an independent analysis of the S-wave resonance profile at six scattering angles. The average values of the phaseshifts were given without error analysis and were $\eta_0 = 1{\cdot}937$, $\eta_1 = 0{\cdot}297$ and $\eta_2 = 0{\cdot}052$. If we associate a 1% statistical error with the measurements of the resonance profile and accept all fits which deviate from the measured profile by less than two standard deviations, we find the errors in determining the phaseshifts from the fitting to be about ±2%, ±6% and ±22% for η_0, η_1 and η_2, respectively. They assumed that these phaseshifts do not change appreciably between 19·35 and 19·1 eV and that the higher order partial waves do not make significant contributions to the differential cross section at 19·1 eV. Therefore, they calculated the differential cross section using only the first three phaseshifts. At 19·1 eV the ratio of the raw data to the calculated values yields a set of correction factors which they used to normalise the raw data at all energies. It was pointed out by Andrick (1973) that the higher order partial waves do affect the differential cross sections and he renormalised the data of Gibson and Dolder (1969b) at 19·1 eV. We have extended this renormalisation to the rest of their data. While the inclusion of higher order partial waves has a significant effect on the structure of the calculated differential cross section, this effect is much less significant in a resonance profile. The partial waves for $l \geqslant 2$ have a significant effect on the differential cross section at 19·1 eV. However, there are four angles (31, 62, 82 and 137°) where the contribution of the higher order partial waves vanishes, and thus resonance measurements at these angles are more easily analysed. The maximum effect of the higher order partial waves on the differential cross section at 19·1 eV is 4% for the angles studied by Gibson and Dolder (1969a). These small changes in the level of the background do not significantly affect the resonance profile. In order to see the size of this effect one may calculate the resonance profile with and without the inclusion of the higher order partial waves. The two calculated profiles differ by a maximum of about 1%. The data could be re-analysed taking the higher order partial waves into account. However, lacking the original data we have accounted for this effect by considering the statistical error to be 2%, although this may overestimate the actual error. A statistical error of 2% would result in errors of ±4%, ±12% and ±44% for η_0, η_1 and η_2, respectively.

The procedure of Gibson and Dolder (1969a) to account for instrumental broadening was to fold a Gaussian of variable half-width with the calculated profile before comparing it to the measurement. Andrick (1973) argued that the measurement of

Gibson and Dolder (1969a) at 25° reveals an asymmetric energy distribution because the measurement contains a minimum followed by a maximum of equal amplitude, but smaller width. However, if the P-wave resonance structure postulated by Gibson and Dolder (1969a) is in fact real, this could account for the small asymmetry. For a further discussion of this possible P-wave resonance see Golden (1978). Gibson and Dolder (1969b) used the average phaseshifts obtained from an independent analysis of the S-wave resonance profile at six scattering angles, but did not assess the errors of these average phaseshifts or the possible effects of these errors on the normalisation procedure. Their angular distributions for 17·1 and 5·1 eV, corrected for higher order partial waves, are shown in figures 1(*a*) and 1(*b*), respectively. The error bars are those given by Gibson and Dolder (1969b) and the full curves are our best fits to their data. The χ^2_{min} are 2·9 at 17·1 eV and 7·4 at 5·1 eV. It is clear that the errors introduced by the normalisation process must be larger than the errors given.

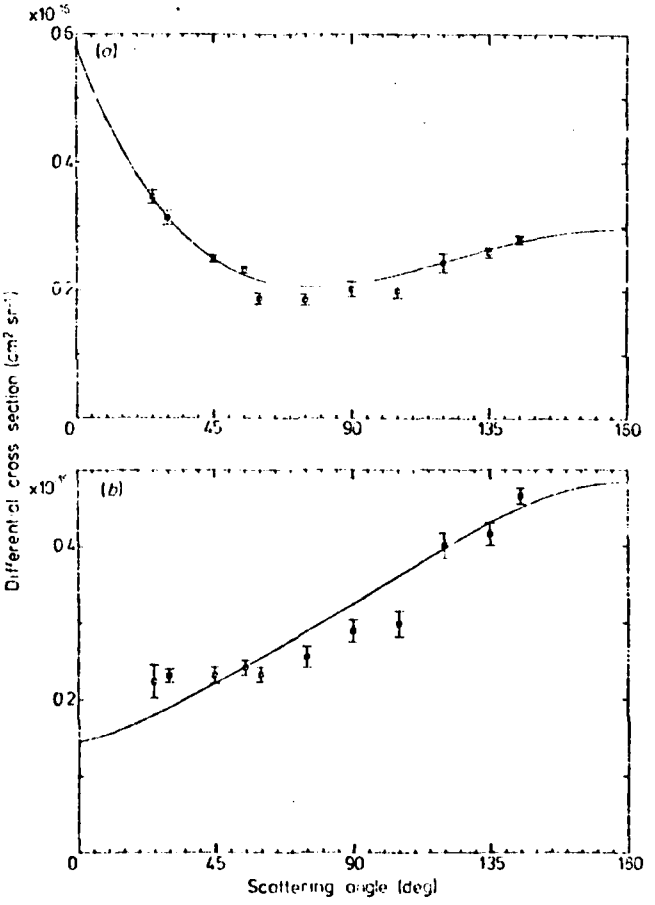

Figure 1. The angular distribution measurements of Gibson and Dolder (1969b) at the energies (*a*) 17·1 eV and (*b*) 5·1 eV. The error bars are those quoted by the authors. Both results have been corrected for the effect of the higher order waves as discussed in § 5. The full curves are the best fits from our analysis.

An electron-beam–gas-cell experiment was also performed by McConkey and Preston (1975). They also analysed the S-wave resonance and used the phaseshifts of LaBahn and Callaway (1970) to account for partial waves up to $l = 50$. Their result for η_0 was 1·972, only 1·8% above the value obtained by Gibson and Dolder (1969a). Their results for η_1 and η_2 were the same as those obtained by Gibson and Dolder (1969a). McConkey and Preston (1975) quote a maximum error of 3% for their current measurement and less than 1% statistical error. If we thus assume a 4% total error for their resonance profile measurements, the errors in η_0, η_1 and η_2 from their resonance profile measurements would be about ±4%, ±12% and ±44%, respectively.

In addition to studying the resonance, McConkey and Preston (1975) also measured the differential cross section for energies between 1·5 and 100 eV. These authors measured the angular distribution of their electron beam, the angular acceptance profile of their analyser, and the pressure in the interaction region. Thus they were able to relate their raw data to absolute differential cross sections experimentally. Their data may be analysed for phaseshifts giving the best fit using the procedure of § 3, with $\kappa = 1$. Our best fit to their data of 19·1 eV has a $\chi^2_{\min} = 0{\cdot}17$, yields phaseshifts of $\eta_0 = 1{\cdot}868 \pm 40\%$, $\eta_1 = 0{\cdot}291 \pm 72\%$, and $\eta_2 = 0{\cdot}052 \pm > 100\%$ and is shown in figure 2 as a full curve together with their data. The best fit has more curvature than the data. In fact a very good fit could also be obtained with $\eta_2 = 0$. This possibly indicates that the data may include an angularly dependent systematic error due to the enclosed interaction region as discussed in § 2. The primary electron beam and the electrons scattered at the angle being studied leave the shielded interaction region through a small hole. At high energies, where small-angle scattering predominates, the electrons scattered through small angles are not removed from the interaction region when larger angles are being studied. These electrons may bounce off the interaction region walls and possibly enhance large-angle scattering. At small energies, large-angle scattering predominates and the situation is reversed. The net effect could be to flatten the angular distribution at all energies. In figure 2 we also show, as a broken curve, the fit predicted by the

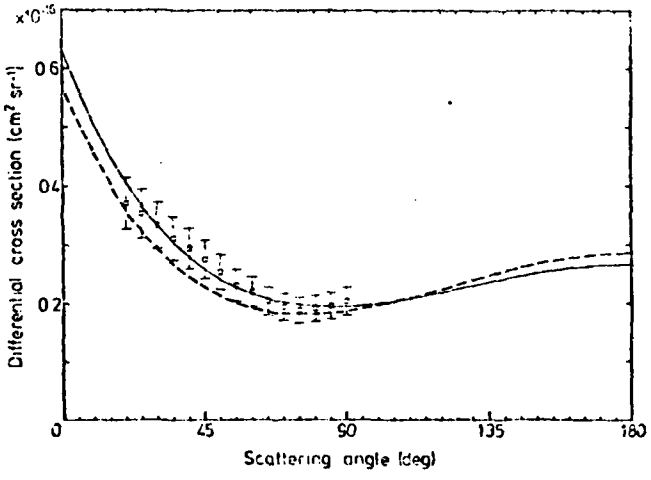

Figure 2. The angular distribution measurement of McConkey and Preston (1975) at 19·1 eV with 12% error bars. The full curve is the best fit from our analysis. The broken curve is the fit predicted by the phaseshifts these authors deduced from their analysis of the S-wave resonance profile. The χ^2 of this fit is 1·3.

phaseshifts McConkey and Preston deduced from their measurements of the S-wave resonance profile. The difference between the broken curve and the data shown is very similar to the possible systematic effect just discussed. It should also be noted that the 12% error for their angular distribution measurements quoted by McConkey and Preston is the root sum of the squares of several very different types of error. A simple sum of these errors is 21% which may be a more accurate assessment of their errors.

These authors chose to put more weight on the values of the phaseshifts obtained by fitting to the shape of the non-resonant angular distribution at 19·1 eV, than those obtained by studying the resonance. However, our analysis indicates that much smaller errors can be obtained from the analysis of a resonance.

Andrick and Bitsch (1975) were the first authors to undertake a complete phaseshift analysis of angular distribution measurements over a wide range of energies. They performed a crossed electron-beam–gas-beam experiment and used the subtraction technique discussed in § 2. They extrapolated these relative cross section data and found the relative total cross section by numerical integration. They then performed a phaseshift analysis of their data using the following method. Each set of phaseshifts considered was given a value of κ defined as the ratio of the cross section predicted from the phaseshifts to the integrated total cross section. The values of κ were used in equation (18) as fixed parameters. This extrapolation and integration is unnecessary and may have hindered their ability to find the best fit. We present some of their data (adjusted for $\kappa = 1$) and their fitting results for 2, 5, 12 and 19 eV in table 1. Their χ^2_{min} were calculated using statistical error only. The precision of their measurements, as given by their statistical error, is sufficient to define the shape of their angular

Table 1. Analysis of the angular distribution data of Andrick and Bitsch (1975). The numbers in parentheses indicate per cent errors determined as discussed in the text.

Energy (eV)	Analysis	χ^2	η_0 (rad)	η_1 (rad)	η_2 (rad)	κ	σ_T (Å^2)	σ_{MT} (Å^2)
2	Andrick and Bitsch	1·58	2·616(5)	0·052(37)		1	6·20(50)	7·20(40)
	Present	1·14	2·517(8)	0·067(52)	0·010(>100)	1·37(52)	8·51(52)	9·88(53)
	Present (η_2 Born)	1·88	2·642	0·049	0·006	0·91	5·68	6·60
5	Andrick and Bitsch	2·99	2·323(2)	0·135(19)		1	5·64(11)	6·64(11)
	Present	1·77	2·338(5)	0·126(40)	0·011(>100)	0·96(27)	5·42(26)	6·41(27)
	Present (η_2 Born)	3·85	2·319	0·138	0·015	1·01	5·70	6·72
12	Andrick and Bitsch	0·81	1·985(3)	0·259(12)		1	4·15(4)	4·28(3)
	Present	1·12	1·993(6)	0·255(22)	0·036(99)	1·00(10)	4·11(8)	4·26(5)
	Present (η_2 Born)	1·13	1·994	0·255	0·037	0·99	4·11	4·26
19	Andrick and Bitsch	1·96	1·814(5)	0·325(12)		1	3·19(4)	2·86(4)
	Present	1·56	1·823(11)	0·325(30)	0·063(56)	1·00(8)	3·20(8)	2·86(9)
	Present (η_2 Born)	2·61	1·826	0·332	0·058	1·01	3·21	2·89

distributions clearly. However, the presence of systematic errors makes the accuracy of this shape questionable. These authors state that there could have been a systematic error due to inhomogeneities in the magnetic field of their apparatus. They estimated this error to be a maximum of 3 to 4% and they used this estimate as described in § 4 to assign errors to η_0, η_1, σ_T and σ_{MT}. However, they included no explicit determination of the error in κ or η_2.

We have re-analysed the data of Andrick and Bitsch (1975) using our method described in § 3 and also give our results in table 1. We considered three additional sources of systematic error. No mention is made in the work of Andrick and Bitsch (1975) of a Faraday cup. If the unscattered electron beam is not collected by a Faraday cup, such electrons can introduce systematic errors as discussed in § 2. However, these systematic errors are difficult to estimate. Another systematic error may be present if the angular spread of the electron beam is large. The measured cross section is actually an average of the 'true' cross section over the angular spread of the beam. If the slope of the 'true' cross section is changing rapidly, as is the case at small angles at 19 eV, this would result in an angularly dependent error. Since Andrick and Bitsch did not measure the angular distribution of their electron beam, the size of this error is difficult to estimate. Their electron beam was sufficiently wide that they considered their 10° data unreliable. If we assume that the beam had a Gaussian distribution of 10° half-width, then the error is such that the measured value would be too large at small angles. The maximum error would be 2% at about 30° and this error would decrease uniformly to zero at about 100°. Another systematic error is possible if the zero of the angular scale is incorrect. As mentioned in § 2 the electron beam which determined this 0° direction can be subjected to instabilities. Therefore a mechanical alignment is not adequate and a direct measurement of the unscattered beam is necessary for accurate determination of 0°. Indeed this measurement should be made often, since instabilities in the electron beam can cause variations of several degrees (see Sutcliffe *et al* 1978). Since the measurement of Andrick and Bitsch at 19 eV is changing by 2% per degree at the small angles, an uncertainty of only 0·5° in the zero of the angular scale would introduce an error of 1% into the measurement.

In the light of these possible additional sources of error, we conclude that the error analysis of Andrick and Bitsch underestimated the errors in η_0, η_1, σ_T and σ_{MT}. We believe it is more reasonable to take the estimated error of 3 to 4% as a probable error. In this case the total probable error is 5%. We then calculate χ^2 using the total probable error and retain any fit with a $\chi^2 \leq 2$. In the course of searching for acceptable sets of phaseshifts, maximum and minimum values of κ are developed at each energy. These extreme values form the basis of the error in κ listed in table 1. Using statistical error only, we are able to find χ^2_{min} which are significantly lower at all energies than those given by Andrick and Bitsch.

At 19 eV our best fit yields a set of values of η_0, η_1, κ, σ_T and σ_{MT} in good agreement with the set obtained by Andrick and Bitsch.

It seems that the values for 12 eV given by Andrick and Bitsch in table 1 do not represent their data. The χ^2 of the fit found by us using the set of phaseshifts given by Andrick and Bitsch at 12 eV is 4·33, while they gave a value of 0·81. We cannot find a set of phaseshifts which yield a fit with $\chi^2 < 1$. The value of σ_1 predicted by our best fit at 12 eV is 4·11 (1% lower than the value given by Andrick and Bitsch).

At the lower energies of 2 and 5 eV our best fits yield results which are different than those of Andrick and Bitsch (1975). In particular, we find values of $\kappa \neq 1$. At 2 eV our best fit yields values of σ_1 and σ_{MT} which are almost certainly too large. This fact and

the very large error in κ show the breakdown of the normalisation procedure at low energies. The values of η_2 predicted by our best fits at 2 and 5 eV are significantly different from the values of η_2 given by the Born approximation. We have analysed the 2, 5, 12 and 19 eV data with η_2 fixed at its Born value in order to investigate the effect of η_2 on the best fit. These results are also presented in table 1 without error analysis. It should be noted in table 1 that our best fit to the data of Andrick and Bitsch (1975) with η_2 fixed at its Born value yields very different values of the fitting parameters at the lower energies than when η_2 is allowed to vary. Furthermore, very different total and momentum transfer cross sections are obtained at the lower energies. Thus the energy dependence of the total or momentum transfer cross section at low energies is not very well defined by analysis of angular distribution measurements. It has been argued by Andrick and Bitsch (1975) that all direct measurements agree regarding the shape of the total cross section. However the most recent measurement of Kennerly and Bonham (1977) does not have the same shape as that of Golden and Bandel (1965). Furthermore, the results of Andrick and Bitsch (1975) do not predict a definite shape at the lower energies.

At all energies, the errors predicted by our analysis are about a factor of two larger than those predicted by Andrick and Bitsch. Since the shape of the angular distribution is so vital to the normalisation process in both the method of Andrick and Bitsch and our own, the effect of unknown systematic errors on the shape of a measurement must not be underestimated. In the absence of experimental checks to determine the size and effect of possible systematic errors, no absolute values of such errors can be determined.

We have discussed four possible sources of systematic error in the experiment of Andrick and Bitsch and we believe that our error analysis gives a more accurate estimate of the errors of their measurements and derived quantities. Andrick and Bitsch also used effective-range theory to analyse their phaseshift results. They fitted the effective-range formulae developed by O'Malley *et al* (1962) and O'Malley (1963) to their derived phaseshifts as a function of energy over the range from 2 to 19 eV and found that such formulae could reproduce their phaseshifts with a $\chi^2 < 0{\cdot}1$. They argued that this small χ^2 implied that the error in their phaseshifts could be substantially reduced. However, it is quite unclear what physical meaning, if any, can be attached to effective-range theory for $l < 2$ for energies much higher than 1 or 2 eV.

Williams and Willis (1975) measured the helium ^{2}S resonance at 19·35 eV in a crossed electron-beam–gas-beam experiment. They deduced the first three phaseshifts by analysis of the resonance profile at various scattering angles using a method similar to that discussed in § 3. They accounted for higher order partial waves up to $l = 10$ by using the values calculated from equation (12). They obtained the values $\eta_0 = 1{\cdot}852 \pm 1\%$, $\eta_1 = 0{\cdot}309 \pm 2{\cdot}6\%$ and $\eta_2 = 0{\cdot}066 \pm 11\%$. These errors are consistent with a $\pm 1\%$ statistical error in the measurement of the resonance profile. In fact $\pm 1\%$ is one standard deviation of the statistical error in the experiment of Williams and Willis (1975). As discussed in § 4, we would use two standard deviations when fitting the data. Therefore, we believe that the error bars on the phaseshifts of Williams and Willis (1975) should be increased by a factor of two. Another analysis of this resonance has been recently made by Williams (1978). He accounted for higher order partial waves up to $l = 19$ by using the values calculated from equation (12) and obtained the values $\eta_0 = 1{\cdot}822 \pm 0{\cdot}5\%$, $\eta_1 = 0{\cdot}31 \pm 1{\cdot}5\%$ and $\eta_2 = 0{\cdot}061 \pm 4{\cdot}0\%$. These error bars represent one standard deviation. We would use two standard deviations when fitting the data so as to achieve errors at the 95% confidence level. Furthermore, unless two standard deviations are used to describe the data of Williams and Willis (1975) and

Williams (1978), the values of η_0 of the two measurements do not agree within their respective errors. Williams (1978) also analysed angular distributions for energies from 0·5 to 20 eV. However, no data for angular distributions were included and we are thus unable to draw any conclusions about his results.

6. Discussion of experimental results and conclusion

In this section we discuss the difference between the various angular distribution measurements in the light of our analyses.

The non-resonant angular distribution measurements of Gibson and Dolder (1969b) are in agreement with those of McConkey and Preston (1975) at all common energies studied. The angular distribution measurements of McConkey and Preston (1975) at 19 eV are compared with those of Andrick and Bitsch (1975) in figure 3. It should be noted that after we have increased the error bars on the measurements of Andrick and Bitsch (1975) to account for the error in the determination of κ, the two sets of error bars overlap for $\theta \geq 25°$. As has been discussed in § 5, the error bars on the measurements of McConkey and Preston (1975) might also be increased. If this were done, the angular distribution measurements of McConkey and Preston and those of Andrick and Bitsch at 19 eV would be in agreement at all angles. Nevertheless, the errors associated with the phaseshifts of either set of measurements at this energy are sufficiently large that the phaseshifts or cross sections derived from them cannot be determined to sufficient accuracy to distinguish between various direct measurements or the various theories. These errors are given in table 2 where we summarise the results of our analyses at 19 eV. The direct total cross section measurements of Golden and Bandel (1965) and Kennerly and Bonham (1977) as well as the calculation of

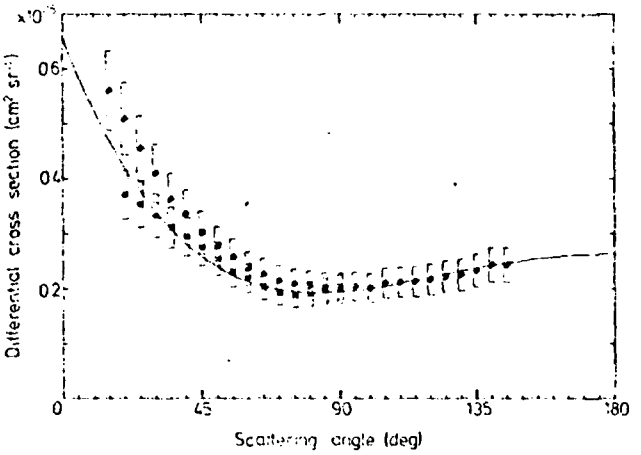

Figure 3. The angular distribution measurements of McConkey and Preston (1975) at 19·1 eV (■), and the angular distribution measurements of Andrick and Bitsch (1975) at 19 eV (◆), with their respective error bars as discussed in the text. The full curve is the differential cross section predicted by the values of η_0, η_1 and η_2 determined by a weighted average of the values obtained by Gibson and Dolder (1969a), McConkey and Preston (1975), Williams and Willis (1975) and Williams (1978). These authors deduced the values of η_0, η_1 and η_2 by fitting to the S-wave resonance as discussed in the text.

Duxler *et al* (1971) are also included. It can be seen from table 2 that the errors in the phaseshifts obtained from the resonance profile measurements are much smaller than those obtained from the non-resonant angular distribution measurements. Therefore we have made an average of the phaseshifts determined from analyses of the resonance profiles given in table 2 weighted by their respective errors. These values are also given in table 2 as our best estimates. The differential cross section predicted by these phaseshifts and f_B^2 is shown in figure 3 as a full curve. This curve calculated from the phaseshifts deduced by analyses of resonance profiles is in excellent agreement with the non-resonant angular distribution measurements for $\theta \geq 55°$. As $\theta \to 0$ this calculated curve tends to predict values roughly midway between the two measurements. This behaviour could be expected on the basis of our previous discussion of the systematic errors of the measurements. It should be noted that all of the values of σ_{MT} determined from all of the angular distribution measurements given in table 2, on or off resonance, are in agreement with each other within 3% while the corresponding values of σ_T only agree to within 14%.

Table 2. Phaseshifts, total and momentum transfer cross sections for e^-–He scattering at 19 eV. The numbers in parentheses indicate per cent errors at the 95% confidence level.

	η_0 (rad)	η_1 (rad)	η_2 (rad)	σ_T (Å)	σ_{MT} (Å)
Experiment					
Fitting to the resonance					
Gibson and Dolder (1969a)	1·937(4)	0·297(12)	0·052(44)	2·87(12)	2·89(5)
McConkey and Preston (1975)	1·972(4)	0·297(12)	0·052(44)	2·81(12)	2·75(5)
Williams and Willis (1975)	1·852(2)	0·309(5)	0·066(22)	3·07(5)	2·82(3)
Williams (1978)	1·822(1)	0·310(3)	0·061(8)	3·12(2)	2·85(1)
Fitting to the angular distribution					
McConkey and Preston (1975)	1·868(40)	0·291(72)	0·052(100)	2·95(40)	2·81(20)
Andrick and Bitsch (1975)	1·823(11)	0·325(30)	0·063(56)	3·20(8)	2·86(9)
Measurement of Total Cross Section					
Golden and Bandel (1965)				2·87(7)	
Kennerly and Bonham (1977)				3·13(3)	
Theory					
Duxler *et al* (1971)	1·811	0·316	0·06	3·16	2·84
Nesbet (1975)	1·831	0·316	0·056	3·13	2·86
Best estimate	1·863(4)	0·307(10)	0·060(34)	3·05(10)	2·83(4)

Below 19 eV, at all common energies studied the non-resonant angular distribution measurements of Gibson and Dolder (1969b), McConkey and Preston (1975) and Andrick and Bitsch (1975) are in agreement with each other within the respective errors which we have associated with the measurements. Values of σ_T or σ_{MT} derived from these non-resonant angular distribution measurements have very large associated errors. Therefore they span all direct measurements and calculations of these quantities and cannot be used to decide which results are to be preferred.

It is quite clear from the present work that in order to establish properly the absolute values of elastic cross sections in e^-–He scattering one must begin with precise measurements of the resonance profile at 19·35 eV. The analysis of resonance measurements does not involve the use of the parameter κ and thus is free of the error

associated with κ. Furthermore, the method of analysis of resonances discussed in § 3 may be used at the angles of 31, 62, 82 and 137° to determine the first three phaseshifts without inclusion of the higher order phaseshifts. Therefore by analysing the resonance at other angles one may check the validity of f_B^2 (equation (14)). While the resonance measurements of Gibson and Dolder (1969a) were made with an energy resolution of about 65 meV, those of Williams and Willis (1975) were made with an energy resolution of 30 meV. However, in neither case does the energy resolution contribute significantly to the errors in η_0, η_1, η_2, σ_T or σ_{MT}. Therefore, if the statistical errors of this kind of measurement can be reduced to 0·05%, the values of η_0, η_1 and η_2 can be determined to about 0·1, 0·3 and 1%, respectively. Then σ_T and σ_{MT} will be established to better than 1%. This is easier to do than to make sufficiently precise measurements of angular distributions at energies where there are no resonances. Following the precise measurement of the resonance profile, relative angular distribution measurements at all energies may be placed on an absolute scale to better than 1% by normalising them to measurements at 19·35 eV and using the procedure discussed in § 3 with $\kappa = 1$. However, it should be cautioned that in making such measurements one needs to pay attention to the considerations discussed in §§ 2–4.

We have given in table 2 best estimates of the values of η_0, η_1 and η_2 at 19 eV based on the available resonance profile measurements. We offer no best estimate for phaseshifts at other energies pending additional measurements.

Acknowledgments

We would like to thank Professor R W Crompton for bringing this problem to our attention and for his advice and suggestions throughout the course of the work. We would also like to thank Professor Stanley Dabb for his help in the analysis of the data.

References

Andrick D 1973 *Adv. Atom. Molec. Phys.* **9** 207–42
Andrick D and Bitsch A 1975 *J. Phys. B: Atom. Molec. Phys.* **8** 393–409
Andrick D and Ehrhardt H 1966 *Z. Phys.* **192** 99–106
Bederson B and Kieffer L J 1971 *Rev. Mod. Phys.* **43** 601–41
Berrington K A, Burke P G and O'Malley T F 1978 unpublished
Bevington P R 1969 *Data Reduction and Error Analysis for the Physical Sciences* (New York: McGraw-Hill)
Blum K and Burke P G 1975 *J. Phys. B: Atom. Molec. Phys.* **8** L410–3
Boyd R J 1977 *J. Phys. B: Atom. Molec. Phys.* **10** 2283–91
Bransden B H and Hutt P K 1975 *J. Phys. B: Atom. Molec. Phys.* **8** 603–11
Bransden B H and McDowell M R C 1969 *J. Phys. B: Atom. Molec. Phys.* **2** 1187–201
Bullard E C and Massey H S W 1931 *Proc. R. Soc.* A **133** 637–51
Bullis R 1977 *PhD Thesis* University of Connecticut
Burke P G and Robb W D 1975 *Adv. Atom. Molec. Phys.* **11** 144–214
Byron F W, de Heer F J and Joachain C H 1975 *Phys. Rev. Lett.* **35** 1147–50
Collins R E, Bederson B and Goldstein M 1971 *Phys. Rev.* A **3** 1976–87
Crompton R W, Elford M T and Jory 1967 *Aust. J. Phys.* **20** 369–95
Crompton R W, Elford M T and Robertson A G 1970 *Aust. J. Phys.* **23** 667–81
Crompton R W and Jory 1965 *Proc. 4th Int. Conf. on Physics of Electronic and Atomic Collisions, Quebec* (Hastings on Hudson, Science Bookcrafters) p 118
Duxler W M, Poe R T and LaBahn R A 1971 *Phys. Rev.* A **4** 1935–44
Frost L S and Phelps A V 1964 *Phys. Rev.* A **136** 1538–45

Gerjuoy E 1958 *Ann. Phys., NY* **5** 58–93
Gerjuoy E and Krall N A 1960 *Phys. Rev.* **119** 705–11
—— 1962 *Phys. Rev.* **127** 2105–13
Gibson J R and Dolder K T 1969a *J. Phys. B: Atom Molec. Phys.* **2** 741–6
—— 1969b *J. Phys. B: Atom. Molec. Phys.* **2** 1180–6
Golden D E 1966 *Phys. Rev.* **151** 48–51
—— 1978 *Adv. Atom. Molec. Phys.* **14** to be published
Golden D E and Bandel H W 1965 *Phys. Rev.* **138** A14–21
Hertel I V and Ross K J 1969 *J. Phys. B: Atom. Molec. Phys.* **2** 285–93
Hutt P K, Islam M M, Rabheru A and McDowell M R C 1976 *J. Phys. B: Atom. Molec. Phys.* **9** 2447–60
Kennerly R E and Bonham R A 1977 *Proc. 10th Int. Conf. on Physics of Electronic and Atomic Collisions, Paris* (Paris: Commissariat à l'Energie Atomique) p 396
LaBahn R W and Callaway J 1970 *Phys. Rev.* A **2** 366–9
Massey H S W and Burhop E H S 1969 *Electron and Ionic Impact Phenomena* vol 1 (Oxford: Oxford University Press)
McConkey J W and Preston J A 1975 *J. Phys. B: Atom. Molec. Phys.* **8** 63–74
Milloy H B and Crompton R W 1977 *Phys. Rev.* A **15** 1847–50
Naccache P F and McDowell M R C 1974 *J. Phys. B: Atom. Molec. Phys.* **7** 2382–95
Nesbet R K 1975 *Phys. Rev.* A **12** 444–50
Normand C E 1930 *Phys. Rev.* **35** 1217–25
O'Malley T F 1963 *Phys. Rev.* **130** 1020–9
O'Malley T F, Rosenberg L and Spruch L 1962 *Phys. Rev.* **125** 1300–10
Ramsauer C 1921 *Ann. Phys., Lpz.* **64** 513–40
Ramsauer C and Kollath R 1929 *Ann. Phys., Lpz.* **3** 536–46
—— 1931 *Ann. Phys., Lpz.* **10** 143–54
—— 1932 *Ann. Phys., Lpz.* **12** 529–61
Schmieder C 1961 *Phys. Rev.* **124** 1468–71
Srivastava A L and Nesbet R K 1972 *Phys. Rev.* A **6** 2118–25
Stein T S, Kauppila W E, Pol V, Smart J H and Jesion G 1978 *J. Phys. B: Atom. Molec. Phys.* **11** 1699–7
Sutcliffe V C, Haddad G N, Steph N C and Golden D E 1978 *Phys. Rev.* A **17** 1603–7
Thompson D G 1966 *Proc. R. Soc.* A **294** 160–74
Wichmann E and Heiss P 1974 *J. Phys. B: Atom. Molec. Phys.* **7** 1042–51
Williams J F 1978 unpublished
Williams J F and Willis B A 1975 *J. Phys. B: Atom. Molec. Phys.* **8** 1641–69
Yarlagadda B S, Csanak G, Taylor H S, Schneider B and Yaris R 1973 *Phys. Rev.* A **7** 146–54

Low energy electron impact excitation of the $b\,^3\Sigma^+$ state of CO[a)]

J. R. Twist,[b)] W. C. Paske, T. O. Rhymes, G. N. Haddad, and D. E. Golden

Department of Physics and Astronomy, University of Oklahoma, Norman, Oklahoma 73019
(Received 23 April 1979; accepted 13 June 1979)

The lifetime of the $b\,^3\Sigma^+(v'=0)$ level of CO has been measured using a delayed coincidence technique. Lifetime components of 51.86 ± 0.24, 358 ± 20, and 1500 ± 900 ns at the 95% confidence level have been unfolded by computer fitting and extrapolating to zero pressure. In addition, the collisional quenching cross sections for the prompt decay and the first cascade component were determined to be $(7.7\pm3.8)\times10^{-15}$ and $(7.1\pm3.5)\times10^{-15}$ cm^2 at the 95% confidence level. These results agree with spectroscopic evidence that the $a'\,^3\Sigma^+(v''=32$–$41)$ levels strongly perturb the $b\,^3\Sigma^+(v'=0,1)$ levels. Discrepancies with previous lifetime results are explained.

INTRODUCTION

The lifetime of the $b\,^3\Sigma^+(v'=0)$ state of CO has been studied by a number of authors,[1–8] with widely varying results. While some have reported pressure dependent lifetime components,[4,5,8] others have not.[1–3,6,7]

The most recent lifetime measurement of the $v'=0$ level of this state was made by Van Sprang *et al.*[1] by studying the b–a transition using a delayed coincidence technique with a pulsed electron gun and a monochromator of 5–20 Å resolution. The decay constants were determined by fitting the data to either one or two exponentials for the lifetimes studied as a function of pressure in a scattering cell which was differentially pumped. In this work, the excitation pulse was varied between 100 ns and 10 μs and a short pulse was used in the case of the b state decay. The maximum for the b–a emission function was found to be at 13 eV and the lifetime data were obtained at that energy.

The lifetimes of the $v'=0,1$ levels of the $b\,^3\Sigma^+$ state have been measured by Smith *et al.*[2] These authors reported coincidence measurements between energy analyzed (50 meV resolution) inelastically scattered electrons and emitted photons which were filtered by a 2400–4200 Å bandpass filter. The lifetimes were studied as a function of the pressure in their molecular beam target using a time window of 400 ns. They expected multiple exponentials in the decay of the $v'=1$ level since spectroscopic measurements have shown this state to be strongly perturbed.[9,10] However, their experimental sensitivity to multiple exponentials was low and they only observed one exponential decay, although a 3% background slope correction was made to the higher pressure data before analysis.

The lifetime of the b state was measured by Rogers and Anderson,[3] by studying the $b\,^3\Sigma^+(v'=0)\rightarrow a\,^3\Pi(v''=1,2,3,4)$ transition for a pressure range from 10–125 mTorr. These measurements used a hot cathode invertron[11] and a delayed coincidence detection scheme. Their lifetime data were fitted to a single exponential by graphical techniques using a record length of 0.5 μs.[12] A discussion of the older work[4–8] has been given by Van Sprang *et al.*[1] and will not be given here.

In an effort to understand the rather large differences between some of the previous results we have remeasured the lifetimes and the quenching cross sections of this state and the cascade components in a delayed coincidence experiment between a rapid electron gun shutoff and photons from the $b\,^3\Sigma^+(v'=0)\rightarrow a\,^3\Pi(v''=0,2)$ transitions. In addition, we have also determined the optical excitation function using the time resolved technique of Golden *et al.*[13]

APPARATUS AND PROCEDURE

The experimental apparatus which is shown schematically in Fig. 1 consists of a pulsed electron gun, gas target cell, and Faraday cup all located in an ultra-high vacuum system. Photons which pass through quartz windows in the gas target cell and vacuum wall are filtered by a Bausch & Lomb high intensity UV-visible monochromator and are detected by a RCA C31034A-02 photomultiplier tube (PMT) cooled to −20 °C. The photon pulses are processed with Ortec timing circuitry and stored in a multichannel analyzer (MCA) or in an online LSI-11 minicomputer.

The electron gun described previously[13,14] has been modified for this work as follows: The retarding potential difference (RPD) element (element 3) has an added grid structure which is electrically isolated from the neighboring elements. A coaxial 50 Ω terminator has been connected to the RPD element to terminate a 50 Ω vacuum coaxial cable connecting the grid to a PG-502 Tektronix pulser. The sixth lens element has been redesigned to give increased control of the electron beam. A 0.035 in. i.d. aperture has been added to the seventh lens element to reduce the amount of unscattered electrons collected by the front surface of the target gas cell. This allows a more accurate measurement of the fraction of the current collected by the target gas cell which is due to scattering events inside the cell. The electron multiplier has been replaced by a Faraday cup to permit absolute current measurements of the electron beam transmitted through the gas cell.

The axis of the optical system is perpendicular to the electron beam and is defined by a 25 mm focal length

[a)]Supported in part by grants from NSF and AFOSR.
[b)]Present address: Physics Department, Georgia Institute of Technology, Atlanta, Ga. 30332.

 0021-9606/79/182345-07$01.00

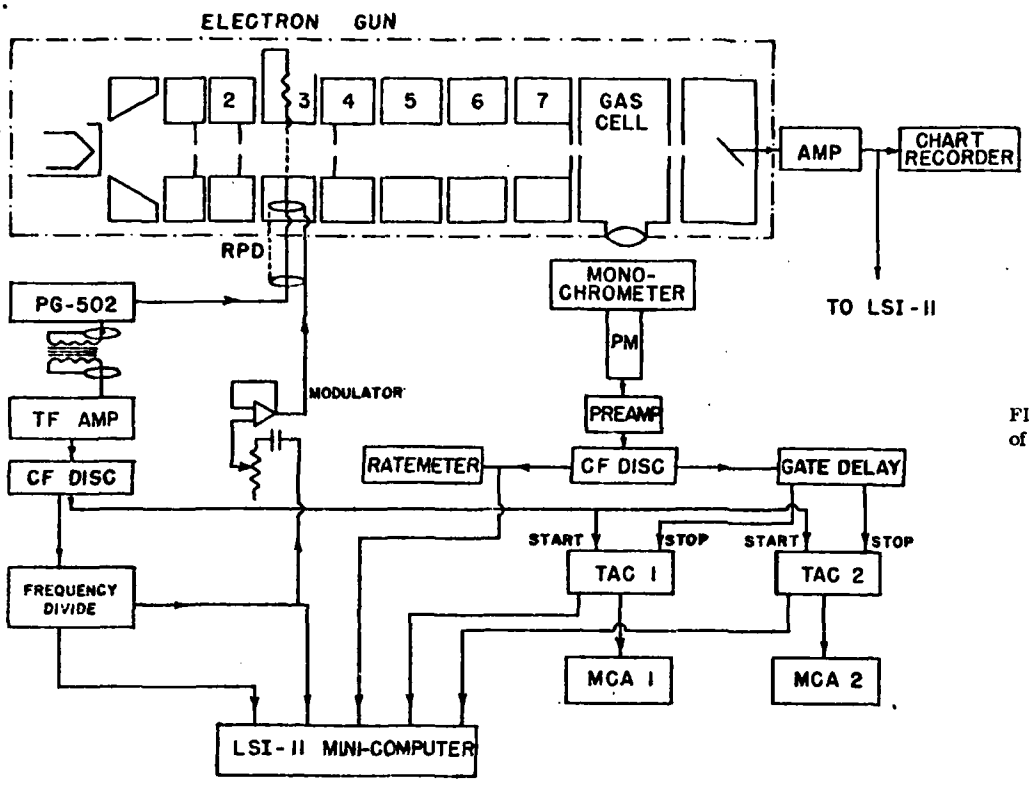

FIG. 1. Schematic diagram of the apparatus.

lens of UV grade fused silica. This lens is mounted 1 in. from the electron beam and provides a $f/1.0$ cone of light to the monochromator. The optical monochromator has a reciprocal dispersion of 76 Å/mm. To obtain the best resolution with an exit slit width of 0.25 mm, the optimum entrance slit width should be 0.50 mm. However we used a 0.75 mm entrance slit and a 0.25 mm exit slit to obtain more light. This combination gives a resolution of approximately 19 Å. A static gas line from the gas cell is connected to an MKS Baratron capacitance manometer. With a pressure of 10 mTorr in the scattering cell, the low pressure region of the vacuum system is approximately 4×10^{-5} Torr as measured by a Varian triode ion gauge.

Photon signals were time resolved with respect to the turn-off of the electron beam. For lifetime studies, the data were recorded using multichannel analyzers (MCAs). The response time of this system is faster than 4 nsec. To record the optical emission functions, a time region was selected by the single channel analyzer in the time to amplitude converter (TAC). The signal in this window was counted into one of six scalars interfaced with the LSI-11 minicomputer and stored on a magnetic disk.

Delayed coincidence experiments may suffer from several kinds of systematic errors in addition to random experimental errors. For an extensive discussion of these errors see Corney,[15] Imhof and Read,[16] and Khayrallah and Smith.[17] In the present work, the most serious errors to be avoided or accounted for are spectral overlap of emission lines due to the finite resolving power of the optical monochromator, cascades from higher lying states, and extraction of the decay constants from the data by computer fitting to a sum of several exponentials.

Wavelength scans were made in the region of interest, i.e., 2000–3500 Å, to determine that the states studied were free from overlapping states.[9,18–20] The spectra were obtained using a resolution of 50 Å FWHM at electron beam energies from 10.5 to 13.5 eV. For the optical resolution used in this work no spectral overlap was found for the third positive system for electron energies just above the $b\,^3\Sigma^+(v'=0)$ threshold. The $b\,^3\Sigma^+(v'=0)\rightarrow a\,^3\Pi(v''=1)$ transition at 2977 Å is nearly overlapped by the $b\,^3\Sigma^+(v'=1)\rightarrow a\,^3\Pi(v''=2)$ line at 2930 Å. However the 2930 Å line is expected to be weak due to the small excitation cross section of the $b\,^3\Sigma^+(v'=1)$ level. The $b\,^3\Sigma^+(v'=0)\rightarrow a\,^3\Pi(v''=0)$ transition at 2833 Å has an adjacent line at 2799 Å $[A\,^1\Pi(v'=0)\rightarrow X\,^1\Sigma^+(v''=22)]$. These lines were resolved in the present case. The 3134 Å line $[b\,^3\Sigma^+(v'=0)\rightarrow a\,^3\Pi(v'=2)]$ is overlapped by a line at 3138 Å $[C\,^1\Sigma^+(v'=0)\rightarrow a\,^3\Pi(v''=2)]$. However by keeping the electron gun energy set at the peak of the $b\,^3\Sigma^+(v'=0)$ excitation cross section, the $C\,^1\Sigma^+(v'=0)$ state will not be populated since its threshold is 0.7 eV above the peak. In addition, since this is an intercombination line it is expected to be weak.

The relative optical excitation function as well as the lifetime of the $b\,^3\Sigma^+(v'=0)$ level were measured by studying the 2833 Å (0,0), 3134 Å (0,2), and 2977 Å (0,1) lines with an electron energy resolution of 0.3 eV. These lines suffer from spectral overlap above the 16.5 eV threshold of the $A\,^2\Pi$ comet tail bands $(A\,^2\Pi\rightarrow X\,^2\Sigma^+)$ and from the first negative system above the 19.7 eV threshold of the $B\,^2\Sigma^+$ state $(B\,^2\Sigma^+\rightarrow X\,^2\Sigma^+)$.

TABLE I. Nonlinear computer fit on test data.[a]

τ_1 (ns)	τ_2 (ns)	τ_3 (μs)	A_1	A_2	A_3	C	Gaussian noise factor (standard deviations)	Calib. (ns/ch)	No. of Exp. used in Fit	Reduced χ^2	Initial Ch.	Final Ch.
51	350	1.50	54000	1600	700	100	1	5	3	...	20	980
56.99	...	...	54406	...	...	352	1	5	1	169	20	980
±0.27			±187			±9						
51.79	692	...	54240	1751	...	160	1	5	2	3.1	20	980
±0.04	±5		±20	±10		±2						
50.93	351	1.50	55970	1582	701	99	1	5	3	1.008	20	980
±0.04	±11	±0.07	±24	±26	±33	±5						
51.69	402	1.79	53855	1548	596	88	2	5	3	4.260	20	980
±0.08	±25	±0.26	±42	±61	±70	±12						
55.37	...	...	54002	...	...	1270	1	0.5	1	7.15	20	980
±0.09			±93			±7						
51.70	278	...	53780	2044	...	657	1	0.5	2	1.050	20	980
±0.10	±32		±110	±56		±71						
50.92	282	1.02	53970	1316	1053	112	1	0.5	3	1.040	20	980
±0.98	±1222	±291	±2050	±140380	±32900	$\pm 10^5$						
50.18	326	1.43	20306	1427	721	102	1	5	3	1.013	30	980
±0.11	±11	±0.62	±26	±24	±31	±4						
51.93	370	1.55	7583	1173	630	97	1	5	3	1.023	40	980
±0.23	±15	±0.91	±21	±28	±34	±5						
51.08	407	2.69	54029	1717	585	10^{-10}	1	5	3	0.890	20	500
±0.05	±17	±0.96	±28	±52	±55							
50.79	339	1.72	54123	1590	825	10^{-10}	1	5	3	0.961	20	250
±0.35	±97	±2.80	±174	±472	±421							

[a]Uncertainties represent one standard deviation of the computer fit to the data.

Cascades have been avoided as much as possible by keeping the electron gun energy near the peak of the $b\,^3\Sigma^+(v'=0)$ cross section at 10.7 eV. It should be noted that this is just above its threshold at 10.39 eV. Analysis of the data sets collected on 5.0 μs full range time scales showed the existence of weak long lived components in the decay of the $b\,^3\Sigma^+(v'=0)$ state, even when the precaution of using near threshold excitation of the state was used. This necessitated lengthening the time scale used in our lifetime work to provide accurate analysis of these long lived components. It also required a computer fit of the data to a sum of exponentials as expected for cascades:

$$N(t) = A_1 e^{-t/\tau_1} + A_2 e^{-t/\tau_2} + A_3 e^{-t/\tau_3} + C \ , \qquad (1)$$

where A_1, A_2, and A_3 are the strengths of the component decays and τ_1, τ_2, τ_3 are the lifetimes of the prompt, first cascade, and second cascade components (which may be pressure dependent) of the levels in question, and C is a constant background due to dark counts in the detector. It should be noted that while we have observed at least two cascade components in the present work, no dipole allowed transitions that end on the $b\,^3\Sigma^+$ were found in the literature.[9,18–20]

A computer program which is more fully described elsewhere,[21] was used to extract the lifetime components by fitting the data to Eq. (1) using a nonlinear method of least squares. The program can fit up to four exponentials plus a constant background and was tested using synthesized data containing chosen exponentials plus varying amount of Gaussian distributed noise.[22] It was found that the program could extract decay constants as long as the noise was less than one standard deviation. The effect of varying the numbers of parameters used in fitting synthesized data and the resulting reduced χ^2 is shown in Table I. The parameters chosen for this test are shown in the first row of the table. It should be noted that the values of τ_1 slowly converge to the chosen value of τ_1 as more exponentials are added. In this case, when too few exponentials are present τ_1 is too large. It can also be seen that doubling the Gaussian distributed noise greatly increases the error associated with each decay constant. The errors listed in Table I are one standard deviation. The lifetime components are obtained with less systematic error when a 5.0 μs record length is used as opposed to that obtained when a 0.5 μs record length is used. Finally, moving the first channel of the analysis to longer times effects the short lived exponentials and similarly moving the last channel of the analysis to shorter times effects the long lived exponentials.

The lifetime data were collected at pressures varying from 1 to 20 mTorr. All data were collected such that the channels just prior to the beam turn-off had at least 50 000 counts. The majority of the data runs were taken at a 100 kHz pulse repetition rate where the beam was "on" for 5 μs and "off" for 5 μs. The MCAs were time calibrated using an Ortec 462 Time Calibrator. In no case did the MCAs show a time drift of more than one channel over the full 1024 channels for a scale of 5 ns/channel. Two data acquisition systems were used, each using a separate MCA and TAC. The first was set at 5 μs full scale and the second was set at 0.5 μs full scale.

To measure the optical emission functions, a total photon signal was taken from the stop channel of the constant fraction discriminator (Ortec 437A). This

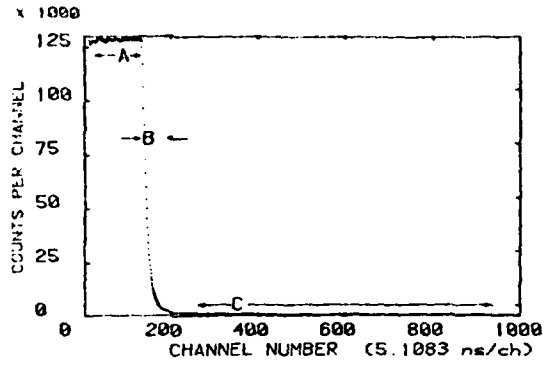

FIG. 2. Decay curve for the $b\,^3\Sigma^+(v'=0) - a\,^3\Pi(v''=2)$ transition in CO at 3134 Å at a pressure of 18.6×10^{-3} Torr after a run time of 21.6 h. Region *A* is the time region for the measurement of the total emission while Region *B* is the time region for the measurement of the prompt emission and Region *C* is the time region for the measurement of the delayed emission for a repetition rate of 1.019×10^5 Hz, a photon count rate of 1.2 kHz, at an electron energy of 10.7 eV.

signal corresponds to the case of an unpulsed electron beam in which all excitation processes have reached equilibrium. Alternatively, a TAC has been used with its time window set so that photons are counted only during the time region marked *A* in Fig. 2. The delayed emission curves were obtained by counting photons in region C in Fig. 2 after the gun had been off for a time greater than 8 or 10 prompt lifetimes of the $b\,^3\Sigma^+(v'=0)$ state. The delayed photons correspond to long lived population mechanisms which populate the state after those molecules which were directly excited to the *b* state have decayed. By comparing total and delayed excitation functions, one has a means of determining the thresholds of these cascade processes.

EXPERIMENTAL UNCERTAINTIES

In our lifetime determinations the statistical errors typically vary between 0.2% right after cutoff to about 3.5% at the longest times used. The data were fit using Eq. (1) to find the best values of all the parameters by the method described above. A grid search which varied each parameter about its best value independently was

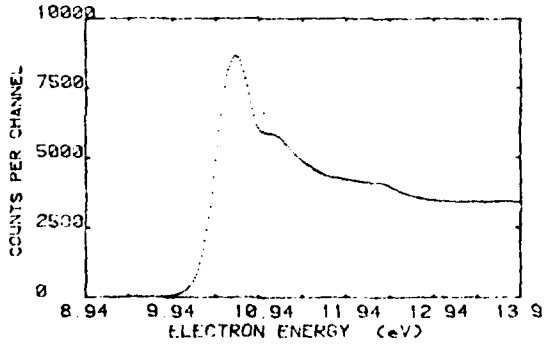

FIG. 3. Total optical excitation function for the $b\to a$ (0, 1) transition in CO at 2977 Å at a pressure of 12.0×10^{-3} Torr using 300 meV resolution, for 20 meV/channel with a dwell time of 660 sec/channel.

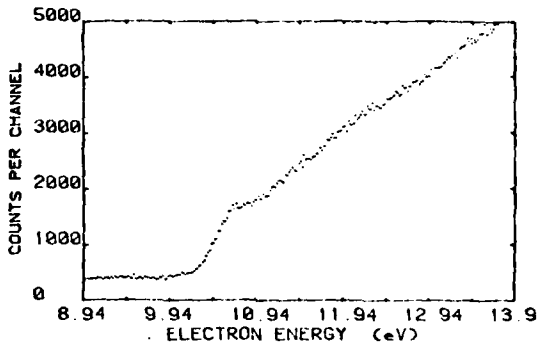

FIG. 4. Delayed optical excitation function (440 nsec delay) for the $b\to a$ (0, 1) transition in CO at 2977 Å at a pressure of 12.0×10^{-3} Torr using 300 meV resolution, for 20 meV/channel with a dwell time of 660 sec/channel. The points are three point averages.

conducted to determine the uncertainties in the parameters. This grid search provided the range through which the data could be fit by the seven parameters (lifetimes and intensities) and still yield a reduced chi square of less than two. The error bars used in Figs. 6 and 7 which are two standard deviations are the result of this search. The uncertainty in the prompt decay at the two standard deviation level (95% confidence) was typically one percent, while the uncertainty at the 95% confidence level for the first cascade was typically about 20%. Five separate lifetime runs at the same pressure yielded lifetimes within the above uncertainty limits. The uncertainty quoted for the quenching cross sections represents one standard deviation in the slope of a weighted least squares fit to the reciprocal lifetimes vs pressure where each data point contains an uncertainty of two standard deviations. In the same manner, one standard deviation for the intercept yields the uncertainty in the zero pressure lifetime at the 95% confidence level.

RESULTS AND DISCUSSION

The total optical excitation function shown in Fig. 3 was obtained using the total electron gun cycle. It should be noted that the prominent resonance peaks and general structure are in good agreement with the results given by Fikui *et al.*[23] and Böse.[24] These structures were used to calibrate the electron energy scale.

A delayed excitation function obtained using the time region marked *C* in Fig. 2 is shown in Fig. 4. Note that even though the excitation pulse has been off for eight prompt lifetimes, an excitation function with a threshold near that of the total function still persists. It is clear from this curve that measurement of the prompt lifetime using threshold excitation does not eliminate cascades.

A semilog decay curve for the $b\to a$ (0, 2) transition in CO is shown in Fig. 5. The best fit to the data using the method previously described is shown as the solid line. The two dashed lines on the expanded scale represent the envelope of the extreme fits to the data as determined by the statistical error limits of the data at the 95% confidence level. Three lifetime components were extracted from data like that shown in Fig. 5. By

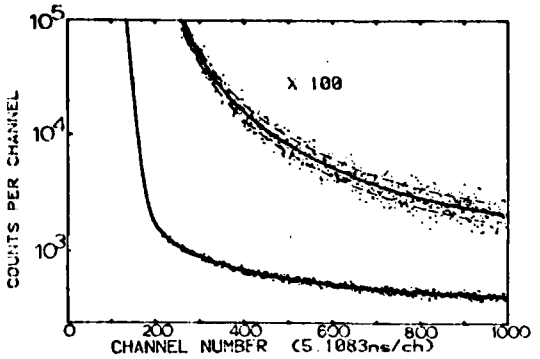

FIG. 5. Semilog decay curve for the data shown in Fig. 2.

taking data such as that shown at various pressures in the range of from $(1-20)\times10^{-3}$ Torr we studied the pressure dependence of the various decay components.

The reciprocal prompt lifetime vs pressure is shown in Fig. 6. The zero pressure extrapolated lifetime for this decay is 51.86 ± 0.24 nsec at the 95% confidence level. The slope of the plot yields the collisional quenching cross section which is $(7.7\pm3.8)\times10^{-16}$ cm^2.

The pressure dependence of the first cascade component feeding the $b-a$ transition is shown in the reciprocal lifetime vs pressure curve in Fig. 7. The zero pressure extrapolated lifetime for this cascade component is 358 ± 20 nsec at the 95% confidence level and the slope of this plot yields a collisional quenching cross section which is $(7.1\pm3.5)\times10^{-15}$ cm^2 at the 95% confidence level.

The second cascade component feeding the $b-a$ transition was very weak and we measured its lifetime to be (1.5 ± 0.9) μsec at the 95% confidence level. The poor statistics associated with this cascade did not allow its pressure dependence to be extracted.

We have summarized the present results in Table II. We have also included the previous results of Van Sprang *et al.*,[1] Smith *et al.*,[2] and Rogers and Anderson,[3] as well as our reanalysis of the data of Rogers and Anderson.[12] As has been discussed above, if either too short an excitation pulse or too short a record length is used, too long a prompt lifetime will be observed. Computer fits for

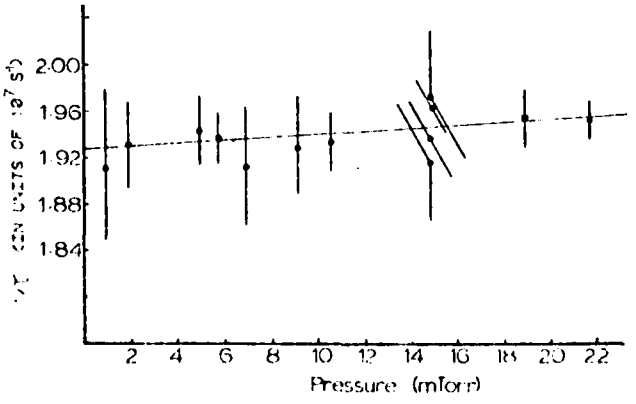

FIG. 6. Reciprocal prompt lifetime vs pressure for the $b-a$ (0, 0)—● and (0, 2)—■ .

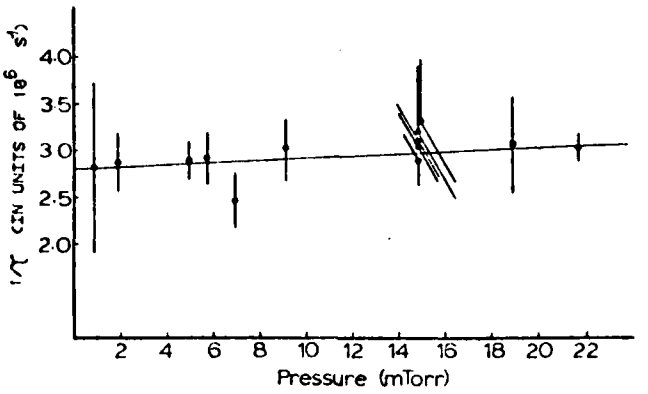

FIG. 7. Reciprocal lifetime vs pressure for the first cascade component feeding the $b-a$ (0, 0)—● and (0, 2)—■ levels of CO.

a single exponential to our data consistently gave a prompt decay lifetime of 56 ns when a data record of 0.5 μs or less was used. This lifetime was also obtained when computer fits for one exponential were made to data sets collected on 0.5 and 5 μs time scales when an 87 ns excitation pulse was used. However, in all cases we did see the 350 ns cascade when a two exponential fit was made. It should be noted that our experiment with a 0.5 μs time scale and an 87 ns excitation pulse is similar to the arrangement used in two of the previous studies.[1,3] This kind of arrangement has been commonly used for measuring lifetimes in the 30–100 ns range since a short excitation pulse and a short record length will allow a higher repetition rate and a shorter collection time. In addition to the systematic errors seen in the prompt decay lifetimes if cascades are present, fitting to short data record lengths makes finding long lived exponentials difficult since usually not even one e-folding is present, and the use of short excitation pulses will not allow the long lived processes to saturate. In both cases the long lived processes are not eliminated but are decreased to the point that they cannot be accurately determined although they may still effect the prompt lifetime of interest. In this work excitation pulses several times longer than the longest lifetime detected have been used so that the long lived components could be fitted with precision.

The difference between the prompt lifetime determined by Smith, Imhof, and Read,[2] and that determined in the present work is about 1 nsec larger than that given by the combined error limits of the two experiments. Smith *et al.* made a 3% slope correction to their data before analysis. The 3% slope could correspond to an exponential with a lifetime of about 450 ns. It is possible therefore that the cascade process was misinterpreted as the photon count rate error commonly encountered in coincidence work. Since in the present work the data rate is less than 0.1% of the pulse repetition rate, we should have an insignificant photon count rate error. In addition, we found that three exponentials were necessary to analyze our data. In our analysis of test data we found that when two exponentials were used for data analysis, a prompt lifetime which was 1 ns too long was recovered. It seems likely that this is the

TABLE II. Lifetimes and collisional quenching cross sections for the $b\,^3\Sigma^+$ ($v' = 0$) state of CO.

Investigator	Prompt lifetime (nsec) (τ_1)	First cascade lifetime (nsec) (τ_2)	Second cascade lifetime (nsec) (τ_3)	Prompt quenching cross section (cm^2)	First cascade quenching cross section (cm^2)
This work	51.86 ± 0.24	358 ± 20	1500 ± 900	$(7.7 \pm 3.8) \times 10^{-15}$	$(7.1 \pm 3.5) \times 10^{-15}$
Van Sprang *et al.* (Ref. 1).	56 ± 1	Not mentioned	Not mentioned	Not mentioned	Not mentioned
Smith *et al.* (Ref. 2).	53.6 ± 0.3	Not mentioned	Not mentioned	$< 2 \times 10^{-14}$	Not mentioned
Rogers and Anderson (Ref. 3).	57.6 ± 1.24	Not mentioned	Not mentioned	Pressure independent	Not mentioned
Rogers and Anderson (present analysis, see Ref. 11).	54.6 ± 5.8	340 ± 200	Indeterminate	$(1.28 \pm 0.51) \times 10^{-11}$	Indeterminate

explanation of the discrepancy. It is also possible that the electron monochromator in the experiment of Smith *et al.*[2] did not exclude electrons that have scattered from the nearby perturbing vibrational levels of the $a'^3\Sigma^+$. In this case long lived a' levels could have been counted as coincidences. However, this effect should be small.

Our computer analysis of the data of Rogers and Anderson[3,12] yields at best two exponential decay curves. Our attempts to fit three exponentials to the data of Rogers and Anderson have not been successful. We attribute this failure to their short data record length (600 ns) and their poor statistics (typically 3000 counts in the initial channels). Our reanalysis of their data yields a pressure dependent lifetime of 54.6 ± 5.8 ns with a quenching cross section of $(1.28 \pm 0.51) \times 10^{-14}$ cm^2 in agreement (within error bars) with the present results. We believe that their result is systematically high due to the short record length used (see Table I). This explanation is also applicable to the difference between the prompt lifetime result of Van Sprang *et al.*[1] and that given by the present work. In addition, Van Sprang *et al.* used an electron energy of 13 eV which is only 1 eV below the ionization potential of CO. This introduces a number of problems which have been discussed above. Furthermore, our reanalysis of the data of Rogers and Anderson,[12] supports the conclusion based on our own data that multiple exponentials are present in this decay. The first cascade component found by us in our reanalysis of the data of Rogers and Anderson has a lifetime of (340 ± 200) ns. However the statistics for this cascade component are so poor that it is difficult to determine if any pressure dependence exists. The lifetime given in Table II for the first cascade from our analysis of the data of Rogers and Anderson is the mean of all of their data. The error given in the table is the square root of the variance of the mean.

Long lived (1 ms) metastable thresholds have been observed in the region of 10–11 eV by Wells *et al.*[25] In order to insure that the cascades observed in the present work were not due to such metastable states, we used an electron gun repetition rate of 12 kHz and a TAC record length of 40 μs. In this way, an extremely weak exponential was detected with a lifetime of (5 ± 10) μsec. Its amplitude was only 25% of the background and no other long components were detected. So we have not found any conclusive evidence for attributing the cascades to such a long lived metastable.

It is likely that the origin of the first cascade into the $b\,^3\Sigma^+$ state is due to the $v'' = 32$–41 levels of the $a'\,^3\Sigma^+$ state, since the high vibrational levels of the a' state are known to strongly perturb the $v' = 0$ and 1 levels of the $b\,^3\Sigma^+$ state.[9,10] This conclusion is supported by the fact that the quenching cross sections of both the prompt and first cascade components of the decay are equal.

[1] H. A. Van Sprang, G. R. Mohlman, and F. J. de Heer, Chem. Phys. 24, 429 (1977).
[2] A. J. Smith, R. E. Imhof, and F. H. Read, J. Phys. B 6, 1333 (1973).
[3] J. Rogers and R. Anderson, J. Quant. Spectrosc. Radiat. Transfer 10, 515 (1970).
[4] J. H. Moore Jr. and W. W. Robinson, J. Chem. Phys. 48, 4870 (1968).
[5] E. H. Fink and K. H. Welge, Z. Naturforsch. Teil A 23, 358 (1968).
[6] T. Wentinck Jr., E. P. Marram, L. Isaacson, and R. J. Spindler, Ablative Material Spectroscopy, AFWL TR 67-30.
[7] R. G. Fowler and T. M. Holzberlein, J. Chem. Phys. 45, 1124 (1966).
[8] R. P. Schwenker, J. Chem. Phys. 42, 1895 (1965).
[9] P. H. Krupenie, 1966 Natl. Stand. Ref. Data Ser. 5, Natl. Bur. Stand.
[10] R. K. Asundi, Indian J. Phys. 50, 241 (1976).
[11] T. M. Holzberlein, Rev. Sci. Instrum. 35, 1041 (1964).
[12] R. Anderson has kindly supplied us his raw data for reanalysis.
[13] D. E. Golden, D. J. Burns, and V. C. Sutcliffe Jr., Phys. Rev. A 10, 2133 (1974).
[14] D. E. Golden and A. Zecca, Rev. Sci. Instrum. 42, 210 (1971).
[15] A. Corney, Adv. Electron. and Electron Phys. 29, 115 (1970).
[16] R. E. Imhof and F. H. Read, Rep. Prog. Phys. 40, 1 (1977).
[17] G. A. Khayrallah and S. J. Smith, Phys. Rev. A 18, 559 (1978).
[18] S. N. Suchard, *Spectroscopic Data—Heteronuclear Diatomic Molecules* (Plenum, New York, 1975).
[19] R. W. B. Pearse and A. G. Gayden, *The Identification of Molecular Spectra* (Wiley, New York, 1976).
[20] B. Rosen, Selected Constants Spectroscopic Data Relative

to Diatomic Molecules (Pergamon, New York, 1970).
[21]See for example, W. C. Paske, Ph.D. dissertation, University of Oklahoma 1974.
[22]G. E. P. Box and M. E. Muller, Ann. Math. Stat. **29**, 610 (1958).
[23]K. Fukui, T. Hirotsu, and K. Kuwata, Chem. Phys. Lett. **44**, 13 (1976).
[24]N. Böse, Chem. Phys. Lett. **61**, 367 (1978).
[25]W. C. Wells, W. L. Borst, and E. C. Zipf, Phys. Rev. A **8**, 2463 (1973).

PHYSICAL REVIEW A VOLUME 21, NUMBER 3 MARCH 1980

Electron-photon angular correlation measurements of He ($1\,^1S_0$-$2\,^1P_1$) excitation by electron impact at 80 eV

N. C. Steph and D. E. Golden
Department of Physics and Astronomy, University of Oklahoma, Norman, Oklahoma 73019
(Received 22 May 1979)

The electron-photon angular correlation function was measured between 80-eV electrons which excited the $2\,^1P_1$ state of helium and 58.4-nm photons from the decay of that state for electron scattering angles ranging from 5° to 100°. The data have been analyzed to yield values of the ratio λ of the differential cross section for exciting the $M_j = 0$ sublevel to the total differential cross section and the magnitude $|\chi|$ of the phase difference between the $M_j = 0$ and $M_j = 1$ excitation amplitudes. The data agree with all previous measurements within one standard deviation, with the exception of the large-angle values of λ obtained by Hollywood, Crowe, and Williams. Possible causes of these discrepancies are discussed. The values of λ and $|\chi|$ obtained in this work agree quite well with those given by the distorted-wave calculations of Madison over the entire angular range.

I. INTRODUCTION

The study of correlation between outgoing components of an electron-atom scattering experiment can yield information about the internal symmetries of the target, provided the experimental geometry is properly prepared. In an inelastic scattering experiment, the angular correlation between scattered electrons which have excited a particular atomic state and photons from the decay of that state, leads to knowledge of the excitation cross sections for the degenerate magnetic sublevels as well as the relative phase of the corresponding excitation amplitudes. Alternatively, the alignment and orientation parameters which describe the polarization and anisotropy of the radiation are specified. Such a scattering experiment is thus the most sensitive test of a theory of atomic excitation because it can measure all of the quantum-mechanical observables.

In the present work we consider the excitation of the $2\,^1P$ state of He. Since both the general subject of electron-photon angular correlations in atomic physics[1] and the specific topic of electron-helium excitation[2] have been recently reviewed, only a brief discussion will be given here.

The first electron-photon angular correlation measurements reported were for the excitation of the $2\,^1P$ state of helium.[3] In these experiments, $2\,^1P \rightarrow 1\,^1S$ photons were detected as a function of angle θ_γ in the scattering plane in delayed coincidence with electrons, which had excited the $2\,^1P$ state and been scattered to various scattering angles θ_e at various electron impact energies E. The wave function of the $2\,^1P$ state is completely determined within an arbitrary phase factor by the cross sections for exciting the magnetic sublevels of the $2\,^1P$ states, $\sigma_0, \sigma_1 = \sigma_{-1}$, and the relative phase χ between the corresponding scattering amplitudes. The standard parameters used to describe the scattering are σ, the differential cross section for exciting the $2\,^1P$ state ($\sigma = \sigma_0 + 2\sigma_1$), $\lambda = \sigma_0/\sigma$, and χ. The parameters λ and χ may be determined from a measurement of the electron-photon coincidence rate which was originally given by Macek and Jaecks.[4]

The 1974 measurementsof Eminyan *et al.*,[3] which were the first to determine λ and $|\chi|$ for the $2\,^1P$ state of helium, covered the energy range from 40 to 80 eV for a range of θ_e from 16° to 40° and the energy range from 100 to 200 eV for a range of θ_e from 16° to 20°. The angular ranges at 80 and 120 eV were extended to 11° and 10°, respecitvely, by Ugbabe *et al.*[5] in 1976. In 1977 Tan *et al.*[6] used a linear polarization filter at 50 eV to cover the angular range from 5° to 42° and at a fixed scattering angle of 42° to cover the energy range from 32 to 80 eV. In 1978 Sutcliffe *et al.*[7] extended the measurements of λ at 80 eV to the range from 5° to 155° by restricting the photon detector to 90°, and thus no determination of χ was made. All of these experiments are in excellent agreement for λ and $|\chi|$ at 80 eV in their common angular ranges. More recently, Hollywood *et al.*[8] measured both λ and $|\chi|$ at 80 eV for the angular range 10° to 130°. Their values of λ at 16° and 25° are lower by 9 and 12%, respectively, than those of Eminyan *et al.*,[3] and their results disagree even if the uncertainties are increased to two standard deviations or 95% confidence limits. In the range from 50° to 70° they agree with the results of Sutcliffe *et al.*,[7] while their value at 90° is substantially lower than the value of Sutcliffe *et al.*[7] Their values of

$|\chi|$ are in good agreement with previous measurements in their common angular ranges.

There are many calculations of both λ and $|\chi|$ using several different techniques.[9-15] The distorted-wave calculations of Madison and Calhoun,[9] give values of λ at 80 eV, in excellent agreement with all of the data of Sutcliffe *et al.*,[7] while another distorted-wave claculation by Baluja and McDowell[15] does not agree with any of the data. The recent R-matrix calculation of Fon *et al.*[14] is in fair agreement with the small-angle data for λ at 80 eV, and, although somewhat lower than the large-angle data of Sutcliffe *et al.*,[7] it is substantially higher than the large-angle results of Hollywood *et al.*[8]

The only measurements of $|\chi|$ at 80 eV which extend to large values of θ_e are those of Hollywood *et al.*[8] The R-matrix calculations of Fon *et al.*[14] and the distorted-wave calculations of Scott and McDowell,[10] and Baluja and McDowell[15] are the only calculations thus far that give results which resemble the measurements. However, none of these calculations is in very good agreement with each other or the measurements of $|\chi|$ over the complete angular range.

II. APPARATUS

The experimental apparatus is shown schematically in Fig. 1. The interaction region is formed by crossed electron and atomic beams. Delayed coincidences are detected in the scattering plane between inelastically scattered electrons which have excited the 2^1P state of helium and the photons from the decay of this state. The apparatus consists of a rotatable electron gun (EG), a rotatable hemispherical electron-energy analyzer (EEA), and atomic beam source, a double-walled Faraday cup (FC), and a fixed photon detector (PD). The EG uses an indirectly heated triple-oxide-coated cathode in a Pierce configuration. Conventional tube lenses focus the electron beam onto the atomic beam and give an operating beam current of between 1 and 20 μA as a function of anode voltage at an electron energy of 80 eV. Minor misalignment of the beam can be compensated by an electrostatic quadrupole lens. The energy distribution is 250 meV full width at half maximum (FWHM), and the full angular spread of the beam is 2.8° (1.2° FWHM). The FC collects the unscattered electron beam and is mounted so that when electron scattering angles of less than 25° are studied, it is displaced by the EEA. A spring lever returns the FC to its stable position when the EEA is returned to angles greater than 25°.

The EEA may be varied in angular position between −5° and 150°. Its angular position is determined by a Vernier scale visible through a window in the vacuum wall. Electrons scattered at a particular angle enter an acceptance cone of solid angle 7.2×10^{-4} sr as seen from the scattering center and are decelerated and focused onto the entrance slit of the radial electrostatic

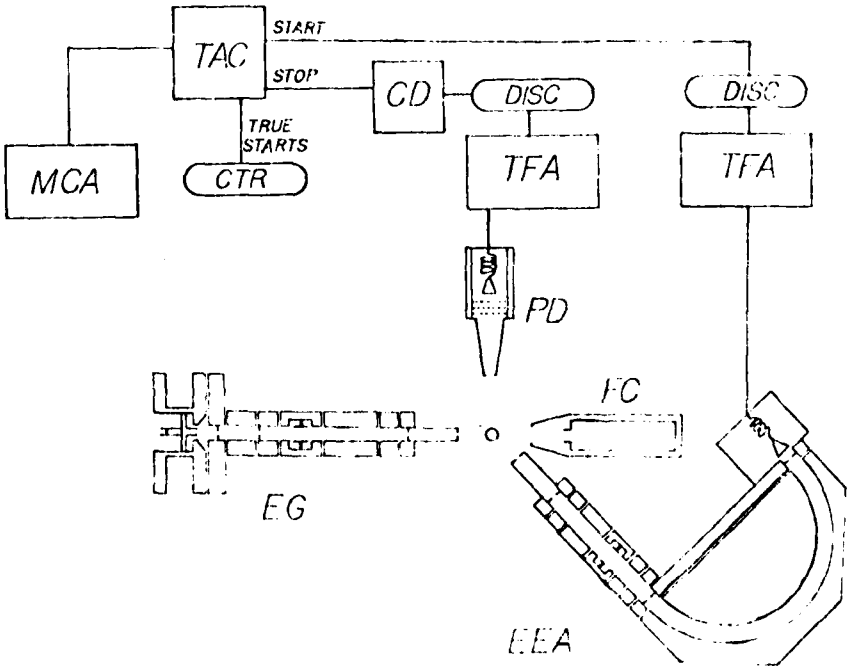

FIG. 1. Schematic diagram of the apparatus (not to scale). The helium beam emerges perpendicular to the plane of the diagram, which represents the scattering plane. The symbols are EG, electron gun; EEA, electron-energy analyzer; FC, Faraday cup; PD, photon detector; TFA, timing filter amplifier; DISC, discriminator; CD, cable delay; CTR, counter; TAC, time-to-amplitude converter; MCA, multichannel analyzer.

field of the EEA. The EEA resolution is 300 meV FWHM and the transmission profile due to the combined energy distribution of the incident beam and the EEA resolution is 400 meV FWHM. This is sufficient to separate $2\,^1P$ from all states except $2\,^3P$, which is a negligible component. The energy-selected electrons are collected by a Galileo-type 4039 channel electron multiplier (CEM).

The 58.4-nm photons from the $2\,^1P \rightarrow 1\,^1S$ transition are detected in the scattering plane with an identical CEM in the photon detector (PD). The PD is fixed and the photon emission angle may be varied between 50° and 145° by rotating the electron gun. Its angular position is determined by a second Vernier scale visible through another window in the vacuum wall. Photons emitted at a particular angle enter an acceptance cone of solid angle 2.4×10^{-2} sr as seen from the scattering center. Three grids are mounted in front of the CEM. Two are biased to prevent the arrival of both positive and negative charged particles at the CEM and the third is grounded to prevent electric field penetration into the scattering region.

A well-collimated atomic beam is produced by effusing helium through a single capillary tube 25 mm long and 0.5 mm in diameter. To further reduce the wings of the atomic beam, a skimmer of 0.5-mm diameter is placed 1 mm from the outlet of the tube and is differentially pumped. For this work, the background system pressure was 4.0×10^{-7} Torr, and the pressure in the beam has been estimated to be 4.0×10^{-5} Torr with a beam width of 0.5 mm.

The EG, EEA, PD, etc. are all shielded by grounded oxygen-free high-conductivity copper (OFHC). The experiment is contained within a Molypermalloy magnetic shield. The maximum field strength in the interaction region was < 8 mG measured with a Rawson-Lush rotating coil Gauss meter. The magnetic shield is contained within a stainless-steel vacuum chamber and the experiment is bakable to 200 °C, and attains a base pressure of $<1\times10^{-8}$ Torr.

III. DATA ACQUISITION

The EG is rotated with respect ot the PD to the desired value of θ_γ. The position of $\theta_e = 0$ is then determined by turning the EEA through the electron beam, and the angular width of the electron beam is checked. The measured FWHM of the beam is consistently found to be 1.2°. The EEA is then rotated with respect to the EG to the desired value of θ_e and an energy-loss spectrum is obtained (see Fig. 2). Photons and electrons are collected in solid angles Ω_γ and Ω_e, respectively, and the corresponding pulses are amplified and fed into a time-to-amplitude converter

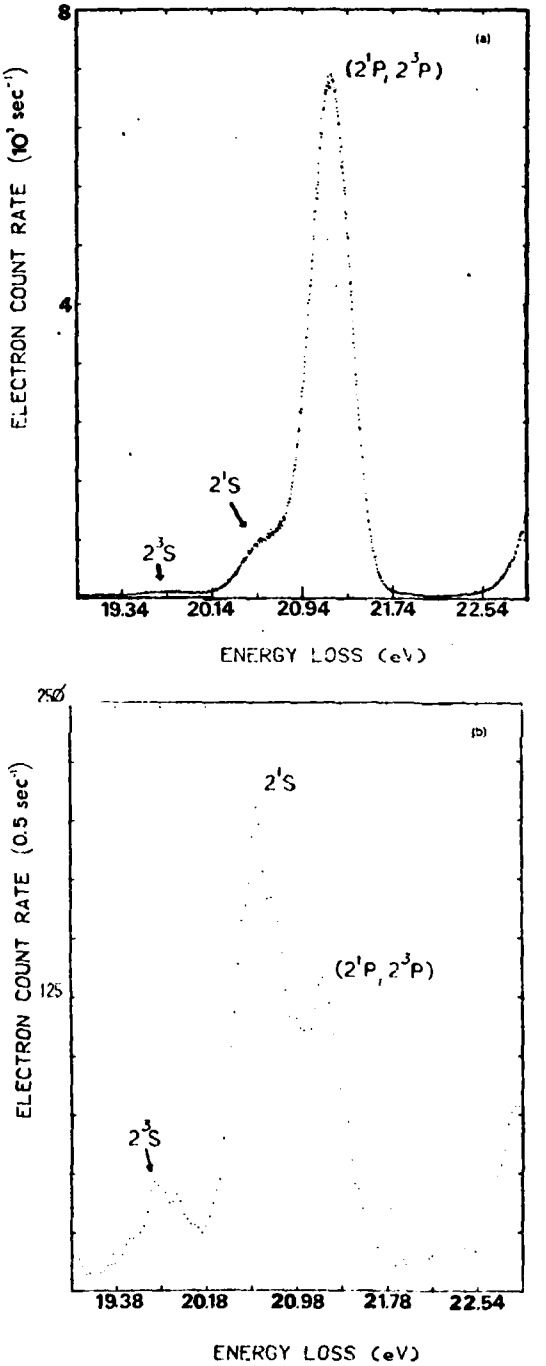

FIG. 2. Helium energy-loss spectra at 80 eV at electron scattering angles (a) $\theta_e = 10$, (b) $\theta_e = 90°$. The total energy resolution is 0.40 eV FWHM. The $2\,^3P$ state is not resolved.

(TAC). The inelastically scattered electrons require about 130 ns to travel to the CEM and these electron pulses are used to start the TAC. Pulses from the photon channel are passed through a 250-ns cable delay and are used to stop the TAC. Electrons and photons from the same scattering event arrive with a definite time correlation. These true coincidences are made to fall into a group of about 20 channels of a 1024-channel multichannel analyzer (MCA) [0.90 ns/channel] corresponding to a range of delays Δt. The width Δt is mainly determined by the time resolution of the apparatus since the lifetime of the excited state is only 0.58 ns. Accidental coincidences occur when the TAC is started and stopped by electrons and photons from different scattering events or by noise counts. This background is determined by fitting a straight line $y_i = a + bi$, where i is the channel number, to the background counts, excluding the 30 channels centered on the coincidence peak.[16] The number of true coincidences and its variance are then determined by

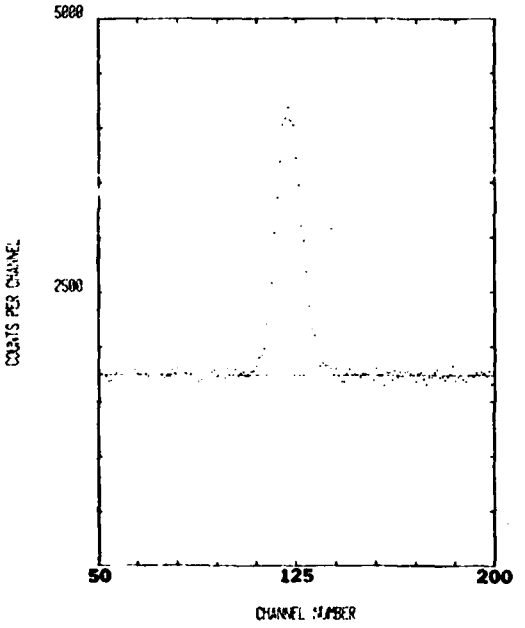

FIG. 3. Delayed coincidence spectrum for an electron energy of 80 eV, $\theta_e = 5°$, $\theta_\gamma = 90°$. The TAC was started on electrons and stopped on photons. Accumulation time ~11 h, channel width 0.9 nsec, inelastic electron rate ~9.5 kHz, photon rate ~4.2 kHz, electron-beam current ~1.1 μA, background pressure 3.5×10^{-7} Torr. The linear least-squares fit to the background has a slope of −0.021 counts per channel, and the intercept is 1741.4 counts. The number of coincidences is 28 400 ± 280, the total number of electrons detected is 3.76×10^8, and the number of true starts is 3.53×10^8. The dead time of the Ortec 457 TAC was ~6.5 μsec.

$$N_c = \sum_i N_i - y_i , \tag{1}$$

$$\sigma^2_{N_c} = \sum_{\Delta t} (N_i + \sigma_a^2 + i^2\sigma_b^2) , \tag{2}$$

where N_i is the number of counts in the ith channel, $\sqrt{N_i}$ is the counting uncertainty of N_i, σ_a^2 is the variance of intercept, and σ_b^2 is the variance of slope. The coincidence rate is $\dot{N}_c = N_c/T$ where T is the collection time. The accidental rate per channel i is $N_a = y_i/T$. An example of a coincidence spectrum and the least-squares fit to the background is shown in Fig. 3.

IV. DATA ANALYSIS AND STATISTICS

The expression relating the rate of coincidences to the parameters λ and χ as given by Golden and Steph[2] is

$$\dot{N}_c(\theta_e, \theta_\gamma) = \frac{3}{8\pi} \frac{I_e}{e} \sigma \epsilon_e \epsilon_\gamma J_c(\theta_e, \theta_\gamma) f(\lambda, \chi, \theta_\gamma) , \tag{3}$$

where I_e is the incident electron beam current, e is the electron charge, ϵ_e and ϵ_γ are the efficiencies of the electron and photon detectors, respectively, and

$$f(\lambda, \chi, \theta_\gamma) = \lambda \sin^2\theta_\gamma + (1-\lambda)\cos^2\theta_\gamma - [\lambda(1-\lambda)]^{1/2} \cos\chi \sin 2\theta_\gamma \tag{4}$$

is the angular correlation function, and

$$J_c(\theta_e, \theta_\gamma) = \int_{l_c} \rho(z) \Delta\Omega_e(z, \theta_e) \Delta\Omega_\gamma(z, \theta_\gamma) dz , \tag{5}$$

where we have taken I_e to be along the z axis, $\rho(z)$ is the density of target atoms, $\Delta\Omega_e$ and $\Delta\Omega_\gamma$ are the solid angles subtended by the electron and photon detectors, respectively, as a function of the position of a scattering event along the z axis, and l_c is the interaction length viewed mutually by the two detectors. Provided that ϵ_γ does not have a significant variation during the measurement, the effect of variations in the electron beam intensity, atomic density, and electron detector efficiency can be eliminated by normalizing the number of real coincidences N_c collected in a time T to the number of electron pulses N_e that started the TAC in this same time T,

$$N_e = T[(I_e/e)\epsilon_e(\sigma + \sigma')J_e(\theta_e) + \dot{n}_e] , \tag{6}$$

where σ' is the cross section for the production of electron counts in the window of the energy analyzer due to states other than $2\,^1P$, $\dot{n}_e$ is the count rate due to electronic noise, and

$$J_e(\theta_e) = \int_{l_c} \rho(z) \Delta\Omega_e(z, \theta_e) dz , \tag{7}$$

where l_e is the interaction length viewed by the electron detector. In performing the experiment, the discriminator in the electron channel is adjusted so that $\dot{n}_e$ is zero. The normalized number of coincidences is then

$$\eta(\theta_e,\theta_\gamma)=\frac{N_c}{N_e}=\frac{3}{8\pi}\frac{\epsilon_\gamma}{1+\sigma'/\sigma}\frac{J_c(\theta_e,\theta_\gamma)}{J_e(\theta_e)}f(\lambda,\chi,\theta_\lambda). \quad (8)$$

Since the analysis is done at fixed θ_e, assuming that ϵ_γ is constant, we may collect all quantities which only vary with θ_e into one term $A(\theta_e)$ and write

$$\eta(\theta_e,\theta_\gamma)=A(\theta_e)J_c(\theta_e,\theta_\gamma)f(\lambda,\chi,\theta_\gamma). \quad (9)$$

The integral J_c may be evaluated analytically as shown in Sutcliffe *et al.*[7] The values of $J_c(\theta_e,\theta_\gamma)$ obtained in the present case are shown in Fig. 4. To insure that ϵ_γ was constant during runs at a fixed θ_e, the photon count rate was measured several times during the run for each value of θ_γ. The variation of ϵ_γ for a given θ_e was always less than 1%.

If angular correlation data at fixed θ_e for various values of θ_γ are normalized to data obtained at $\theta_\gamma=\frac{1}{2}\pi$, $A(\theta_e)$ in Eq. (9) does not need to be determined. Thus,

$$\frac{f(\lambda,\chi,\theta_\gamma)}{\lambda}=\frac{J_c(\theta_e,\frac{1}{2}\pi)}{J_c(\theta_e,\theta_\gamma)}\frac{\eta(\theta_e,\theta_\gamma)}{\eta(\theta_e,\frac{1}{2}\pi)}. \quad (10)$$

Then, using $x=(1-\lambda)/\lambda$ and $z=\cos\chi$ as parameters, we use the method of least squares and derive analytic expressions for the optimum values of λ and $|\chi|$ and their standard deviations in terms of the data and their standard deviations.

V. DISCUSSION OF SYSTEMATIC ERROR

In order to insure that the results are free from any systematic effects, various possible sources of systematic error have been considered. The calculation of the integral given by Eq. (5) accounts for contributions to N_c due to scattering from both beam and background helium. As can be seen in Fig. 4, $J_c(\theta_e,\theta_\gamma)$ has no significant variation for $20°<\theta_e<160°$. This is mainly due to the use of two 1.33-mm apertures which are separated by 1 cm and form the grounded snout of the EEA. Measurements of the electron beam profile with the EEA lens elements grounded gave virtually the same shape as measurements with the EEA lens elements at thier operating potentials. This shows that the EEA acceptance profile is determined solely by geometry. Thus

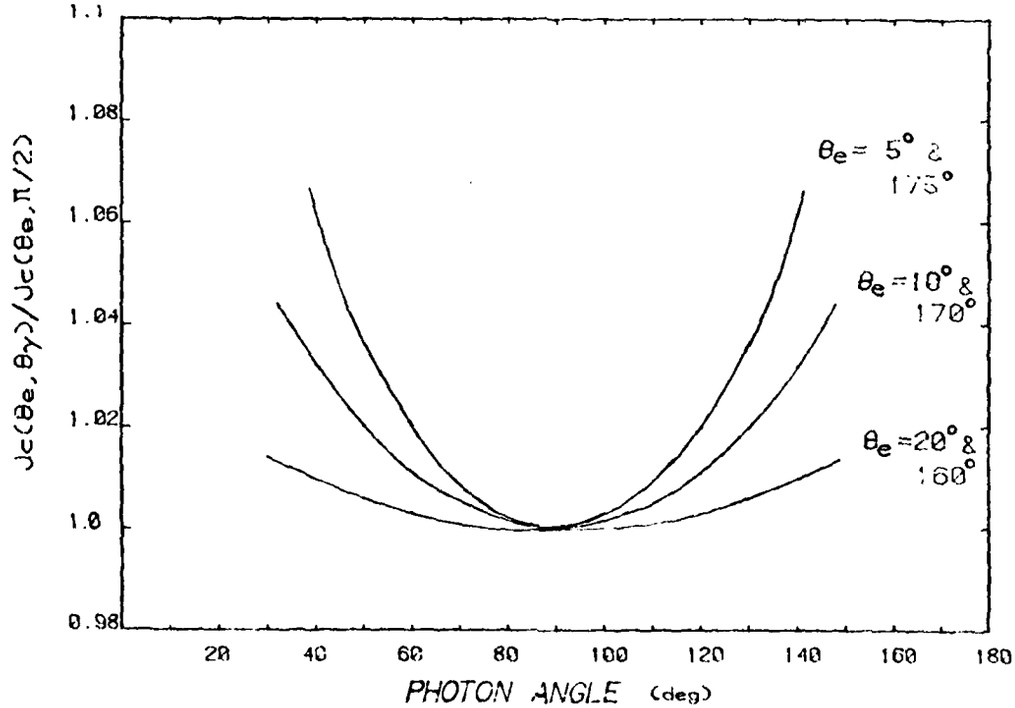

FIG. 4. Multiplicative factor $J_c(\theta_e,\theta_\gamma)/J_c(\theta_e,\frac{1}{2}\pi)$. This factor accounts for scattering from both beam and background helium. The curves are all symmetric about $\theta_e=90°$.

the snout places geometrical limits on the length l_e. In addition, the angular divergence of electrons entering the focusing electrodes is limited to 3°. This alleviates problems with background counts at small electron scattering angles, where elastic scattering is large, and at large electron scattering angles, where N_e is small ($\lesssim 20$ counts/sec) and can be seriously affected by spurious electrons.

When the TAC is started by electrons, it is important to note that the detector efficiency ϵ_e includes both the efficiency of the CEM and the probability that an electron pulse will start the TAC. Thus an electron which is detected but fails to start the TAC is no different from an electron which strikes the CEM but fails to produce a pulse; neither can produce a coincidence. Since this dead-time correction is necessarily count-rate dependent, it varies with both θ_e and θ_γ. This problem is completely eliminated by normalizing the data to N_e, where N_e represents only those electrons which actually start the TAC, during the collection time T.

The normalized number of coincidences given by Eq. (8) is proportional to $(1+\sigma'/\sigma)^{-1}$. The ratio σ'/σ can become quite large for large values of θ_e. This can be seen in the energy-loss spectrum for $\theta_e = 90°$ presented in Fig. 2(b). For a given value of θ_e, the ratio σ'/σ is a minimum when the pass energy of the electron energy analyzer is centered on the energy-loss peak. To ensure that σ'/σ was a minimum, an energy-loss spectrum was taken prior to each data run to establish the position of the $2\,^1P$ peak. To ensure that σ'/σ was constant during a data run, the relevant potentials were monitored and another energy-loss spectrum was taken at the completion of each run to ensure that there was on change in the position of the $2\,^1P$ peak.

When the coincidence data are normalized to the number of electrons, it is prudent to ensure that the energy resolution is sufficient to resolve the $2\,^1P$ peak clearly. The potentials of all power supplies are subject to some drift and instabilities, and several power supplies are involved in maintaining an electron energy analyzer at the proper pass energy. Instability or drift away from this setting decreases the number of true coincidences detected. If the $2\,^1P$ state is clearly resolved, then the number of detected electrons will similarly decrease so that the ratio N_c/N_e is virtually unaffected by power-supply instability. However, if the energy resolution is so broad that the $2\,^1P$ state is not resolved, then instabilities in the analyzer pass energy lead to changes in N_c that are unrelated to the changes in N_e. N_c may decrease more or less than N_e, or N_c may increase. This leads to an additional uncertainty in the ratio N_c/N_e that is difficult to estimate.

We have also analyzed the data by dividing N_c by the number of accidentals in the peak channel of the coincidence spectrum, N_a^p. The pertinent equations for this analysis may be found in Sutcliffe *et al.*[7] This procedure results in larger uncertainties in the parameters because N_a^p must be determined by fitting the background, and the angular distribution of photons must be measured and used in the fit. However, for all angles studied, the optimum values of λ and $|\chi|$ are virtually the same regardless of which of these two normalization procedures is used. Since normalizing by N_a^p removes the dependence on ϵ_γ, this demonstrates the absence of significant instability or drift in the photon detector; and indicates that the effect of dead time on true stops is negligible in this work. For most of the data runs, an additional TAC and MCA were used to obtain a coincidence spectrum starting on photons and stopping on electrons. While the number of coincidences obtained in this configuration is not a different measurement of N_c and cannot be used to lower the counting error,[17] it served as a consistency check on the electronics. In all cases, the ratio N_c/N_a^p was independent of the TAC configuration. However, the raw number of coincidences N_c differed considerably depending upon whether electrons or photon started the TAC.

Since a quadrupole steering lens is included in the EG to correct minor misalignments, it is possible to move the electron beam without a significant change in the current to the FC. Such minor adjustments in this steering lens did not change R_e or R_γ. To eliminate any uncertainty in the angular position of the EEA, the position of the beam is checked prior to each individual point by turning the EEA through the electron beam to determine $\theta_e = 0$. This is particularly important for values of θ_e where λ is a rapidly varying function of θ_e. In addition, since the FC is displaced during runs at $\theta_e < 25°$, the uncollected beam can scatter through the apparatus and cause additional $2\,^1P$ excitations. This effect can be seen in the present work as an increase in the photon count rate of $\lesssim 2\%$ for $\theta_e < 25°$. Because the ratio $\Omega_\gamma/\Omega_e = 33.3$, we would expect this effect on the electron count rate to be much smaller, and the effect on the coincidence rate to be smaller still.

Uncertainty in the value of θ_γ is particularly important in any angular-correlation experiment, since it would alter the phase of the sinusoid described by Eq. (4). In this experiment, the coincidence rate at $\theta_\gamma = 90°$ is used to normalize

the data at other values of θ_γ to enable an analytic determination of λ and $|\chi|$. The position of $\theta_\gamma = 90°$ was established to $\sim \pm 1°$ by measuring the distribution of photons in a plane. This distribution has the form

$$I(\theta_\gamma) = I(90°)(1 - P\cos^2\theta_\gamma), \tag{11}$$

where $I(\theta_\gamma)$ is the intensity of photons emitted at an angle θ_γ with respect to the incident-beam direction, and P is the polarization fraction. The position of the maximum of this distribution determines $\theta_\gamma = 90°$ in this experiment.

The problem of resonant trapping has been considered in some detail by both Eminyan *et al.*[3] and Hollywood *et al.*[6] These authors show that resonance trapping at $\theta_e = 16°$ has a negligible effect on λ but increases the value of $|\chi|$ as pressure increases. As pointed out in Golden and Steph,[2] when $|\chi|$ is small (< 0.5 rad), the amplitude of the angular correlation function $f(\lambda, \chi, \theta_\gamma)$ is solely determined by $|\chi|$ and its phase by λ. This implies that the effect of resonance trapping is to add a uniform background to $f(\lambda, \chi, \theta_\gamma)$ which results in a decrease in its amplitude. Since this uniform background is independent of θ_e then its effect at larger values of θ_e would be to decrease both λ and $|\chi|$. To insure that resonant trapping would not be a problem in this experiment, we studied the background pressure dependence of the photon detection rate at $\theta_\gamma = 90°$, and the results are shown in Fig. 5. The linearity and the zero intercept of the results indicate that resonant trapping is not present at a significant level and also shows that there are no charged particles affecting the photon count rate.

One final systematic effect considered is the angular resolution imposed by the finite size of the detectors. In the absence of a known shape for $\lambda(\theta_e)$ and $\chi(\theta_e)$, it is difficult to determine the effect of the angular resolution of the EEA, $\Delta\theta_e$. For this work $\Delta\theta_e$ was restricted to a flat response of $\pm 1°$, and therefore any significant effect would require an extremely sharp maximum or minimum in $\lambda(\theta_e)$ or $\chi(\theta_e)$. Thus no effect was attributed to $\Delta\theta_e$. Since the shape of $f(\lambda, \chi, \theta_\gamma)$ is known, the effect of the angular resolution of the PD $\Delta\theta_\gamma$ is readily calculated.[19] The effect of a finite angular resolution on a measurement of a sinusoidal function such as $f(\lambda, \chi, \theta_\gamma)$ is to decrease its amplitude. This change in amplitude is a function only of the shape of the angular resolution, and the fractional decrease is independent of amplitude. Therefore, if the shape of the angular resolution is known, the data can be corrected in the following way. De-

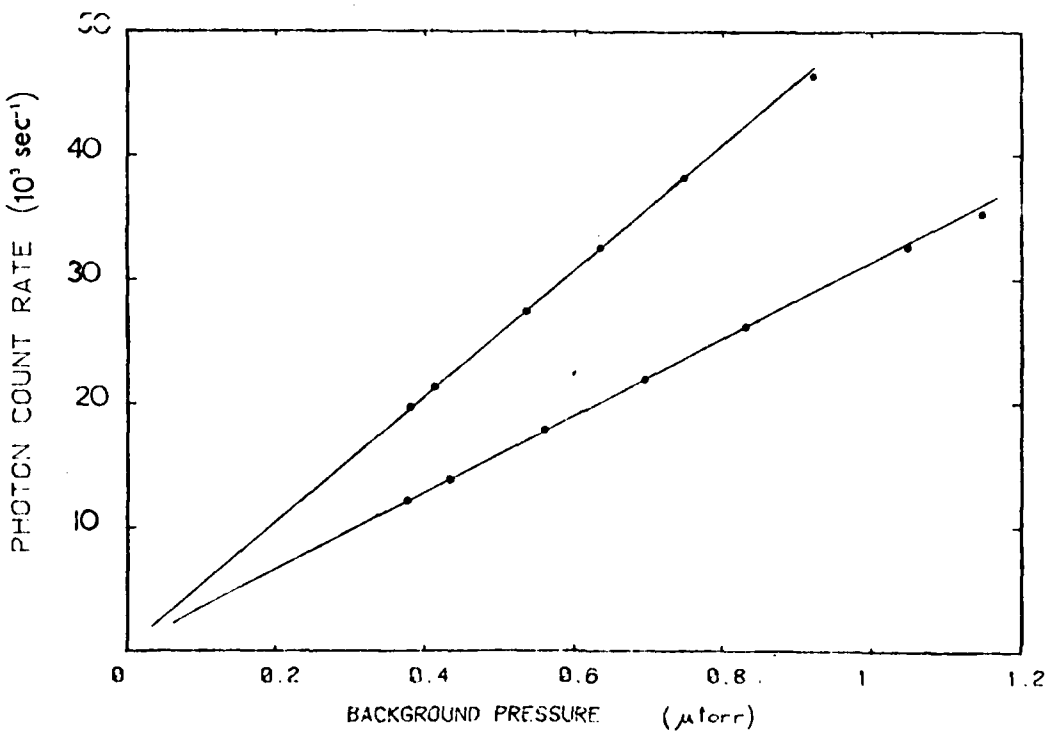

FIG. 5. The pressure dependence of the photon count rate for two values of ϵ_γ. The curves are linear up to a background pressure of 1 μtorr.

termine the fractional change in amplitude ΔA of sine wave by folding it with the known angular resolution function of the detector. Find the best fit of the uncorrected data $f(\theta_\gamma)$, and from this fit determine the inflection angle $\theta_I[f(\theta_I) = 0.5]$. The correction for any point $f^{\rm corr}(\theta_\gamma)$ is then

$$f^{\rm corr}(\theta_\gamma) = f(\theta_\gamma) + \Delta A[f(\theta_\gamma) - f(\theta_I)]. \quad (12)$$

Assuming that the detection efficiency is constant across the face of the photon detector, it has a flat angular response of ±5°. This implies that $\Delta A = 0.006$, and, since the maximum possible amplitude of $f(\lambda, \chi, \theta_\gamma)$ is 0.5, the maximum possible correction is 0.003. This is only significant for points near $\theta_{\rm min}$, the minimum of $f(\lambda, \chi, \theta_\gamma)$, and then only for $\theta_e < 20°$. The effect of small changes in amplitude on $|\chi|$ is detailed in Ref. 2.

VI. RESULTS AND DISCUSSION

The present experimental results are summarized in Table I, where values of λ, $|\chi|$, and $\theta_{\rm min}$ are presented for various values of θ_e. The angular-correlation function measured in this work for $\theta_e = 10°$ is shown in Fig. 6. Since the use of Eq. (10) allows an analytic solution for the parameters λ and $|\chi|$, it is only necessary to measure $N_c(\theta_e, \theta_\gamma)$ and $N_c(\theta_e, \theta_\gamma)$ at two other values of θ_γ. When the $\theta_e = 10°$ data are analyzed using all 11 data points shown in Fig. 6, the results obtained are $\lambda = 0.488 \pm 0.016$ and $|\chi| = 0.371 \pm 0.038$. When the data are analyzed using only the three points $\theta_\gamma = 52.5°$, 90°, and 135°, the results are $\lambda = 0.485 \pm 0.018$ and $|\chi| = 0.376 \pm 0.059$. Thus the results are not significantly different. However, when only three points are used, there is an increase in the uncertainty which is accompanied by a significant reduction in the data-accumulation time. Even though we need to measure $N_c(\theta_e, \theta_\gamma)$ at only three values of θ_γ, the data accumulation time can become prohibitively long at large values of θ_e. A total of 28 days was required to accumulate the data used to obtain the angular-correlation function at $\theta_e = 100°$. In order to reduce the uncertainties in λ and $|\chi|$ by a factor of 2, it would be necessary to increase the data-accumulation time or the product $\Omega_e\Omega_\gamma$ by a factor of 4. Increasing the product $\Omega_e\Omega_\gamma$ carries with it an angular averaging problem, and increasing the data-accumulation time is not practical.

TABLE I. Values of the parameters derived from the measured angular correlations as a function of the electron scattering angle θ_e, for an incident energy of 80 eV. Uncertainties quoted represent one standard deviation.

θ_e (deg)	λ	$\lvert\chi\rvert$ (rad)	$\theta_{\rm min}$ (deg)
5	0.766 ± 0.020	0.231 ± 0.220	28.57 ± 1.71
10	0.488 ± 0.015	0.370 ± 0.038	45.71 ± 0.94
20	0.297 ± 0.014	0.568 ± 0.054	58.86 ± 1.08
30	0.444 ± 0.023	1.182 ± 0.053	53.27 ± 3.34
50	0.919 ± 0.054	1.994 ± 0.146	−7.47 ± 3.86
60	0.903 ± 0.074	2.424 ± 0.416	−14.45 ± 7.70
80	0.861 ± 0.102	2.570 ± 0.402	−19.44 ± 9.02
90	0.871 ± 0.103	2.001 ± 0.243	−10.33 ± 7.70
100	0.838 ± 0.103	1.842 ± 0.175	−8.16 ± 6.64

The measured variation of λ with θ_e is presented in Fig. 7(a) for the range $5° \leq \theta_e \leq 50°$ and in Fig. 7(b) for the range $60° \leq \theta_e < 155°$, together with the results of previous measurements. The measured variation of $|\chi|$ with θ_e is shown in Fig. 8, together with the results from previous measurements and calculations. The present results for $|\chi|$ agree with all previous measurements in their common angular ranges. The present results for λ agree with all previous measurements for values of $\theta_e < 70°$. Our value of λ at $\theta_e = 90°$ agrees with the result of Sutcliffe *et al.*,[7] but our values of λ for $\theta_e = 80°$, 90°, and 100° are about 20–40% larger than the corresponding values obtained by Hollywood *et al.*,[8] who state that their angular correlation data were obtained by starting a TAC with photons and stopping with electrons, and that the values of N_c obtained were normalized by dividing by the total number of electrons detected during the accumulation time. As we have discussed in Sec. V, values of N_c obtained using photon starts should be normalized to the number of accidentals to eliminate TAC dead-time effects on the value of N_c. We have measured coincidence spectra at $\theta_e = 20°$ and 90° using photon starts. When we analyzed the 20° data using the technique discussed by Hollywood *et al.*, we obtained a value for λ of 0.285 and a value for $|\chi|$ of 0.578. When we analyzed the data at $\theta_e = 90°$, we obtained a value for λ of 0.760 and a value for $|\chi|$ of 1.996. The values of λ and $|\chi|$ obtained at $\theta_e = 10°$ are 4% less and 1.6% greater than those obtained using our method. At $\theta_e = 90°$, the value of $|\chi|$ is unchanged, while the value of λ is 14.6% less than that obtained using our method. Thus the major effect of the analysis discussed by Hollywood *et al.*[8] is to obtain too small a value of λ at large values of θ_e, where the photon count rate is large compared to the electron count rate. Since this effect is count-rate dependent, it is difficult to estimate how much the values of λ obtained at large values of θ_e by Hollywood *et al.* would be depressed by this normalization procedure. However, because the background helium

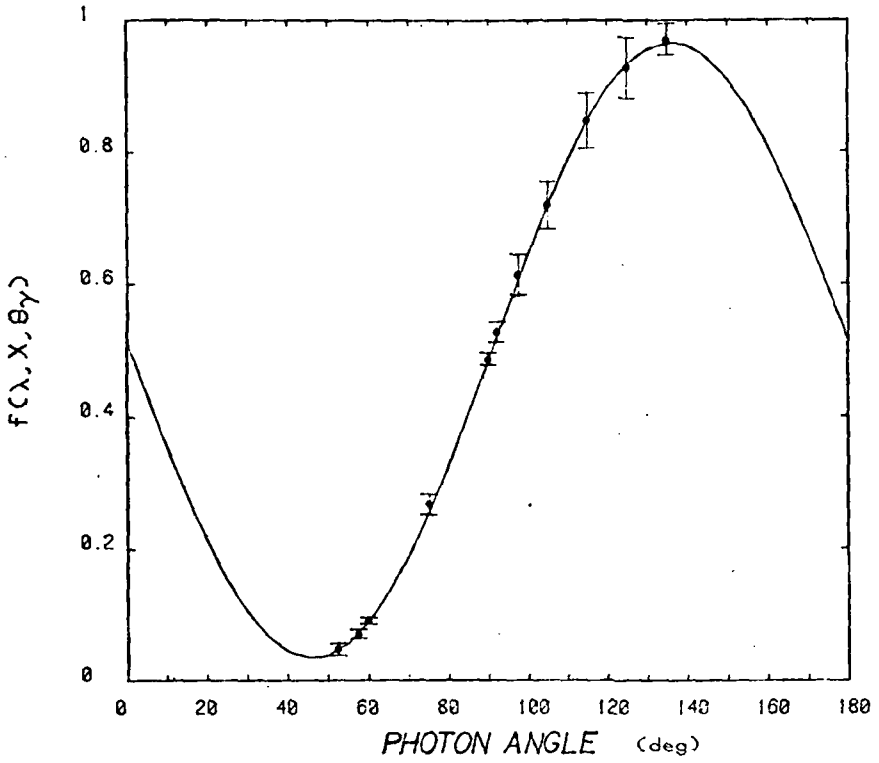

FIG. 6. The electron-photon angular correlation for the present work for $\theta_e = 10°$ at 80 eV.

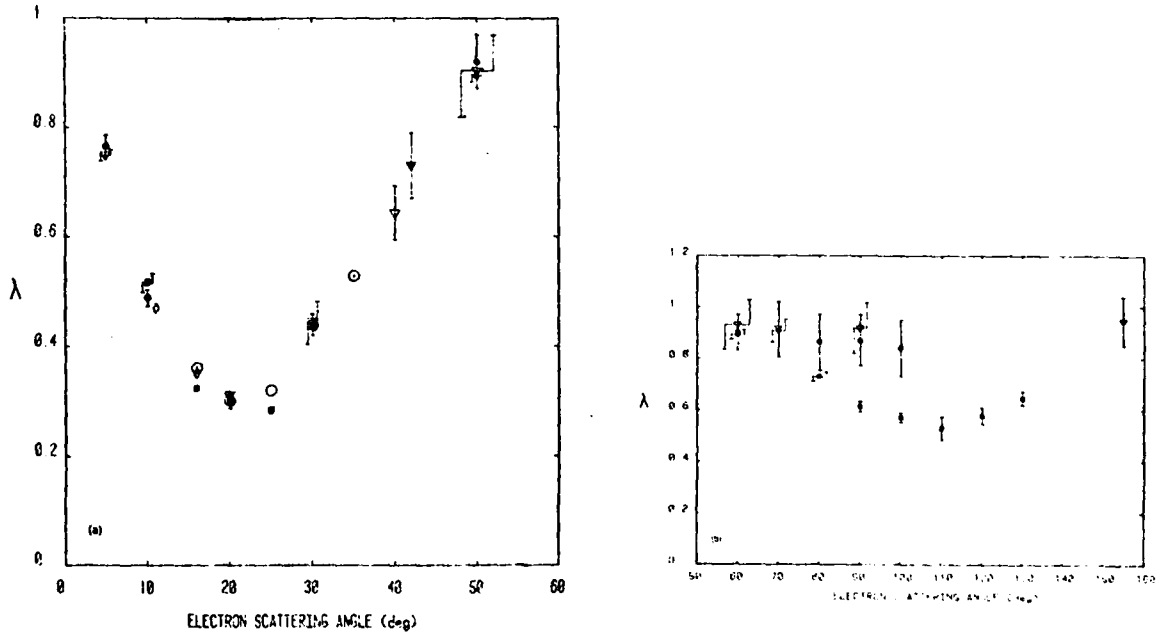

FIG. 7. Variation of λ with electron scattering angle (a) $0° \leq \theta_e \leq 50°$ and (b) $60° \leq \theta_e \leq 180°$ at an incident electron energy of 80 eV: ●, present data; ○, results of Ref. 3; ◇, results of Ref. 5; ▼, results of Ref. 6; ▽, results of Ref. 7; ■, results of Ref. 8.

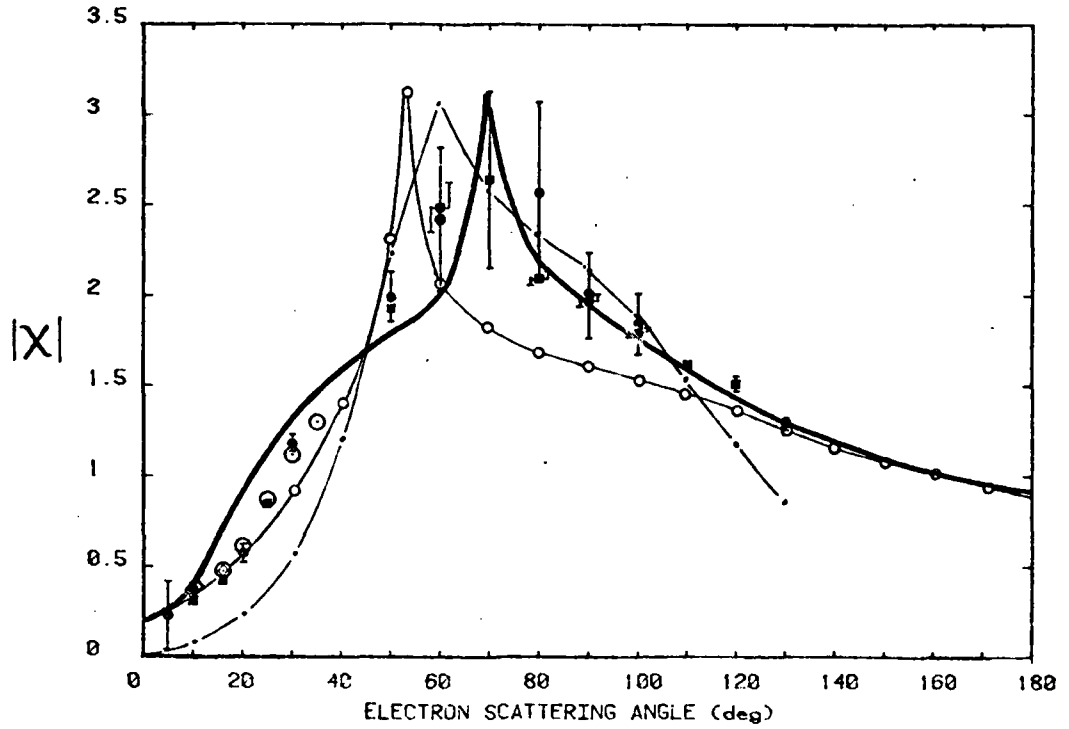

FIG. 8. Variation of $|\chi|$ with electron scattering angle for an incident electron energy of 80 eV. ●, present data; ○, results of Ref. 3; ◇, results of Ref. 5; ■, results of Ref. 8; —O—, calculation of Ref. 14; — • —, calculation of Ref. 10; —, calculation of Ref. 19.

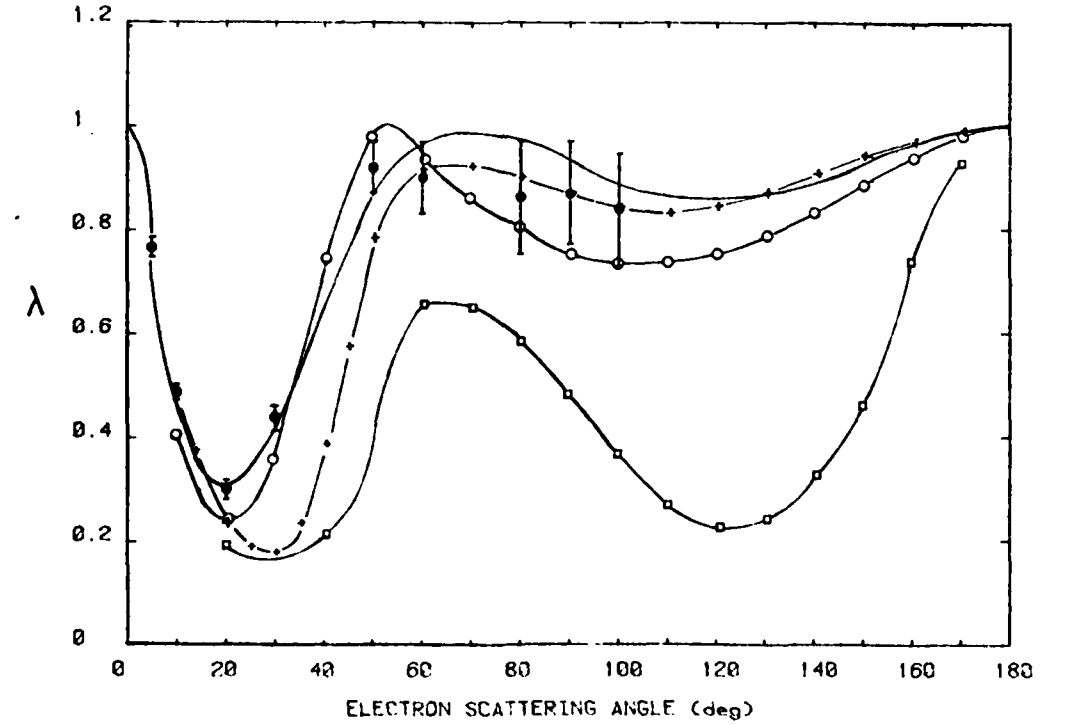

FIG. 9. Calculation of the variation of λ with electron scattering angles compared with the present data; ——, calculation of Ref. 18; —+—, calculation of Ref. 13; — □ —, calculation of Ref. 15; —○—, calculation of Ref. 14.

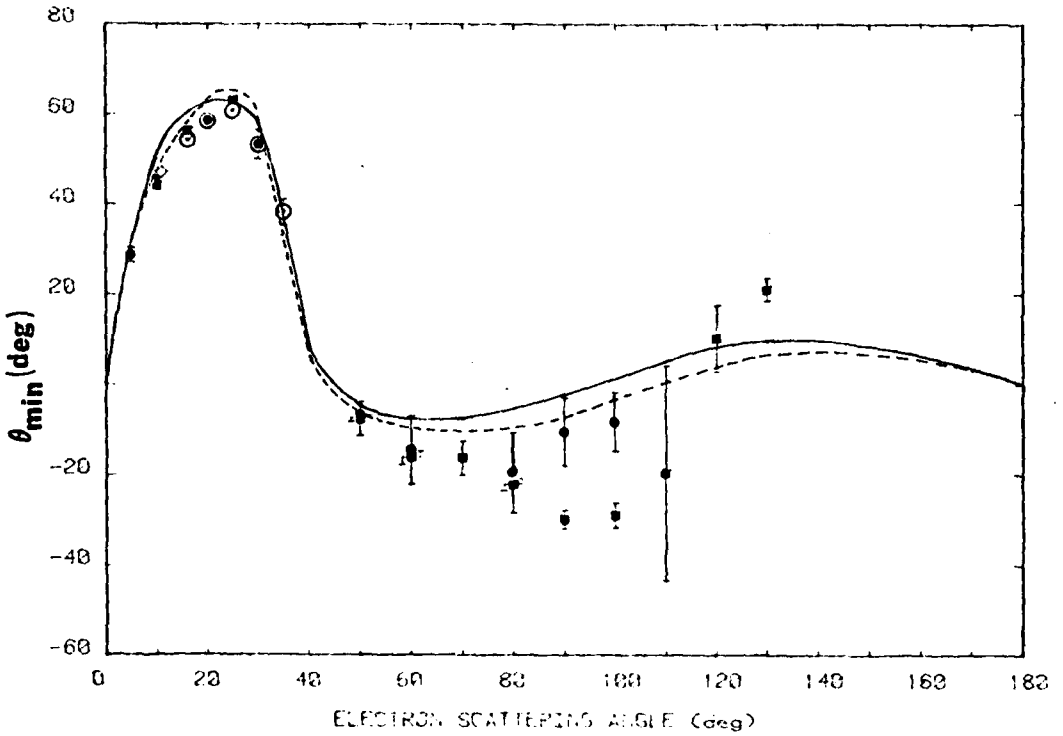

FIG. 10. Variation of θ_{min} with electron scattering angle for an incident electron energy of 80 eV: ●, present work; ⊙, results of Ref. 3; ◇, results of Ref. 5, ■, results of Ref. 8; solid curve, calculation of Ref. 14; dashed curve, calculation of Ref. 18.

is a negligible effect in the work of Hollywood *et al.*,[8] we would expect that $\dot{N}_\gamma$ had a larger variation with θ_γ than in our experiment and therefore this count-rate-dependent effect would be larger in their apparatus than in ours. Our analysis leads to the conclusion that, for a large ratio of $\dot{N}_\gamma/\dot{N}_e$, the method of analysis discussed by Hollywood *et al.*[8] yields an angular correlation function with too small an amplitude and an altered phase.

It should also be noted that the energy resolution of the apparatus of Hollywood *et al.* was 900 meV. Thus they were unable to resolve the $2\,^1P$ peak at large values of θ_e. This could have increased the uncertainty of their results, as discussed in Sec. V.

The present results for λ are compared with the results of several calculations in Fig. 9. All of the present data points are in agreement within one standard deviation with the calculation of Madison and Calhoun.[9] It should be noted that the most recent *R*-matrix calculation of Fon *et al.*[14] agrees fairly well with the present large-angle data, and the only serious disagreement is at the minimum ($\theta_e \sim 20°$). In contrast, their results for $|\chi|$ agree remarkably well with all of the data of $\theta_e \leq 20°$, while their results disagree with all of the data at larger angles. A recent paper by Madison[18] details the results of Madison and Calhoun[9] and includes a calculation of χ which is shown in Fig. 8. While this calculation gives values of $|\chi|$ somewhat large than the measurements in the range of θ_e from 15° to 30°, it is in excellent agreement with all of the experimental results at all other angles.

Finally, in Fig. 10 we present the values of θ_{min}, the position of the minimum in the angular correlation function $f(\lambda, \chi, \theta_\gamma)$ as a function of θ_e. Since this function depends upon the values of both λ and $|\chi|$, it gives a much clearer picture of the agreement between various theories and the experimental results. All of the experimental data are in agreement wit the exception of the points at 90° and 100°. The *R*-matrix calculation of Fon *et al.*[14] agrees reasonably with the present results at all angles. The distorted-wave calculation of Madison[18] is in even better agreement with the present results. The deep minimum seen by Hollywood *et al.*[8] at about 95° is not predicted by either of the calculations.

ACKNOWLEDGMENTS

This work was supported in part by the NSF and in part by the Air Force Office of Scientific Research.

[1]K. Blum and H. Kleinpoppen, Phys. Rep. 52, 203 (1979).
[2]D. E. Golden and N. C. Steph, in *Coherence and Correlation in Atomic Physics*, edited by H. Kleinpoppen and J. Williams (Plenum, New York, to be published).
[3]M. Eminyan, K. B. MacAdam, J. Slevin, and H. Kleinpoppen, Phys. Rev. Lett. 31, 576 (1973); J. Phys. B 7, 1519 (1974).
[4]J. Macek and D. H. Jaecks, Phys. Rev. A 4, 2288 (1971).
[5]A. Ugbabe, H. Arriola, P. J. O. Teubner, and E. Weigold, J. Phys. B 10, 72 (1977).
[6]K. H. Tan, J. Fryar, P. S. Farago, and J. W. McConkey, J. Phys. B 10, 1073 (1977).
[7]V. C. Sutcliffe, G. N. Haddad, N. C. Steph, and D. E. Golden, Phys. Rev. A 17, 100 (1978).
[8]M. T. Hollywood, A. Crowe, and J. F. Williams, J. Phys. B 12, 819 (1979).
[9]D. H. Madison and R. V. Calhoun (unpublished).
[10]T. Scott and M. R. C. McDowell, J. Phys. B 8, 1851 (1975).
[11]M. R. Flannery and K. J. McCann, Phys. Rev. A 12, 846 (1975).
[12]L. D. Thomas, G. Csanak, H. S. Taylor, and G. S. Yarlagadda, J. Phys. B 10, 1073 (1977).
[13]G. D. Meneses, N. T. Padial, and Gy Csanak, J. Phys. B 11, L237 (1978).
[14]W. C. Fon, K. A. Berrington, and A. E. Kingston, J. Phys. B 12, L171 (1979).
[15]K. L. Baluja and M. R. C. McDowell, J. Phys. B 12, 835 (1979).
[16]It was found that fitting the background to a straight line, an exponential or the expression given by Ref. 7 did not alter the results.
[17]Sutcliffe *et al*. in Ref. 7 used both photon starts and electron starts at the same time in two TAC's to reduce the counting error. I have determined experimentally that only ~5% of the coincidences detected using photon starts are different from those detected using electron starts. Thus their uncertainties should be increased by about 1.414.
[18]D. H. Madison, J. Phys. B 12, 3399 (1979).
[19]It should be pointed out that Eq. (12) does not account for the effects of averaging out of the scattering plane. However, these effects are negligible in the present work. The procedure for complete circular averaging is given in Ref. 3.

Alignment and orientation in the electron-impact excitation of the $2\,^1P$ state of He from 40 to 500 eV

N. C. Steph and D. E. Golden
Department of Physics and Astronomy, University of Oklahoma, Norman, Oklahoma 73019
(Received 14 November 1979)

Electron-photon angular correlations between electrons which have excited the $2\,^1P$ state of He and photons from the $2\,^1P \rightarrow 1\,^1S$ transition have been studied for 100-, 200-, and 500-eV incident electrons. Values of λ and $|\chi|$ obtained from these measurements are compared to values which have been obtained in other experiments and calculations. The results are in good agreement with the recent distorted-wave calculation of Madison. The values of λ and $|\chi|$ from all experiments have been combined to examine the behavior of the Fano-Macek alignment and orientation parameters for electron energies from 40 to 500 eV.

I. INTRODUCTION

Electron-photon angular correlation measurements were first reported by Eminyan *et al.* in 1973.[1] These measurements covered the energy range from 40 to 200 eV, but the range of electron scattering angles θ_e was restricted to $\theta_e > 15°$ at all energies, and to $\theta_e \leq 25°$ for energies >80 eV. The only other measurements for energies above 80 eV were those of Ugbabe *et al.*[2] at 120 eV for values of θ_e of 10° and 16°. A summary of the other measurements for energies ≤ 80 eV may be found in Steph and Golden.[3]

The results of such angular correlation measurements are usually expressed in terms of the parameters λ and $|\chi|$ which describe the excited state. For excitation of the $2\,^1P$ state from the $1\,^1S$ ground state, the excited-state wave function is given by

$$\psi(2\,^1P) = a_0|10\rangle + a_1|11\rangle + a_{-1}|1-1\rangle , \tag{1}$$

where the complex excitation amplitudes a_{M_L} describe the excitation of the different magnetic sublevels. Since the scattering process has mirror symmetry in the scattering plane, $a_1 = -a_{-1}$, and the total differential cross section is given by

$$\sigma = |a_0|^2 + 2|a_1|^2 . \tag{2}$$

The parameter $|\chi|$ is the absolute value of the phase difference between the complex scattering amplitudes a_0 and a_1 and

$$\lambda = |a_0|^2/\sigma . \tag{3}$$

The dimensionless parameters λ and $|\chi|$ are functions of the electron energy E and the electron scattering angle θ_e. They describe the excited state of the atom after undergoing a collision and (together with σ) provide a complete determination of the excitation amplitudes. The approximations used in a calculation can give insight into the relative importance of various effects, such as exchange, in the scattering process provided the calculation predicts the correct values of λ, $|\chi|$, and σ. Thus it is important to obtain accurate values of these quantities.

For an excitation at a given E and θ_e, the angular distribution of deexciting radiation in the scattering plane is given in terms of λ and χ as

$$f(\lambda,\chi,\theta_\gamma) = \lambda \sin^2\theta_\gamma + (1-\lambda)\cos^2\theta_\gamma - [\lambda(1-\lambda)]^{1/2}\cos\chi \sin 2\theta_\gamma , \tag{4}$$

where θ_γ is the angle of photon emission. Although the $2\,^1P$-$1\,^1S$ photons result from an electric dipole transition, studying electron-photon angular correlations leads to a knowledge of the electric quadrupole and magnetic dipole distributions for the excited state. The excited-state population has been described by Fano and Macek[4] in terms of an orientation vector $\vec{O}$ and an alignment tensor $\underline{A}$ in order to separate the geometrical and dynamical effects. For $1\,^1S$-$2\,^1P$ excitation in helium by electron impact, $\vec{O}$ has one nonvanishing component which is proportional to the average value of the net angular momentum of the excited state and is related to λ and χ by

$$O_{1^-}^{col} = \langle L_y\rangle/[L(L+1)] = -[\lambda(1-\lambda)]^{1/2}\sin\chi . \tag{5}$$

The alignment tensor has three nonvanishing components:

$$\begin{aligned} A_{0}^{col} &= \langle 3L_z^2 - L^2\rangle/[L(L+1)] = (1-3\lambda)/2 , \\ A_{1^-}^{col} &= \langle L_xL_z + L_zL_x\rangle/[L(L+1)] \\ &= [\lambda(1-\lambda)]^{1/2}\cos\chi , \\ A_{2^-}^{col} &= \langle L_x^2 - L_z^2\rangle/[L(L+1)] = (\lambda-1)/2 . \end{aligned} \tag{6}$$

It should be noted that $O_{1^-}^{col}$ and $A_{1^-}^{col}$ are not independent and that A_0^{col} and $A_{2^-}^{col}$ are not independent. The third independent parameter in this formulation is the monopole moment, which is propor-

tional to σ.[5]

It has been shown by Blum and Kleinpoppen[5] that the induced magnetic moment of the excited atom is determined by the orientation vector and that the electric quadrupole tensor is proportional to the alignment tensor, while all higher multipoles vanish. The orientation vector is directly given by the transfer of angular momentum to the atom, and its behavior as E and θ_e are varied can give physical insight into the scattering process. The alignment tensor specifies the distribution of the electronic charge in the atom and this, in turn, specifies the anisotropy of the emitted radiation. Therefore Eq. (4) may be rewritten as

$$f(\lambda,\chi,\theta_\gamma)=\tfrac{3}{3}+\tfrac{1}{3}A_0^{\rm col}(3\cos^2\theta_\gamma-1) - A_{1,}\sin2\theta_\gamma+A_{2,}\sin^2\theta_\gamma . \quad (7)$$

Equation (7) may be rewritten in terms of the associated Legendre function, $P_l^m(\cos\theta_\gamma)$,

$$f(\lambda,\chi,\theta_\gamma)=\tfrac{3}{3}[1+A_0^{\rm col}P_0^2(\cos\theta_\gamma)-A_{1,}^{\rm col}P_2^1(\cos\theta_\gamma) +\tfrac{1}{2}A_{2,}^{\rm col}P_2^2(\cos\theta_\gamma)] . \quad (8)$$

The first term in Eq. (8) represents the monopole contribution to the radiation distribution. The remaining terms represent contributions to the radiation distribution from linear quadrupoles in the scattering plane along the z axis, at 45° to the z axis, and at 90° to the z axis, respectively. The nonvanishing components of $\underline{A}$ are coefficients which determine the intensity of radiation with a given angular distribution.

The simplest theory which makes clear predictions of λ and χ is the first Born approximation (FBA). The results of the FBA depend only on the kinematics of the collision. Accordingly, no angular momentum may be transferred to the atom along the direction of linear-momentum transfer $\vec{K}$. Thus, along the K axis there is a $\Delta M_L=0$ selection rule. This implies that there will be no radiation emitted along the direction of $\vec{K}$. This means that $\chi=0$ independent of E and θ_e. The FBA predicts that $\lambda=\cos^2\theta_K$ where θ_K is the angle between $\vec{K}$ and the incident electron beam. Because of the nature of this approximation, one might at first expect this prediction to be valid for small scattering angles and high energies. However, while the FBA prediction for λ is in reasonable agreement with the results of Eminyan *et al.*[1] at 50 eV, the agreement becomes worse as the energy increases. The FBA places emphasis on the role played by the direction of linear-momentum transfer $\vec{K}$. The angle θ_K in the FBA corresponds to the angle where the angular distribution of radiation is a minimum, $\theta_{\rm min}$. This prediction is in much better agreement with the data of Eminyan *et al.*,[1] even where the FBA predictions for λ and χ are in very poor agreement. The value of $\theta_{\rm min}$ may be expressed in terms of λ and χ as

$$\tan2\theta_{\rm min}=2[\lambda(1-\lambda)]^{1/2}\cos\chi/(2\lambda-1) . \quad (9)$$

So it is clear that if the FBA correctly predicts $\theta_{\rm min}$ when χ is not zero, then its prediction of λ must be incorrect.

Another fairly simple approximation which in general has a broader range of applicability than the FBA, is the Glauber approximation. (The Glauber approximation satisfies the optical theorem in contrast to the FBA in which the scattering amplitudes are purely real.) However, it was pointed out by Eminyan *et al.*[1] that the Glauber approximation, despite some success in predicting differential cross sections, predicts that λ and χ are both independent of E and θ_e. Therefore we must turn to more elaborate theoretical calculations.

The various theoretical calculations prior to 1978[6-10] have been reviewed by Bransden and McDowell.[11] A meaningful comparison of the various calculations is difficult because they differ in the nature of the approximations and within a given approximation they may differ in the choice of atomic potentials and wave functions. For example, the recent distorted-wave calculation of Baluja and McDowell[12] gives very different results than the distorted-wave calculation of Madison.[13] The only significant difference between these two calculations is the choice of atomic wave functions. Baluja and McDowell used a simple analytic form while Madison used numerical Hartree-Fock orbitals. If these two calculations had used the same wave functions, they would in principle have given the same results.

The only calculation in reasonable agreement with all of the results of Eminyan *et al.*[1] for $E \geq 100$ eV, is the distorted-wave calculation of Madison.[13] However, this calculation gives values of $|\chi|$ about 20% larger than those measured by Eminyan *et al.*[1] The distorted-wave calculation of Bransden and Winters[8] using the second-order potential method gives the best agreement for $|\chi|$ but it is in very poor agreement with the results for λ. It should be noted that the calculation of Bransden and Winters[8] neglects final-state distortion which should be an important consideration.

In a recent publication, Steph and Golden[3] have reported electron-photon angular correlation measurements in electron-helium collisions for $2\,^1P$ excitation at an incident electron energy of 80 eV. In this paper we present further angular correlation measurements for $2\,^1P$ excitation of helium at electron energies of 100, 200, and 500

eV. In addition, we have combined the data of Sutcliffe *et al.*[14] with that of Steph and Golden[3] to give results for the full angular range from 5° to 100° and 155° at 80 eV. And finally, we combine all of the present results with the results of the other experiments[1,2] at all energies to examine the behavior of the Fano-Macek[4] alignment and orientation parameters as a function of energy.

II. THE EXPERIMENT

The theory of electron-photon angular correlations first given by Macek and Jaecks[15] has since been fully discussed by several authors.[1,5] The experimental apparatus and procedures used in the present work are identical to those described by Steph and Golden[3] and will only be briefly discussed here. The experimental geometry is shown in Fig. 1. The electron beam is incident along the z axis and intersects the atomic beam which is incident along the y axis. (This choice of axes is referred to as the collision frame.) The scattered electrons are energy analyzed by a hemispherical electron-energy analyzer which is tuned to pass electrons which have lost 21.22 eV. A channel electron multiplier is used to detect the transmitted electrons. The overall resolution of the system is independent of the incident electron energy and is 0.40 eV. The xz plane is the scattering plane. The electron detector may be rotated in the range $-5° \leq \theta_e \leq 150°$. The photons emitted by the excited helium atoms are detected by a suitably housed channel electron multiplier whose axis is also in the scattering plane. The angular position of the photon detector θ_γ may be varied in the range $50° \leq \theta_\gamma \leq 145°$. A Faraday cup is provided to collect the unscattered electron beam. The electron-beam current is typically 1 μA and the background pressure with the target-gas beam on is $\sim 3\times10^{-7}$ Torr. The pressure in the helium beam has been estimated to be $\sim 3\times10^{-5}$ Torr.

The pulses from the electron detector are used to start a time-to-amplitude converter (TAC), and suitably delayed pulses from the photon detector are used to stop the TAC. The output of the TAC is fed into a multichannel analyzer operated in the pulse-height analysis mode in order to generate the time spectrum of coincidence events. Electrons and photons from the same scattering event arrive with a definite time correlation. When counted for a time T these true coincidences form a peak on a background of accidental coincidences due to electrons and photons from different scattering events. For fixed values of θ_e and E, the number of true coincidences N_c will vary with θ_γ according to Eq. (4).

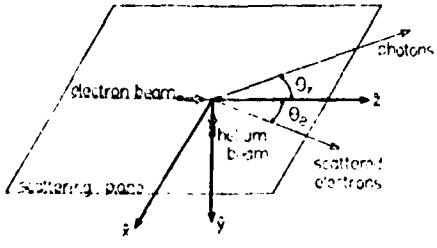

FIG. 1. The geometry of the experiment in the collision frame.

Measurements of N_c at several values of θ_γ are analyzed using the method of least squares to extract optimum values of λ and $|\chi|$. This procedure is discussed in Steph and Golden[3] and involves solving the equations which minimize the χ^2 analytically. This solution yields the optimum values of λ and $|\chi|$ and enables the development of analytic expressions for the statistical uncertainties in λ and $|\chi|$. Prior to analysis, the data must be corrected for the systematic effects of the finite solid angle of the photon detector and for scattering from the background helium. In addition, one must ensure that resonant trapping of the photons is not significant. These points have been fully discussed in Steph and Golden.[3]

The cross section σ decreases as the electron energy is increased from 80 eV. In addition, σ decreases sharply for increasing values of θ_e at all values of E. The decreasing rate of scattered electrons at large values of E and θ_e leads to increasing counting times. When the scattered electron rate falls to ~ 20 sec^{-1}, the rate of accidental coincidences falls to ~ 0.2 sec^{-1} and the rate of true coincidences is less than 1% of the accidental rate. Thus, coincidences must be counted for as long as one week at each value of θ_γ in order to reduce statistical uncertainty to an acceptable level. In this work, no measurements were made for values of θ_e where the scattered electron rate was ≤ 20 sec^{-1}.

III. RESULTS

The present experimental results are tabulated in Table I where the values of λ and $|\chi|$ and their uncertainties are listed as a function of energy and electron scattering angle. We also list the values of $\theta_{\rm min}$ calculated from Eq. (8) and the results of the FBA and the distorted-wave calculation of Madison[13] (MDW) for λ, $|\chi|$, and $\theta_{\rm min}$. The experimental values of λ at 80 eV were obtained by combining the results obtained in the present apparatus by Steph and Golden[3] with those obtained by Sutcliffe *et al.*[14] in an earlier version of the apparatus. The values of Sutcliffe *et al.*[14] were normalized to the 10° result of the calculation of

TABLE I. Experimental results and comparison with theory. (The distorted-wave calculations of Madison is denoted by MDW and the first Born approximation is denoted by FBA.)

		λ			χ (rad)		θ_{max} (deg)		
			Theory			Theory[b]		Theory	
Energy (eV)	θ_e (deg)	Expt.[a]	MDW	FBA	Expt.[a]	MDW	Expt.[a]	MDW	FBA
80[c]	5	0.749 ± 0.015	0.761	0.79	0.231 ± 0.220	0.259	29.7 ± 1.0	28.8	27.3
	10	0.488 ± 0.015	0.470	0.52	0.370 ± 0.038	0.425	44.3 ± 1.0	43.1	43.9
	20	0.305 ± 0.012	0.306	0.31	0.568 ± 0.054	0.905	58.3 ± 1.0	62.1	56.2
	30	0.445 ± 0.023	0.413	0.27	1.182 ± 0.053	1.304	53.1 ± 1.5	61.9	58.7
	40	0.642 ± 0.060	0.651	0.28	(1.60)[d]	1.527	−2.8 ± 15.0	3.9	58.1
	50	0.913 ± 0.048	0.860	0.32	1.994 ± 0.146	1.666	−7.8 ± 3.2	−2.6	55.6
	60	0.950 ± 0.062	0.965	0.37	2.424 ± 0.416	1.948	−10.0 ± 6.6	−4.1	52.5
	70	0.927 ± 0.140	0.990	0.44	(3.0)[d]	3.075	−15.5 ± 12.3	−5.7	48.4
	80	0.861 ± 0.120	0.968	0.50	2.570 ± 0.402	2.260	−19.4 ± 7.2	−6.7	45.0
	90	0.894 ± 0.079	0.925	0.58	2.001 ± 0.243	1.944	−9.0 ± 5.5	−6.4	40.4
	100	0.838 ± 0.108	0.885	0.65	1.842 ± 0.175	1.738	−8.1 ± 5.5	−3.9	36.3
	155	0.920 ± 0.150	0.962	0.96		1.082		5.5	11.5
100	5	0.67 ± 0.03	0.660	0.69	0.25 ± 0.18	0.243	34.8 ± 1.0	35.4	33.8
	10	0.36 ± 0.01	0.365	0.40	0.40 ± 0.04	0.456	53.8 ± 1.0	53.7	50.8
	16	0.28 ± 0.01	0.267	0.27	0.52 ± 0.03	0.778	59.7 ± 1.0	63.2	58.7
	30	0.49 ± 0.03	0.447	0.21	1.40 ± 0.05	1.318	49.4 ± 2.7	56.5	62.7
	40	0.76 ± 0.05	0.736	0.24	1.70 ± 0.12	1.455	−6.0 ± 5.4	6.1	60.7
200	5	0.34 ± 0.014	0.318	0.33	0.25 ± 0.07	0.260	54.6 ± 1.0	56.0	54.9
	10	0.20 ± 0.010	0.161	0.15	0.43 ± 0.06	0.601	64.8 ± 1.0	69.1	67.2
	20	0.19 ± 0.022	0.245	0.11	0.95 ± 0.12	1.082	71.8 ± 2.5	70.8	70.6
	30	0.64 ± 0.031	0.627	0.13	1.31 ± 0.14	1.160	20.7 ± 7.5	28.3	68.9
	40	0.95 ± 0.050	0.925	0.17	1.00 ± 0.20	0.760	7.3 ± 4.2	12.1	65.7
500	5	0.19 ± 0.02		0.08	0.29 ± 0.20		64.8 ± 1.5		73.6
	10	0.09 ± 0.01		0.04	0.58 ± 0.17		74.9 ± 1.6		78.5
	15	0.14 ± 0.02		0.05	0.70 ± 0.20		71.8 ± 2.5		77.8

[a] Uncertainties quoted for λ and χ represent one standard deviation.

[b] The FBA predicts $\chi = 0$ for all E and θ_e.

[c] The experimental values of λ and their uncertainties at 80 eV are the combined results of Refs. 3 and 14 as discussed in the text.

[d] These values of χ are interpolated as discussed in the text.

Madison and Calhoun,[9] $\lambda = 0.479$. We have renormalized their values to the 10° result of Steph and Golden,[3] $\lambda = 0.488$. Although this renormalization results in only ~2% change in the values of λ, it frees the data from dependence on a particular calculation. The two sets of data are combined by taking the average of their values weighted by their uncertainties. The values of $|\chi|$ listed for $\theta_e = 40°$ and 70° at 80 eV are based on a smooth interpolation of the results of Steph and Golden[3] for $|\chi|$ as a function of θ_e. An additional criterion used was that the interpolated values of $|\chi|$ combined with the measured values of λ yielded values of θ_{max}, O_1^{col}, and A_1^{col} which were also consistent with the smooth interpolation of the results of Steph and Golden[3] for these quantities. Figure 2 shows the data for λ and $|\chi|$ for 100, 200, and 500 eV plotted as a function of θ_e. We have also plotted the previous results of Eminyan *et al.*[1] at 100 and 200 eV along with the results of three distorted-wave (DW) calculations.[8,10,13] At each energy we have measured one point in common with Eminyan *et al.*[1] and these results all agree within one standard deviation. The three DW calculations differ in their choice of wave functions and potentials. The calculation of Madison,[13] which is the only DW calculation that includes distortion of the final state, is in good agreement with the present results for λ. The agreement is also fairly good for $|\chi|$ except for the small range of angles from 15° to 25° where the calculation of Madison[13] gives larger values of $|\chi|$ at all energies. The calculation of Bransden and Winters[8] is in fairly good agreement with the present results for $|\chi|$ but it is in very poor agreement with the results for λ. In contrast, the results of Scott and McDowell[10] are in fair agreement with the results for λ, at least at 200 eV, but they are in very poor agreement with the results for $|\chi|$. The results of these three calculations indicate that further refinement of the wave functions and potentials in the

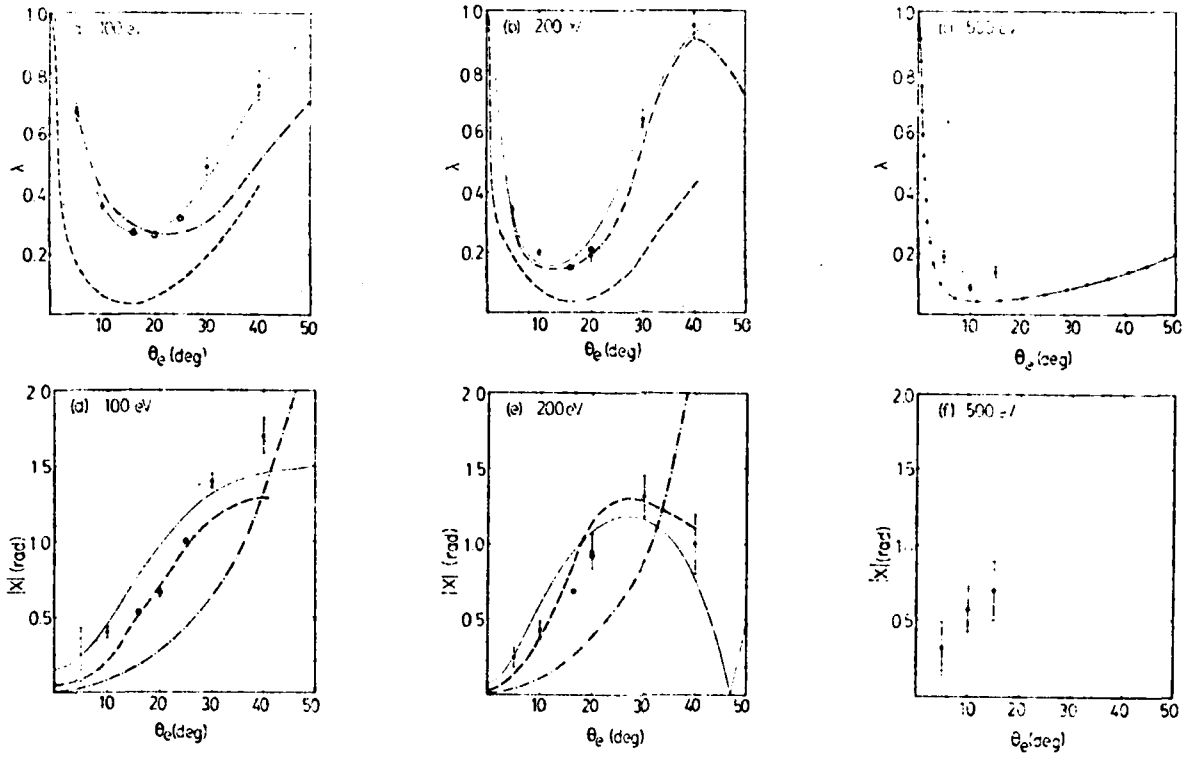

FIG. 2. The variation of λ with electron scattering angle at different electron energies: (a) 100 eV, (b) 200 eV, and (c) 500 eV. The variation of $|\chi|$ with electron scattering angle at different electron energies: (d) 100 eV, (e) 200 eV, and (f) 500 eV. ●, present work; ⊙, results of Ref. 1; ——, calculation of Ref. 13; ---, calculation of Ref. 8; – · –, calculation of Ref. 10; ⊖, FBA.

distorted-wave theory should yield very good agreement with experimental results.

The FBA for λ is in reasonable agreement with the results for λ, $\theta_e \leq 20°$, at 100 eV (see Table I). At 200 eV this agreement is only good for $\theta_e \lesssim 5°$. The FBA does not agree with any of the data for λ at 500 eV which can be seen in Fig. 2. Thus, as the energy is increased, the FBA is in increasingly poorer agreement with experimental results. This is in contrast to the FBA prediction for σ which is in better agreement with experiment at higher energies. This fact, along with the prediction that χ is zero for all energies, is sufficient to conclude that the FBA is inadequate to describe the excitation process in detail. However, it should be noted that the FBA prediction for θ_{min} is in good agreement with the data for $\theta_e \leq 20°$ for $E \approx 200$ eV, and is in good agreement with the present results at 500 eV, at least for $\theta_e \leq 15°$. Thus the importance that the FBA places on the direction of linear-momentum transfer for the excitation process seems to be well founded for small scattering angles. It is clear however that the $\Delta M_L = 0$ selection rule along the K axis is not correct.

IV. DISCUSSION OF RESULTS AND CONCLUSIONS

The behavior of λ and χ as a function of θ_e and E has been discussed. These parameters may be combined to form the alignment and orientation parameters which can then be used to describe the multipole moments of the excited state. Since these quantities are more closely related to the structure and anisotropy of the excited atom, we will consider the behavior of $\vec{O}$ and $\underline{A}$ in some detail.

The nonvanishing component of the orientation vector O_1^{col} is directly related to the dynamics of the excitation process. Equation (5) shows that O_1^{col} is directly proportional to the expectation value of angular momentum transferred to the atom perpendicular to the scattering plane. Indeed, since $L = 1$, we may write

$$\langle L_y \rangle = 2O_1^{col}. \tag{10}$$

Further, we know that $L_y = M_L \hbar$ so that the average $\langle L_y \rangle$ varies between −1 and +1. This reflects the fact that the atom is in a coherent mixture of states and does not generally possess a definite M_L value. We may rewrite Eq. (1) as

$$\psi(2\,^1P) = |a_0|\psi_z + \sqrt{2}\,|a_1|e^{i\chi}\psi_x, \qquad (11)$$

where $\psi_z = |10\rangle$ and $\psi_x = (1/\sqrt{2})(|11\rangle - |1-1\rangle)$. Thus, when $\lambda = 1$ the atom is in the pure state ψ_z, and L_y vanishes so that $\langle L_y\rangle$ also vanishes. When $\lambda = 0$ the atom is in the pure state ψ_x, and L_y may be ± 1 with equal probability so that $\langle L_y\rangle$ again vanishes. Thus, the nonvanishing values of O_{1-}^{e0} may only occur when the atom is in a coherent mixture of ψ_x and ψ_z, and there is interference between the complex scattering amplitudes a_0 and a_1. The maximum value of O_{1-}^{e0} is realized when $|a_0| = 2|a_1|$ (i.e., $\lambda = 0.5$), and $\chi = \pi/2$. When $\chi = 0$ or is an integral multiple of π, O_{1-}^{e0} vanishes. When the value of χ passes through 0 or $\pm\pi$, the sign of O_{1-}^{e0} changes. The experiment only measures the principal value of χ. Thus, values of χ reported are in the range $0 \le \chi \le \pi$. However, theory suggests that χ does pass through $-\pi$ at 80 and 100 eV, and through 0° at 200 eV.[10,12,13] Restricting the discussion to 80 eV, and considering only the theory of Madison,[13] χ is negative in the range $0° \le \theta_e \le 180°$ and passes through $-\pi$ at $\theta_e \simeq 70°$. Thus, O_{1-}^{e0} is positive for $\theta_e \le 70°$ and negative for $\theta_e > 70°$.

In order to relate the behavior of O_{1-}^{e0} to the collision process we shall look at the collision semiclassically. When an electron is scattered to a given angle, θ_e, the scattering may take either of the two principal paths shown in Fig. 3. In Fig. 3(a), the electron approaches the He atom with a negative impact parameter and scatters from the attractive polarizability potential to a positive scattering angle. In order to conserve angular momentum, the atom in Fig. 3(a) must obtain positive angular momentum perpendicular to the scattering plane; i.e., L_y must lie along the positive y axis. So, referring to Eq. (5), this implies that O_{1-}^{e0} is positive for this collision. In Fig. 3(b) the electron must be incident with a positive impact parameter if it is to scatter from the repulsive potential of the helium electrons and reach a positive scattering angle. In order to conserve angular momentum in this case, the atom must obtain negative angular momentum which implies that O_{1-}^{e0} is negative. Using this semiclassical model, we may explain the behavior of O_{1-}^{e0} as follows: When the electron is scattered to $\theta_e = 0°$, there can be no change in the angular momentum of the atom perpendicular to the scattering plane. Therefore O_{1-}^{e0} vanishes at $\theta_e = 0°$. As the scattering angle increases from 0°, the amount of angular momentum transferred to the atom perpendicular to the scattering plane, L_y, increases. Since the dominant scattering potential for small angles is the long-range attractive potential due to atomic polarizability, L_y is positive. Thus, O_{1-}^{e0} is positive and increases towards its extremal value of 0.5. However, as the scattering angle continues to increase, the impact parameter decreases and scattering from the repulsive potential of the helium electrons begins to become significant. Since the sign of the angular-momentum transfer due to repulsive scattering is opposite to that for attractive scattering, these processes compete and the value of O_{1-}^{e0} may or may not reach the value of 0.5 before it decreases with θ_e. Then at some value of θ_e where the contributions from the two types of scattering are equal in magnitude, O_{1-}^{e0} vanishes. As θ_e increases from this angle, the repulsive scattering becomes dominant and O_{1-}^{e0} becomes negative and decreases to another extremum. As θ_e increases further, the transfer of angular momentum perpendicular to the scattering plane again decreases until at $\theta_e = 180°$, O_{1-}^{e0} vanishes.

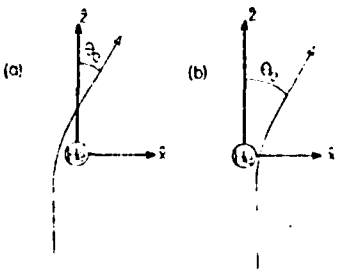

FIG. 3. The two principal paths for semiclassical scattering of electrons from helium. (a) The electron is incident with a negative impact parameter and scatters from the attractive polarizability potential to the positive angle, θ_e. (b) The electron is incident with a positive impact parameter and scatters from the repulsive potential of the He electrons to the same positive angle, θ_e.

The experimental results for $|O_{1-}^{e0}|$ at 80 eV are plotted in Fig. 4 along with the results of calculations by Madison[13] and Fon *et al.*[16] The experimental results are generally in good agreement with the semiclassical description given above and with the calculation of Madison[13] for $\theta_e \le 70°$ at 80 eV. Despite some disagreement in the range from 15° to 25°, the experimental results show an extremal value of $|O_{1-}^{e0}| \simeq 0.5$ at $\theta_e \sim 35°$, and show that O_{1-}^{e0} vanishes at $\theta_e \sim 70°$. The second extremum is much broader than the extremum at $\theta_e \sim 35°$, which indicates that there is little change in the relative importance of the two types of scattering in the backward direction. Using the results of Madison,[13] $[O_{1-}^{e0}(\theta_e = 110°) \simeq 0.35]$ the ratio of repulsive scattering to attractive scattering has a maximum value of ~3. For $\theta_e > 70°$, there are two sets of measurements that disagree. The results of Steph and Golden[3] are in agreement with the calculation of Madison.[13] The calculation of Fon *et al.*[16] lies roughly half-

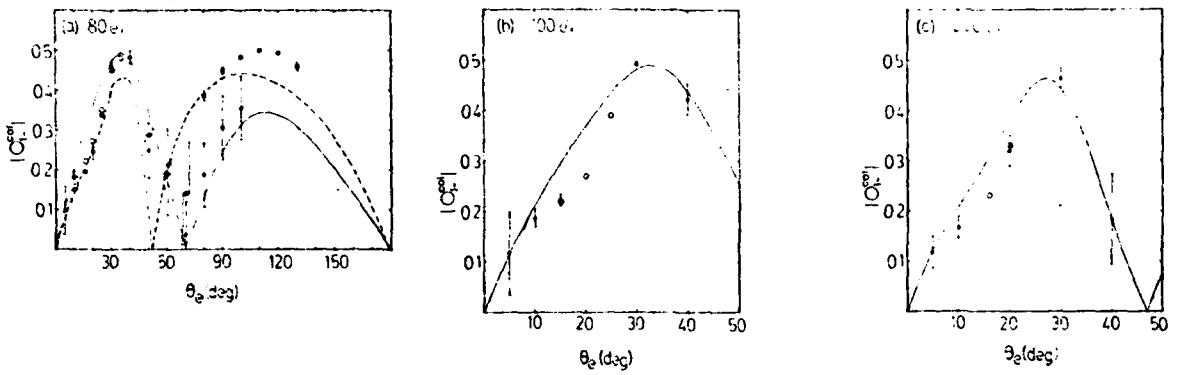

FIG. 4. The variation of $|O_{1-}^{col}|$ with electron scattering angle at different electron energies: (a) 80 eV, (b) 100 eV, and (c) 200 eV. ●, present work; ⊙, results of Ref. 1; ■, results of Ref. 17; ——, calculation of Ref. 13; ---, calculation of Ref. 16.

way between these results and the results of *Hollywood et al.*[17] which predict that $|O_{1-}^{col}|$ reaches its maximum value of 0.5 at $\theta_e \sim 110°$. So, the results of Hollywood *et al.*[17] would indicate that repulsive scattering is virtually the only process for back scattering, while the two calculations and the results of Steph and Golden[3] indicate that repulsive and attractive scattering are competing processes with repulsive scattering dominant by a maximum of a factor of 3 or 4.

We have discussed the disagreement between the two sets of experimental results for λ and $|\chi|$ in Steph and Golden[3] where we argued that the experimental technique discussed by Hollywood *et al.*[17] could impose systematic error on their data in the direction of the observed disagreement. It is also difficult to see how the attractive potential scattering could become completely insignificant for back scattering at 80 eV, although this would certainly be true at much larger energies as we discuss below. In any case, our semiclassical model is in qualitative agreement with the experimental results.

The behavior of O_{1-}^{col} as the electron energy is increased may also be explained in our semiclassical model. As E increases, the velocity of the electron increases and the electron spends less time in the long-range field of the attractive potential. However, the influence of the repulsive potential is not significantly affected by increasing electron velocity. Thus, as E increases, the first extremum of O_{1-}^{col} should occur at smaller values of θ_e and O_{1-}^{col} should no longer reach its maximum value of -0.5 at the first extremum. In addition, the angular position of the zero crossing of O_{1-}^{col} should decrease from 70°. The angular position of the second extremum should decrease from 110° and the value of O_{1-}^{col} at this extremum should decrease toward its minimum value of -0.5 as energy increases and repulsive scattering becomes more dominant. This is precisely the behavior seen by the experimental results at 100 and 200 eV for $\theta_e \leq 40°$ shown in Fig. 4. The calculation of Madison is generally in good agreement with the present results in this energy range and also predicts the behavior of O_{1-}^{col} for $\theta_e > 40°$ discussed above.

The orientation at fixed scattering angles as a function of energy is shown in Fig. 5. The experimental points at fixed angles are joined by straight lines for clarity. The results show that for $\theta_e \leq 20°$, $|O_{1-}^{col}|$ is virtually unaffected by increasing energy. Within our semiclassical model, this indicates that small-angle scattering is due solely to scattering from the long-range polarizability potential. The results also show that as energy increases, the position of the first extremum moves to smaller angles.

The nonvanishing components of the alignment tensor (A_0^{col}, A_{1-}^{col}, and A_{2-}^{col}) are related to the average values of quadratic expressions in the angular-momentum vector and its components. Thus it is more difficult to visualize the physical process that they represent. However, we may

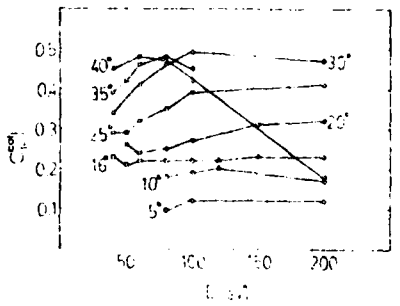

FIG. 5. The variation of $|O_{1-}^{col}|$ with electron energy at different scattering angles. ○, present results; □, results of Ref. 1; △, results of Ref. 2.

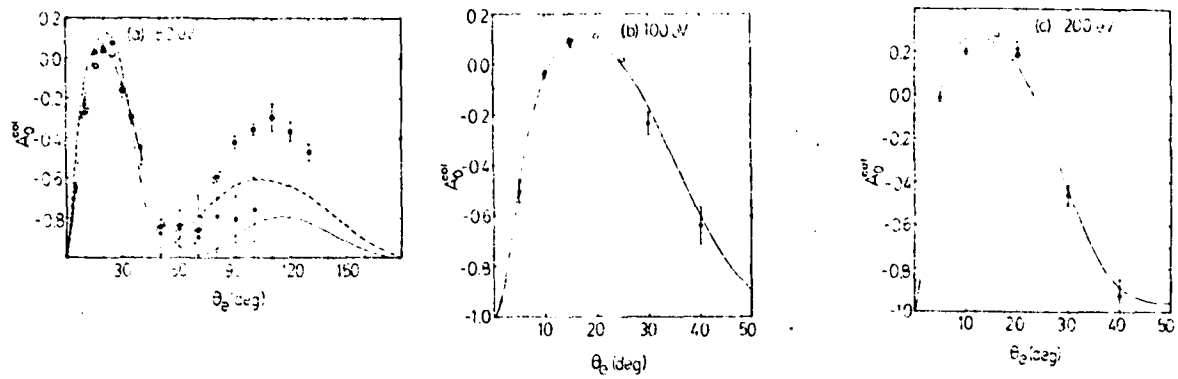

FIG. 6. The variation of A_0^{col} with electron scattering angle at different electron energies: (a) 80 eV, (b) 100 eV, and (c) 200 eV. The symbols are the same as Fig. 4.

note some marked similarities between the components of $\underline{A}$ and $\vec{O}$. It is clear from Eqs. (5) and (6) that the behavior of O_{1-}^{col} and A_{1+}^{col} will be similar. The two remaining components of $\underline{A}$ are also not independent, so we need only consider one of them. In Fig. 6 we show the data and calculations for A_0^{col} at 80, 100, and 200 eV. The qualitative behavior of A_0^{col} is strikingly similar to that of O_{1-}^{col}. At 80 eV, there is a narrow extremum at about 30° and a broad extremum at about 110°. Between these extrema, at 70°, A_0^{col} returns to the value it had at $\theta_e = 0°$. As the energy is increased, the small-angle extremum occurs at decreasing values of θ_e and the size of the extremum decreases. The similarities in the qualitative behavior of $\vec{O}$ and $\underline{A}$ imply that the interplay between long-range attractive potential scattering and repulsive potential scattering is responsible for the observed variations.

ACKNOWLEDGMENTS

This work was supported in part by grants from the National Science Foundation and the U. S. Air Force Office of Scientific Research.

[1]M. Eminyan, K. B. MacAdam, J. Slevin, and H. Kleinpoppen, Phys. Rev. Lett. 31, 576 (1973); J. Phys. B 7, 1519 (1974).
[2]A. Ugbabe, H. Arriola, P. J. O. Teubner, and E. Weigold, J. Phys. B 10, 72 (1977).
[3]N. C. Steph and D. E. Golden, Phys. Rev. A 21, 759 (1980).
[4]U. Fano and J. H. Macek, Rev. Mod. Phys. 45, 553 (1973).
[5]K. Blum and H. Kleinpoppen, Phys. Rev. 52, 203 (1979).
[6]C. J. Jochain and R. Vanderpoorten, J. Phys. B 7, L528 (1974).
[7]M. R. Flannery and K. J. McCann, J. Phys. B 8, 1716 (1975).
[8]B. H. Bransden and K. H. Winters, J. Phys. B 9, 1115 (1976).
[9]D. H. Madison and R. V. Calhoun (unpublished).
[10]T. Scott and M. R. C. McDowell, J. Phys. B 9, 2235 (1976).
[11]B. H. Bransden and M. R. C. Dowell, Phys. Rep. 30, 207 (1977); 46, 250 (1978).
[12]K. L. Baluja and M. R. C. McDowell, J. Phys. B 12, 835 (1979).
[13]D. H. Madison, J. Phys. B 12, 3399 (1979).
[14]V. C. Sutcliffe, G. N. Haddad, N. C. Steph, and D. E. Golden, Phys. Rev. A 17, 100 (1978).
[15]J. H. Macek and D. H. Jaecks, Phys. Rev. A 4, 2288 (1971).
[16]W. C. Fon, K. A. Berrington, and A. E. Kingston, J. Phys. B 12, L171 (1979).
[17]M. T. Hollywood, A. Crowe, and J. F. Williams, J. Phys. B 12, 819 (1979).

Low energy electron impact excitation and radiative decay of the $d^3\Delta$ state of CO[a)]

W. C. Paske, J. R. Twist,[b)] A. W. Garrett, and D. E. Golden

Department of Physics and Astronomy, University of Oklahoma, Norman, Oklahoma 73019
(Received 28 December 1979; accepted 7 February 1980)

The lifetimes of the $d\,^3\Delta(v'=4,5)$ levels of CO have been measured using a delayed coincidence technique. The lifetime for the $^3\Delta_1$ subbands were found to be 9% shorter than the $^3\Delta_2$ and $^3\Delta_3$ subbands while none of the lifetimes showed the J dependence previously reported. The lifetimes of the $^3\Delta_{2,3}$ subbands of the $v'=4$ and $v'=5$ levels were found to be 4.67 ± 0.33 μs and 4.02 ± 0.32 μs while the lifetimes of the $^3\Delta_1$ subbands of the $v'=4$ and $v'=5$ levels were found to be 4.27 ± 0.31 μs and 3.69 ± 0.34 μs, respectively. Long lived cascades with lifetimes of 16.1 ± 0.9 μs and 13.3 ± 1.1 μs were found to feed the $v'=4$ and $v'=5$ levels, respectively. Quenching cross sections and the $(d\rightarrow X):(d\rightarrow a)$ branching ratio are given for $v'=4,5$ and discrepancies with previous works are discussed.

I. INTRODUCTION

The radiative decay lifetimes for several of the vibrational levels of the $d^3\Delta$ state of CO have been studied by a number of authors.[1-5] Some authors[3,4] have reported lifetimes which are influenced by a perturbation[6-13] between the $d^3\Delta$ and $A^1\Pi$ states while several authors[1,2,5] have not mentioned this perturbation. Furthermore, none of these authors have indicated the presence of cascades.

Lifetimes for the triplet system were first reported by Fowler and Holzberlein[1] who used a high pressure (2–50 Torr) discharge and studied the 4100 to 5000 Å region with a bandpass filter. This work reported a single pressure independent fast decay of 31 ± 4 ns. In this initial work vibrational levels were not resolved and the possible perturbation of the $d^3\Delta$ state by the $A^1\Pi$ state was not discussed.

The lifetime of the $d^3\Delta(v'=6-10)$ levels were measured by Wentink *et al.*[2] in a pulsed rf discharge in a flowing gas using a gated pulse sampling technique. A prism monochromator was used and spectrally resolvable states were studied for a range of pressures from 3 to 100 mTorr. An excitation pulse of 10 μs with a fall time of 40 ns was used to obtain lifetimes in the range of 4.2 to 5.2 μs. However, these authors found their measured lifetimes to increase with increasing v', which was counter to expectation. In addition, they found all lifetimes to be pressure dependent with quenching cross sections within $0.9-1.4\times10^{-15}$ cm^2, but perturbations with the $A^1\Pi$ state were not discussed.

The radiative lifetime of the $d^3\Delta(v'=5)$ level was later found by Slanger and Black[3] to be strongly dependent on the rotational quantum number J for the case where $\Omega=1$. They found the subband lifetime to vary from 50 ns to 6 μs with increasing J. A weaker dependence was reported for the $\Omega=2$ subband and no dependence was reported for the $\Omega=3$ subband. These results are consistent with the explanation that the d state is perturbed by the $A^1\Pi$ state. That is, the mixing allows strong $d^3\Delta_1(v'=5)-X^1\Sigma^+$ radiation to compete with the $d^3\Delta_1(v'=5)-a^3\Pi$ transition for depopulation of the d state. In this work the d state was pumped with $d-X$ radiation from a lamp filled with a mixture of Kr and CO_2. The intensity of the fluorescence from the $d-a$ transition was observed as a function of various quenching gases. Three filters were used to separate the subbands. One, centered at 5625 Å with a 10 Å half-width was used to monitor the $^3\Delta_1$ subband. This filter had a 10% peak transmission width of 21 Å. A second filter centered at 5690 Å with a 60 Å half-width provided the predominantly unperturbed $^3\Delta_2$ and $^3\Delta_3$ subband intensities. This filter transmitted only 1% of the $^3\Delta_1$ subband relative to the $^3\Delta_3$ subband. A third filter centered at 5660 Å with a 50 Å half-width was used to pass most of the $d^3\Delta(v'=5)-a^3\Pi(v''=0)$ band. The quenching of the $d^3\Delta$ state was discussed only in terms of the different quenching gases used.

The lifetime of the $v'=3$ level of the $d^3\Delta_3$ state was more recently measured by Phillips *et al.*[4] by using a N_{1V} emission source to photodissociate CO_2 into the CO $d^3\Delta(v'=3)$ state. The decay curve was generated by multiscaling the intensity of the fluorescence from the $d^3\Delta_1(v'=3)-X^1\Sigma^+$ transition in 1 μs increments. The extracted lifetime was 4.7 ± 0.5 μs. Since this transition is doubly forbidden, Phillips *et al.*[4] concluded that the d state must be perturbed. They discussed this perturbation of the $d^3\Delta$ state as being due to an interaction with the $A^1\Pi$ state. Although the pressure dependence of the d state was not discussed, the branching ratio $(d-X):(d-a)$ was calculated for the second and third vibrational levels of the $d^3\Delta_1$ state.

The most recent and most comprehensive lifetime measurements of the $d^3\Delta(v'=1-16)$ states were made by Van Sprang *et al.*[5] In this work a delayed coincidence technique was used with an electron gun pulse duration of 10 μs. The energy of the incident electron beam was 13 eV which is near the maximum[14] of the electron excitation cross section for the $d^3\Delta$ state. The radiation was wavelength selected by a monochromator with a bandpass which was varied from 5 to 25 Å. It is unclear whether the quenching cross section reported for the $d^3\Delta(v'=2)-a^3\Pi(v''=0)$ transition (4.35×10^{-15} cm^2) is

[a)] Supported in part by grants from NSF and AFOSR.
[b)] Present address: Physics Department, Georgia Institute of Technology, Atlanta, GA 30332.

 0021-9606/80/116134-06$01.00

TABLE I. Previously reported lifetimes for the $d^3\Delta$ state of CO.

		τ (μs)				
v'	λ (Å)	Van Sprange *et al.* (Ref. 5) 1977	Phillips *et al.* (Ref. 4) 1976	Slanger and Black (Ref. 3) 1973	Wentink *et al.* (Ref. 2) 1967	Fowler and Holzberlein (Ref. 1) 1955
1	7515	7.30[b]				
2	6925	6.62				
3	6433	5.75	4.7 ± 0.5			
4	6010	5.40		0.058 → 6.40 ($^3\Delta_1$)		
5[a]	5647	4.05		2.17 ($^3\Delta_2$)		
6	5330	4.90		6.40 ($^3\Delta_3$)		
7	5052	4.18			5.03[c,d]	
8[a]	4806	5.23			4.18	
9	4586	4.56			4.36	
10	4747	4.46			4.45	
11	4541	4.46			4.57	
12[a]	4718	4.65				0.031
13	4505	4.67				
14	4328	4.54				
15[a]	4171	4.16				
16	4023	2.94				

[a]Reported as highly perturbed (Ref. 10).
[b]The reported error for all lifetimes was ± 0.6 μs.
[c]Different wavelengths were used in every lifetime measurement.
[d]The (6, 1) band was reported as 5.2 μs but this may be due to the $a'\,^3\Sigma^+ (v' = 9) \rightarrow a\,^3\Pi (v'' = 0)$ transition.

representative of all the transitions studied. No perturbations with the $A\,^1\Pi$ state or any other state were reported in this work.

A tabulation of the previously described work on the $d^3\Delta$ state of CO is presented in Table I. The results of Wentink *et al.*[2] and Van Sprang *et al.*[5] agree to better than 3% for all but the $v' = 8$ level where a 20% discrepancy exists. The lifetime results of Phillips *et al.*[4] for the $v' = 3$ level disagree with the results of Van Sprang *et al.*[5] by 22%, and the perturbation observed by Phillips *et al.*[4] is not even mentioned by Van Sprang *et al.*[5] The results for the $v' = 5$ level reported by Van Sprang *et al.*[5] and those reported by Slanger and Black[3] for the $d^3\Delta_2$ subband disagree by more than 80%. Furthermore, the perturbation reported by Slanger and Black[3] is not mentioned by Van Sprang *et al.*[5] Finally, the very fast decay reported by Fowler and Holzberlein[1] has not been seen in the subsequent work except perhaps by Slanger and Black[3] for the low J levels of the $^3\Delta_1$ subband of the $v' = 5$ level (58 ns).

Throughout the previous lifetime work on the $d^3\Delta$ state, no cascades have been reported. This is somewhat surprising since several cascade mechanisms have been discussed[11-13] during perturbation arguments. In particular, the $A\,^1\Pi - d^3\Delta$ and the $A\,^1\Pi - c\,^3\Sigma^- - d^3\Delta$ population schemes have been discussed. If the $A\,^1\Pi$ state is coupled to the $d^3\Delta$ state, either radiatively or through collisional transfer, a very fast (9–16 ns) cascade would be evident in the decay of the $d^3\Delta$ state.[15] If the $c\,^3\Sigma^-$ state is coupled radiatively or collisionally to the $d^3\Delta$ state, two very similar lifetimes should be evident since the lifetime of the $c\,^3\Sigma^-$ state is suspected to be about 3 μs.[6] Apparently neither of these mechanisms have been observed in the previous work on the $d^3\Delta$ state.

Clearly two questions persist about the radiative lifetime of the $d^3\Delta$ state. First, are the vibrational levels of the $d^3\Delta$ state perturbed by the $A\,^1\Pi$ state and does this perturbation effect the radiative lifetime of the state by opening an additional decay channel ($d - X$) causing the strong J dependent lifetimes reported by Slanger and Black? Second, are cascades present which could indicate the population mechanisms involved in exciting the $d^3\Delta$ state?

In order to answer these questions we remeasured the radiative lifetimes of the $d^3\Delta (v' = 4, 5) - a^3\Pi (v'' = 0)$ transitions in a delayed coincidence experiment. In the analysis of the data we have specifically looked for cascades and the effect of any perturbation between the $A\,^1\Pi$ and $d^3\Delta$ states. Since this perturbation should only effect the $^3\Delta_1$ subband,[8-13] we have examined the radiative decay for each subband individually. We have also calculated the branching ratio $(d - X)/(d - a)$ for the $v' = 4, 5$ vibrational levels of the $d^3\Delta$ state.

II. APPARATUS AND PROCEDURE

The experimental apparatus consists of a pulsed electron gun,[16] gas target cell and Faraday cup all located in an ultrahigh vacuum system which has been described previously.[17] The emitted photons are filtered by a Jarrell Ash 1/4 meter monochromator with a variable band pass of from 10 to 25 Å. The filtered photons are detected by an RCA C31034A-02 photomultiplier which has been cooled to ~ 20 °C. For lifetime measurements, the resultant signal is pulse height analyzed using a delayed coincidence technique.

The lifetime data were collected for a pressure range from 1 to 25 mTorr simultaneously by two Time to Amplitude Converters (TAC's) and two multichannel analyzer (MCA) systems. Typically, one MCA–TAC sys-

tem was used to acquire data suitable for the analysis of long-lived excited states (e.g., 82 ns/channel) while the second MCA–TAC system was set to look for short lived states (e.g., 0.5 ns/channel). This double MCA–TAC system allows an unambiguous analysis of the $d^3\Delta$ system since this state has a lifetime reported to be between 30 ns and 6 μs.[1–5] Clearly, a 30 ns decay could be improperly analyzed if the data were only collected at 82 ns/channel. The data were analyzed using a nonlinear least squares computer fit with multiple exponentials and the experimental error of the best fit was determined by a grid search technique previously described.[17] The errors stated for the lifetimes determined in this work are at the 95% confidence level (two standard deviations).

Wavelength spectral scans were conducted in the region of interest at different energies to determine the extent of possible spectral overlap. The two spectra shown in Fig. 1 were obtained at 9.8 and 11.3 eV, respectively. The transitions observed depended on the electron energy and were $d^3\Delta - a^3\Pi$, $e^3\Sigma^- - a^3\Pi$, $a'^3\Sigma^+ - a^3\Pi$, and $B^1\Sigma^+ - A^1\Pi$ which have threshold energies of 7.519, 7.879, 6.863, and 10.776 eV as given by Krupenie.[8] These spectra were obtained by multiscaling for 0.8 s/channel using 0.5 mm slits (25 Å resolution) in the Jarrell Ash monochromator. The upper trace in Fig. 1 shows that the $B^1\Sigma^+(v'=0) - A^1\Pi(v''=0)$ transition is not resolved from the $d^3\Delta(v'=4) - a^3\Pi(v''=0)$ transition. However, this $B-A$ transition does clearly distort the spectra when the electron gun energy is increased from 9.8 to 11.3 eV. This overlap poses a particularly interesting problem at higher gun energies since the $B^1\Sigma^+ - A^1\Pi$ transition has a 34 ns lifetime.[5] Since we wish to determine whether the presence of a fast (30–60 ns) decay is indeed associated with the decay of the $d^3\Delta$ state, and in order to avoid misinterpreting the results, we must insure that our electron gun energy is always below the threshold of the $B^1\Sigma^+$ state. To stress this point, parts of two decay curves at 9.8 and 11.3 eV are shown in Fig. 2 for the unperturbed $d^3\Delta_2(v'=4) \rightarrow a^3\Pi(v''=0)$ transition at 6010 Å. In the upper curve the electron energy was 11.3 eV and a fast decay is quite evident. The lifetime of this fast component was determined to be 34 ns when analyzed on a more suitable time scale, in excellent agreement with Van Sprang *et al.*[5] for the $B^1\Sigma^+(v'=0) - A^1\Pi$ transition. The electron energy was decreased to 9.8 eV in the lower curve of Fig. 2, which is below the $B-A$ threshold. It can be seen on Fig. 2 that in this latter case the fast component is totally gone. The $B^1\Sigma^+(v'=0) - A^1\Pi(v''=3)$ transition is clearly resolved from the $d^3\Delta(v'=5) - a^3\Pi(v''=0)$ transition and should only pose a problem when studying the $d^3\Delta_1$ subband. Therefore, all lifetime data used in this study were collected with the electron gun energy below the $B^1\Sigma^+$ threshold.

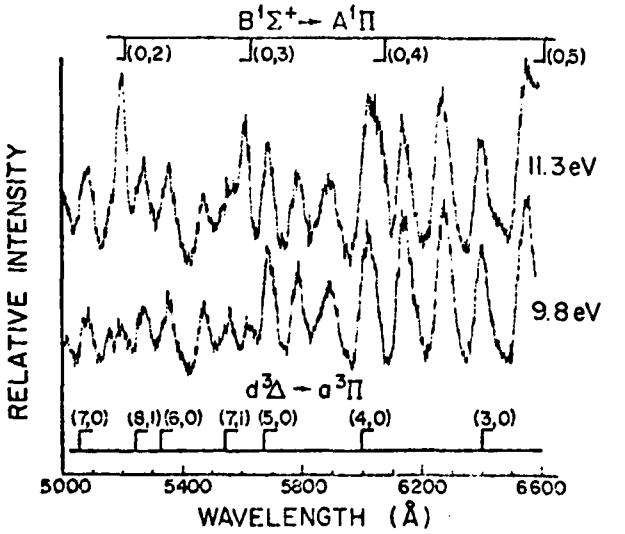

FIG. 1. Optical spectra of CO obtained by multiscaling for 0.8 s/channel using 25 Å resolution. Two excitation energies were used to show the spectral overlap of the $B^1\Sigma^+ - A^1\Pi$ transitions on the $d^3\Delta \rightarrow a^3\Pi$ transitions. The unlabeled peaks in the figure belong to the $e^3\Sigma^- \rightarrow a^3\Pi$ and $a'^3\Sigma^+ \rightarrow a^3\Pi$ transitions and were omitted for clarity.

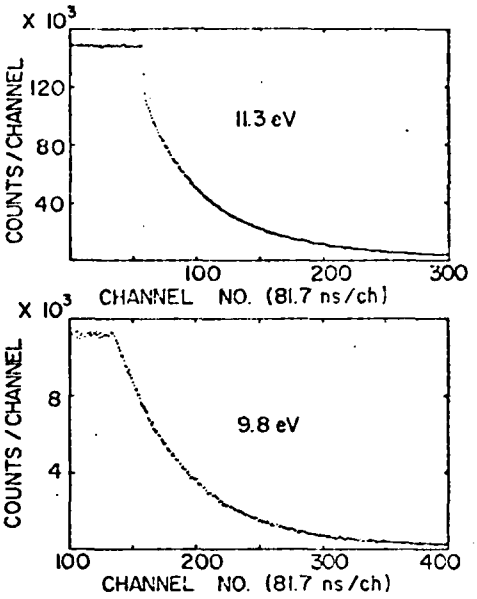

FIG. 2. Sections of the decay curves for the unperturbed $d^3\Delta_2(v'=4) \rightarrow a^3\Pi(v''=0)$ transition of CO for excitation energies of 9.8 and 11.3 eV. The presence of a fast decay in the upper curve in which the excitation energy is above the $B^1\Sigma^+$ threshold is clearly evident.

III. RESULTS AND DISCUSSION

All lifetime measurements made on the $d^3\Delta(v'=4, 5) - a^3\Pi(v''=0)$ transitions indicated the presence of two exponentials. However, the cascade found was too long lived to be due to the $A^1\Pi$ or $e^3\Sigma^-$, as expected. This will be discussed more fully below.

The reciprocal lifetimes of the prompt decays of the subbands of the $d^3\Delta(v'=4, 5) - a^3\Pi(v''=0)$ transitions are plotted as a function of pressure in Fig. 3. The zero pressure extrapolated lifetimes for the subbands of the $d^3\Delta(v'=4, 5)$ states are listed in Table II along with the previously reported lifetimes for $v'=4, 5$. It

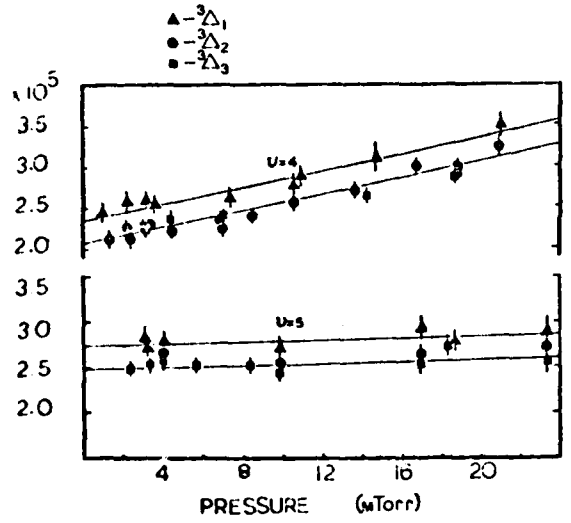

FIG. 3. Reciprocal promp lifetimes vs pressure for the $d\,^3\Delta(v'=4,5) \rightarrow a\,^3\Pi\,(v''=0)$ transitions. The respective subbands are identified as follows: ▲ $^3\Delta_1$ (5982, 5624 Å), ● $^3\Delta_2$ (6010, 5647 Å), and ■ $^3\Delta_3$ (6034, 5670 Å).

is clear from Fig. 3 that the $^3\Delta_1$ subband does indeed have a slightly shorter lifetime than the $^3\Delta_{2,3}$ subbands for both vibrational levels of the d state. Furthermore the lifetimes for the $^3\Delta_2$ and $^3\Delta_3$ subbands are identical within experimental uncertainty. The faster decay observed for the $^3\Delta_1$ level is probably due to the additional decay channel, $d-X$, which is open due to the perturbation by the $A\,^1\Pi$ discussed by Slanger and Black.[3,5,11–13] However, we do not see the strong J dependence reported by Slanger and Black[3] for $v'=5$. We did see a very intense fast (34 ns) lifetime in our studies. This was discussed above as being due to a near spectral overlap with the $B\,^1\Sigma^+(v'=0)-A\,^1\Pi(v''=3)$ transition. This transition (5610 Å) would be passed by the filter centered at 5625 Å used by Slanger and Black. For all energies above the $B\,^1\Sigma$ threshold used in our lifetime studies we found that a 20 Å bandpass would allow this fast B state to overlap the $^3\Delta_1$ subband but not the $^3\Delta_{2,3}$ subbands. It is then possible that the J dependence reported was in reality a spectral overlap with the $B\,^1\Sigma^+-A\,^3\Pi$ transition. However we cannot rule out the J dependence on the basis of this work. Rather we can state that if there is a J dependence present, it does not strongly affect the lifetimes of these states. While this could account for the differences reported[3,5] for the $^3\Delta_1$ and $^3\Delta_2$ lifetimes, it can not account for the differences in the $^3\Delta_3$ lifetime.[3,5] However, the 6.4 μs given by Slanger and Black[3] for the lifetime of the $^3\Delta_3$ level was arrived at through consideration of the data presented by Wentink *et al.*[2] and was not directly measured. If we consider the $^3\Delta_2$ and $^3\Delta_3$ levels to be unperturbed as previously reported, then we must conclude that the $v'=4$ level is as influenced by the $A\,^1\Pi$ state as the $v'=5$ state because the transition probabilities for the $d-X$ branches are $0.20\times10^5\ s^{-1}(v'=4)$ and $0.22\times10^5\ s^{-1}(v'=5)$. We have listed the branching ratio $(d-X):(d-a)$ in Table III for comparison. The values shown in Table III for the $v'=2,3$ $(d-X):(d-a)$ branching ratios are those reported by Phillips *et al.*[4] If we believe that the additional decay channel $(d-X)$ is open solely because of this perturbation, then the almost equal branching ratios for $v'=4,5$ would seem to indicate that the two vibrational levels are equally perturbed by the $A\,^1\Pi$ state. However, only the $v'=5$ level is reported to be strongly perturbed[10] by the $A\,^1\Pi$ state. The $v'=4$ and $v'=5$ levels are both reported to be more perturbed

TABLE II. Lifetimes and collisional quenching cross sections for the $d\,^3\Delta(v'=4,5)$ states of CO.

Investigator	$v'\rightarrow v''$	λ (Å)	Prompt lifetime τ_p (μs)	Cascade lifetime τ_c (μs)	Prompt quenching cross section (Å²)	Cascade quenching cross section (Å²)
This work	4→0	5982	4.27 ± 0.31	16.1 ± 0.9	33.3 ± 4.2	25.5 ± 3.4
	4→0	6010	4.68 ± 0.33		27.8 ± 1.1	
	4→0	6034	4.65 ± 0.33		22.5 ± 2.1	
	5→0	5624	3.69 ± 0.31	13.3 ± 1.1	4.0 ± 2.8	22.8 ± 6.2
	5→0	5647	4.02 ± 0.32		3.65 ± 2.21	
	5→0	5670	4.02 ± 0.32		3.65 ± 2.21	
Slanger and Black (Ref. 3)	4→0	5982	···	···	···	···
	4→0	6010	···	···	···	···
	4→0	6034	···	···	···	···
	5→0	5624	0.058 → 6.40[a]	···	···	···
	5→0	5647	2.17	···	···	···
	5→0	5670	6.40	···	···	···
Van Sprang *et al.* (Ref. 5)	4→0	5982	···	···	···	···
	4→0	6010	5.40 ± 0.60	···	43.5[b]	···
	4→0	6034	···	···	···	···
	5→0	5624	···	···	···	···
	5→0	5647	4.05 ± 0.60	···	43.5[b]	···
	5→0	5670	···	···	···	···

[a] Reported as strongly J dependent.
[b] Reported for the d state. May have been measured for only the (2→0) transition.

TABLE III. Extracted $(d \rightarrow X) : (d \rightarrow a)$ branching ratios for four vibrational levels of the $d^3\Delta$ state of CO.

v'	$(d \rightarrow X) : (d \rightarrow a)$
2	0.021[a]
3	0.076[a]
4	0.093[b]
5	0.088[b]

[a]Reported by Phillips *et al.* (Ref. 4).
[b]Extracted in this work.

than the $v' = 2$ and $v' = 3$ levels, consistent with the trend observed in Table III.

Although our measured lifetime for the $d^3\Delta(v' = 4) - a^3\Pi(v'' = 0)$ transition and that reported by Van Sprang *et al.*[5] overlap within experimental error, we believe all of their results are systematically high due to presence of the cascade discussed above. The effects on a measured lifetime due to the neglect of a cascade have been discussed in detail previously.[17] In general, errors of 10%–20% are common if the intensity of the cascade component is a sizable fraction of the prompt decay. This point is borne out in that the cascade component observed with the $d^3\Delta(v' = 4) - a^3\Pi(v'' = 0)$ decay is 25% of the prompt decay, whereas the cascade component observed with the $d^3\Delta(v' = 5) - a^3\Pi(v'' = 0)$ decay is only 3% of the prompt decay. When a one-exponential fit is made to the data sets instead of a two-exponential fit, the $d^3\Delta(v' = 5) - a^3\Pi(v'' = 0)$ prompt decay lifetime is only effected by about 1% whereas the $d^3\Delta(v' = 4) - a^3\Pi(v'' = 0)$ prompt decay lifetime is affected by 15–20%. This is why we agree so well with the lifetime reported for the $d^3\Delta(v' = 5)$ state by Van Sprang *et al.*[5] but are close to one microsecond (15%) less than the lifetime reported by them for the $d^3\Delta(v' = 4)$ state.

The quenching cross section reported by Van Sprang *et al.*[5] for the $d^3\Delta$ state is considerably larger than that observed by us for either of the $d^3\Delta(v' = 4, 5)$ states. However, as discussed above, it is not clear from their paper whether the quenching cross section given by them was calculated for just the $d^3\Delta(v' = 2) - a^3\Pi(v'' = 0)$ transition or for several transitions. The quenching cross sections given by Wentink *et al.*[2] for $v' = 6$–10 range from 9 to 14 Å^2 which are smaller than our quenching cross sections for $v' = 4, 5$. If we accept the value of 43.5 Å^2 of Van Sprang *et al.*[5] as being the quenching cross section of the $v' = 2$ level and the 9–14 Å^2 values of Wentink *et al.*[2] as the quenching cross sections for the $v' = 6$–10 levels, then we can conclude that the quenching cross section decreases with increasing v' for the $d^3\Delta$ state. However, this work has shown that the quenching cross section is also a function of Ω which is consistent with the $d \rightarrow X$ channel being open.

The reciprocal lifetime of the cascade observed in this study is plotted as a function of pressure in Fig. 4. The zero pressure extrapolated lifetimes are also given in Table II as are their collisional quenching cross sections. While the quenching cross sections are about the same within experimental uncertainties, the lifetimes are not the same. Moreover, the cascade lifetimes are independent of Ω which means that the same upper level feeds all three subbands. However, there are no known long-lived levels which could be the source of this cascade. The lower vibrational levels of the $a'^3\Sigma^+$ state have lifetimes of this order, but the measured lifetimes of the vibrational levels decrease with increasing v' and consequently, upper levels of the a' state must be ruled out as a possible source. The $e^3\Sigma^-$ state was mentioned by Slanger and Black as a possible cascade source. However, the only estimate of a lifetime for the $e^3\Sigma^-$ state[6] indicates that the $e^3\Sigma^-$ is too short lived to be the source of this cascade. Currently we are undertaking a study of the $e^3\Sigma^-$ state and our preliminary results confirm Slanger and Black's estimate for the lifetime of the e state. Therefore this work indicates that either a new triplet state exists or, more probably, that the $I^1\Sigma^-$ or $D^1\Delta$ cascades into the $d^3\Delta$ state.

To check for a possible instrumental error, the amplitude ratio of the prompt and cascade decay components were measured as a function of the excitation pulse width. To determine the theoretical effect that the excitation pulse width should have on the ratio of the prompt decay amplitude to the cascade decay amplitude, we need to solve the rate equations for a two level system. At the time of cut-off T, the ratio of the prompt decay amplitude A_p, to the cascade decay amplitude A_c, is given by

$$\frac{A_p}{A_c} = \frac{\lambda_c}{\lambda_p}\left[\frac{Q_p}{Q_c}\left(\frac{\lambda_p - \lambda_c}{\lambda_{cp}}\right) - 1\right]\left[\frac{1 - e^{-\lambda_p T}}{1 - e^{-\lambda_c T}}\right],$$

where Q_p and Q_c are the production cross sections for the prompt and cascade levels. The pressure dependent transition probabilities, λ_p and λ_c, are given by $\lambda_j = A_j + N_0\sigma_j\bar{v}$ where A_j is the Einstein coefficient, N_0 is the

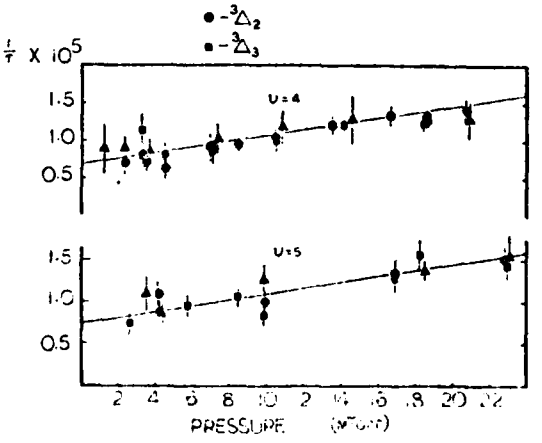

FIG. 4. Reciprocal lifetimes vs pressure for the cascade feeding the $d^3\Delta(v' = 4, 5)$ levels of CO. The respective subbands monitored are as follows: ▲ $^3\Delta_1$ (5952, 5524 Å) ● $^3\Delta_2$ (6010, 5617 Å), and ■ $^3\Delta_3$ (6031, 5670 Å).

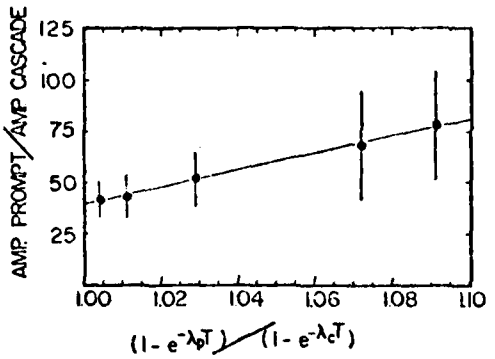

FIG. 5. Plot of the ratio of the measured amplitudes of the prompt and cascade decay modes vs the calculated ratio of the amplitudes as a function of the excitation pulse width, T. The pulse width was varied from 6–80 μs.

population of the ground state, $\bar{v}$ is the mean velocity of the gas, and σ_j is the quenching cross section of the particular level of interest. The pressure dependent transition probability λ_{cp} describes the particular transfer from the cascade state directly to the prompt state.

If the observed cascade is real, a plot of the ratio of the measured amplitudes A_p/A_c, versus the calculated ratio of the amplitudes as a function of the excitation pulse width, $(1-e^{-\lambda_p T})/(1-e^{-\lambda_c T})$ will yield a straight line. The plot in Fig. 5 indicates the cascade is real and not an artifact. However, until further work is concluded, the slope of this graph cannot be interpreted, as both the production cross section Q_c and the pressure dependent transition probability λ_{cp} from the unknown state to the $d^3\Delta$ state are not known.

Two conclusions may be drawn from this work. First, the $^3\Delta_1$ subbands are perturbed as previously reported[6,11] and this perturbation allows a small mixing with the $A\,^1\Pi$ to take place so that a small but measurable branching occurs to the ground state. This perturbation only affects the $^3\Delta_1$ subband and is not seen for the $^3\Delta_2$ and $^3\Delta_3$ subbands, consistent with the $\Delta\Omega = 0, \pm 1$ selection rule. Because of this rule, Van Sprang *et al.*[5] should not have seen, and did not see, this perturbation. However, the strong J coupling reported earlier[3] appears to have been the result of spectral overlap with the $B\,^1\Sigma^+(v'=0) - A\,^1\Pi(v'=3)$ transition which is only 15 Å away from the center of their 20 Å bandpass filter. This spectral overlap with the $B\,^1\Sigma^+$ state is probably also the source of the fast decay reported by Fowler and Holzberlein.[1]

Second, we can conclude that cascades are present. However, the cascade is not due to the two mechanisms discussed earlier. We will have to wait for further work to identify the source of the cascade but we can estimate its threshold to be between 7.8 and 9.8 eV since it feeds both the $d^3\Delta$ and the $e^3\Sigma^-$ states.

[1]R. G. Fowler and T. M. Holzberlein, J. Chem. Phys. 45, 1123 (1966).
[2]T. Wentink Jr., E. P. Marram, L. Isaacson, and R. J. Spindler, AFWL Tech. Rpt. 67-30, Vol. 1, November, 1967.
[3]T. G. Slanger and G. Black, J. Chem. Phys. 58, 194 (1973).
[4]E. Phillips, L. C. Lee, and D. L. Judge, J. Chem. Phys. 65, 3118 (1976).
[5]H. A. Van Sprang, G. R. Mohlmann, and F. J. de Heer, Chem. Phys. 24, 429 (1977).
[6]T. G. Slanger and G. Black, J. Chem. Phys. 58, 3121 (1973).
[7]P. K. Caroll, J. Chem. Phys. 36, 2861 (1962).
[8]P. H. Krupenie, Natl. Stand. Ref. Data Ser. Natl. Bur. Stand. 5 (1966).
[9]J. D. Simmons, A. M. Bass, and S. G. Tilford, Astrophys. J. 155, 345 (1969).
[10]G. Herzberg, T. J. Hugo, S. G. Tilford, and J. D. Simmons, Can. J. Phys. 48, 3004 (1970).
[11]T. G. Slanger and G. Black, Chem. Phys. Lett. 4, 558 (1970).
[12]T. G. Slanger and G. Black, J. Chem. Phys. 64, 219 (1976).
[13]T. G. Slanger and G. Black, J. Chem. Phys. 48, 356 (1968).
[14]S. Chung and C. C. Lin, Phys. Rev. A 9, 1954 (1974).
[15]T. A. Carlsen, N. Durie, P. Erman, and M. Larsson, Z. Phys. Teil A 287, 123 (1978).
[16]D. E. Golden, D. J. Burns, and V. C. Sutcliffe, Phys. Rev. A 10, 2133 (1974).
[17]J. R. Twist, W. C. Paske, T. O. Rhymes, G. N. Haddad, and D. E. Golden, J. Chem. Phys. 71, 2345 (1979).